Poissonnier, Amanda and Sanseau, Doriane and Le Gallo, Matthieu and Malleter, Marine and Levoin, Nicolas and Viel, Roselyne and Morere, Lucie and Penna, Aubin and Blanco, Patrick and Dupuy, Alain and Poizeau, Florence and Fautrel, Alain and Seneschal, Julien and Jouan, Florence and Ritz, Jerome and Forcade, Edouard and Rioux, Nathalie and Contin, Cecile and Ducret, Thomas and Vacher, Anne-Marie and Barrow, Paul A. and Flynn, Robin J. and Vacher, Pierre and Legembre, Patrick (2016) CD95 recruits PLCγ1 to trigger a calcium response promoting Th17 accumulation in inflamed organs of lupus mice. Immunity . ISSN 1097-4180 (In Press)

Immunity

CD95 recruits PLCγ1 to trigger a calcium response promoting Th17 accumulation in inflamed organs of lupus mice

--Manuscript Draft--

Manuscript Number:	IMMUNITY-D-15-00834R3
Full Title:	CD95 recruits PLCγ1 to trigger a calcium response promoting Th17 accumulation in inflamed organs of lupus mice
Article Type:	Research Article
Keywords:	Calcium, CD95, inflammation, lupus, sphingosine-1 phosphate, Th17 cell
Corresponding Author:	patrick legembre Universite de Rennes-1 Rennes, FRANCE
First Author:	patrick legembre
Order of Authors:	patrick legembre
	sanseau doriane
	marine malleter
	amanda poissonnier
	levoin nicolas
	aubin penna
	patrick blanco
	alain dupuy
	florence poizeau
	alain fautrel
	roselyne viel
	seneschal julien
	contin cecile
	thomas ducret
	anne-marie vacher
	paul a barrow
	robin j flynn
	pierre vacher
	matthieu Le gallo
	nathalie rioux
	Lucie morere
	florence jouan
Abstract:	CD95 ligand (CD95L) is expressed by immune cells and triggers apoptotic death. Metalloprotease-cleaved CD95L (cl-CD95L) is released into the bloodstream but does not trigger apoptotic signaling. Hence, the pathophysiological role of cl-CD95L remains unclear. We observed that skin-derived endothelial cells from systemic lupus erythematosus (SLE) patients expressed CD95L, and that after cleavage, cl-CD95L promoted T helper 17 (Th17) lymphocyte transmigration across the endothelial barrier at the expense of T regulatory cells. T cell migration relied on a direct interaction between the CD95 domain called calcium-inducing domain (CID) and the Src homology 3 domain of phospholipase Cγ1. Th17 cells stimulated with cl-CD95L

	produced sphingosine-1-phosphate (S1P), which promoted endothelial transmigration by activating the S1P receptor 3. We generated a cell-penetrating CID peptide that prevented Th17 cell transmigration and alleviated clinical symptoms in lupus mice. Therefore, neutralizing the CD95 non-apoptotic signaling pathway may be attractive therapeutic approach for SLE treatment.
Suggested Reviewers:	eric solary, MD, PhD eric.solary@gustaveroussy.fr death receptor specialist
Opposed Reviewers:	

Oncogenesis, Stress & Signaling Laboratory
Université de Rennes-1 - INSERM ERL440
Centre de Lutte Contre le Cancer Eugène Marquis

Rennes, 17 June, 2016

To Editors of Immunity,

We are pleased to submit a re-revised version of our manuscript **IMMUNITY-D-15-00834R3**, for publication in Immunity. The title changed according to Miss Kavitha Scranton recommendations; New Title is "**CD95 recruits PLCγ1 to trigger a calcium response promoting Th17 accumulation in inflamed organs of lupus mice**".

All reviewer#2 remarks have been addressed in the main text of the manuscript.

Overall, this work highlighted that cl-CD95L, found in high levels in SLE patients, leads to Th17 accumulation in inflamed organs in this autoimmune disease. Moreover, we revealed that CD95-mediated non-apoptotic signaling can be specifically blocked to prevent its pro-inflammatory effect and that treatment designed to halt cl-CD95L actions *in vivo* alleviates both the immune and pathological hallmarks in lupus-prone mice. Ultimately, our findings support further investigations into targeting of the cl-CD95L pathway in autoimmune inflammation and specifically SLE and provide the proof-of-concept for novel therapeutic avenues for this devastating disease.

We are confident that by addressing all reviewer concerns, you now consider this study satisfactory for publication in Immunity.

We look forward to hearing from you at your earliest convenience.

Yours sincerely,

Dr. Patrick Legembre

Reviewer #2: a. The recruitment of PLCg1 to Fas

1. The data about the co-immunoprecipitation in extract of CEM cells, which are presented in supplementary figure 5B and in reviewer-figure 1 are consistent and seem reliable.

Ok.

2. Figure 4A is not reliable. The density within the bands varies (e.g. that of 1 min). At face value this figure implies that the extent of binding of PLCg1 to the receptor decreases (e.g. at 10 minutes) much below the background control (B), which is an absurd. This figure must not be presented.

Figure 4A has been replaced by reviewer-figure 1 as suggested by the reviewer.

3. The proximity ligation assay (PLA): These data are exciting. However, two things need clarification. (a) Why is the kinetics of association indicated by this assay (prolonged association) so different from the kinetics revealed by co-immunoprecipitation (very transient association). (b) The PLA seems to imply occurrence of one or two foci of association of PLCg1 with Fas per cell. This is strange. Fas normally does not form such loci, not even after ligand binding. To confirm validity of the test the authors should present the patterns of immunostaining with anti-Fas (and if possible also with anti PLCg1). To allow telling where the cell membrane is, the authors should also present superposition of the PLA picture with light microscope image.

You are right. Usually, CD95 stimulation leads to the formation of CD95 aggregation and formation of CD95 "cap" at the membrane of T cells (Algeciras-Schimnich et al., 2002; Chaigne-Delalande et al., 2009). Our data confirmed that CD95 is at the membrane (contrast analyses, data not shown).
It is noteworthy that PLA is a different method from co-localization experiments performed with two fluorochrome-conjugated antibodies. Indeed, PLA requires a step of PCR reaction to reveal the protein co-localization and this process may account for the dot pattern observed in our experiments instead of a larger aggregation of CD95 (cap pattern) as observed upon CD95 stimulation.

b. The involvement of PSGL-1 upregulation and of sphingosine-1-phosphate (S1P) signaling pathway in the CD95L effect The main contribution of this study is the definition of the CID and of its function. Whether upregulation of PSGL-1 and the S1P pathway contribute to this function is of lesser importance and to my mind could have been ignored in this paper without greatly harming its significance. However, if the authors do choose to refer to these issues they must opt for the right terms in qualifying the solidity of their evidence.

We tempered our claim as suggested by reviewer (in red in our main text).

1. Involvement of PSGL-1 upregulation in the increased transmigration. The fact that E-selectin-neutralizing antibody blocked the transmigration teaches that E-

ER440 - Université Rennes 1 - Centre de Lutte Contre le Cancer Eugène Marquis
Rue de la Bataille Flandres Dunkerque - CS 44229-35042 RENNES
CEDEX Phone: (+33) 2 99 25 31 90 - Fax: (+33) 2 99 25 31 64

selectin/PSGL-1 interaction is required for the transmigration (as do may other cellular functions - that of the cytoskeleton for example). It does not teach that this interaction is the target of CD95L ligand. The facts that PSGL-1 is already expressed in the absence of CD95L and that CD95L induces rather limited increase of this expression in fact speak against this possibility. Stating that their findings "established that cl-CD95L promotes a selective Th17 cell transmigration by increasing PSGL-1/E-selectin interactions" is wrong.

Claim has been tempered as suggested by reviewer.

2. In support of the idea that the S1P pathway mediates the effect of CD95L on transmigration the authors show that (a) CD95L upregulates proteins that take part in the pathway. (b) CD95L enhances generation of S1P, (b) chemical inhibitors blocking the pathway abolish the increase in transmigration. What they don't provide is any information of the mechanism by which the S1P pathway might mediate this effect. Given the limitation of specificity of any chemical inhibitor and the possibility that activation of this pathway by CD95L serves other functions I would recommend that the authors will temper their statement about their conclusions from the data. The statement "We demonstrated that this process occurs via activation of the sphingosine-1-phosphate (S1P) signaling pathway" is not justified. In addition, if the authors choose not to present in this paper the evidence that S1P generation is upregulated by CD95L they must at least state in it that they have such evidence and that it will be presented elsewhere.

S1P experiments have been kept in the last version of this study. We have tempered our claim.

References

Algeciras-Schimnich, A., L. Shen, B.C. Barnhart, A.E. Murmann, J.K. Burkhardt, and M.E. Peter. 2002. Molecular ordering of the initial signaling events of CD95. *Mol Cell Biol* 22:207-220.

Chaigne-Delalande, B., W. Mahfouf, S. Daburon, J.F. Moreau, and P. Legembre. 2009. CD95 engagement mediates actin-independent and -dependent apoptotic signals. *Cell Death Differ* 16:1654-1664.

Brinkmann, V., M.D. Davis, C.E. Heise, R. Albert, S. Cottens, R. Hof, C. Bruns, E. Prieschl, T. Baumruker, P. Hiestand, C.A. Foster, M. Zollinger, and K.R. Lynch. 2002. The immune modulator FTY720 targets sphingosine 1-phosphate receptors. *J Biol Chem* 277:2145321457.

Murakami, A., H. Takasugi, S. Ohnuma, Y. Koide, A. Sakurai, S. Takeda, T. Hasegawa, J. Sasamori, T. Konno, K. Hayashi, Y. Watanabe, K. Mori, Y. Sato, A. Takahashi, N. Mochizuki, and N. Takakura. 2010. Sphingosine 1-phosphate (S1P) regulates vascular contraction via S1P3 receptor: investigation based on a new S1P3 receptor antagonist. *Mol Pharmacol* 77:704-713.

ER440 - Université Rennes 1 - Centre de Lutte Contre le Cancer Eugène Marquis
Rue de la Bataille Flandres Dunkerque - CS 44229-35042 RENNES
CEDEX Phone: (+33) 2 99 25 31 90 - Fax: (+33) 2 99 25 31 64

CD95 recruits PLCγ1 to trigger a calcium response promoting Th17 accumulation in inflamed organs of lupus mice

Amanda Poissonnier[1,2,3,§], Doriane Sanséau[1,2,3,§], Matthieu Le Gallo[1,2,3], Marine Malleter[1,2,3,5], Nicolas Levoin[4], Roselyne Viel[3,5], Lucie Morere[1,2,3], Aubin Penna[3,6], Patrick Blanco[7,8], Alain Dupuy[3,9], Florence Poizeau[1,2,9], Alain Fautrel[3,5], Julien Seneschal[7,10], Florence Jouan[1,2,3], Jerome Ritz[11], Edouard Forcade[7,8], Nathalie Rioux[3,6,10], Cécile Contin[7,8], Thomas Ducret[7,12], Anne-Marie Vacher[7,13], Paul A Barrow[14], Robin J Flynn[14,¶], Pierre Vacher[7,13,¶], and Patrick Legembre[1,2,3,5¶,*]

§ Shared first authorship; ¶ Shared senior authorship

[1]Centre Eugène Marquis, rue Bataille Flandres Dunkerque, 35042 Rennes, France

[2]INSERM ERL440-OSS, Equipe Labellisée Ligue Contre Le Cancer,

[3]Université de Rennes-1, 2 av. du Prof. Léon Bernard, 35043 Rennes, France

[4]Bioprojet Biotech, rue du Chesnay Beauregard, 35760 Saint-Grégoire, France

[5]Biosit, Plateforme H2P2, Biogenouest, 2 av. du Prof. Léon Bernard, 35043 Rennes, France

[6]INSERM U1085, 2 av. du Prof. Léon Bernard, 35043 Rennes Cedex, France

[7]Université de Bordeaux, CHU Bordeaux, 146 rue Léo Saignat, 33076 Bordeaux, France

[8]UMR CNRS 5164, 146 rue Léo Saignat, 33076 Bordeaux, France

[9]CHU Rennes, 2 rue Henri Le Guilloux, 35022, Rennes Cedex, France

[10]INSERM U1035, 146 rue Léo Saignat, 33076 Bordeaux, France

[11]Division of Hematologic Malignancies and Department of Medical Oncology, Dana-Farber Cancer Institute, Boston, MA, United States

[12]INSERM U1045, 146 rue Léo Saignat, 33076 Bordeaux, France

[13]INSERM U1218, Institut Bergonié, 33076 Bordeaux Cedex, France

[14]School of Veterinary Medicine and Science, University of Nottingham, Nottingham, United Kingdom

[*]**Corresponding author:**

Patrick Legembre, Centre Eugène Marquis, Rue Bataille Flandres Dunkerque, 35042 Rennes, France

Telephone: (+33)-223237241 ; E-mail: patrick.legembre@inserm.fr

Short title: CD95L drives Th17 accumulation in lupus patients

ABSTRACT

CD95 ligand (CD95L) is expressed by immune cells and triggers apoptotic death. Metalloprotease-cleaved CD95L (cl-CD95L) is released into the bloodstream but does not trigger apoptotic signaling. Hence, the pathophysiological role of cl-CD95L remains unclear. We observed that skin-derived endothelial cells from systemic lupus erythematosus (SLE) patients expressed CD95L, and that after cleavage, cl-CD95L promoted T helper 17 (Th17) lymphocyte transmigration across the endothelial barrier at the expense of T regulatory cells. T cell migration relied on a direct interaction between the CD95 domain called calcium-inducing domain (CID) and the Src homology 3 domain of phospholipase Cγ1. Th17 cells stimulated with cl-CD95L produced sphingosine-1-phosphate (S1P), which promoted endothelial transmigration by activating the S1P receptor 3. We generated a cell-penetrating CID peptide that prevented Th17 cell transmigration and alleviated clinical symptoms in lupus mice. Therefore, neutralizing the CD95 non-apoptotic signaling pathway may be attractive therapeutic approach for SLE treatment.

Key words: Calcium, CD95, inflammation, lupus, sphingosine-1 phosphate, Th17 cell

INTRODUCTION

CD95 ligand (CD95L, also known as FasL) is a transmembrane glycoprotein that acts locally through cell-to-cell contact (Suda et al., 1993). The extracellular domain of CD95L comprises a juxtamembrane stalk region (Orlinick et al., 1997) that is cleavable by metalloproteases (Fouque et al., 2014), and this cleavage releases CD95L into the bloodstream. CD95 (also known as Fas, APO-1, and TNFRSF6) belongs to the tumor necrosis factor receptor (TNF-R) family and is ubiquitously expressed in the body (Peter et al., 2015). When membrane-bound CD95L binds to CD95, the intracellular region of CD95 (designated the death domain - DD) orchestrates the formation of a death-inducing signaling complex (DISC) by recruitment of the adaptor molecule, Fas-associated protein with death domain (FADD), which in turn induces caspase-8 aggregation and subsequent apoptosis (Kischkel et al., 1995). Contrarily, we and others have shown that metalloprotease-cleaved CD95L (cl-CD95L) promotes formation of an atypical molecular complex designated motility-inducing signaling complex (MISC) that stimulates non-apoptotic signaling pathways and increases intracellular calcium (Ca^{2+}) content (Kleber et al., 2008; Malleter et al., 2013; Tauzin et al., 2011).

Systemic lupus erythematosus (SLE) is a chronic autoimmune disorder of largely unknown etiology whose pathogenesis can affect almost all organs and tissues. Human studies and murine models indicate a role for IL-17-producing T helper 17 (Th17) cells in SLE progression (see (Shin et al., 2011) for a review). Lupus-prone mice are partially protected from immunopathology by a reduction in renal Th17 cell accumulation (Steinmetz et al., 2009). Therefore, abnormal Th17 cell trafficking to inflamed organs may promote SLE pathogenesis, and modulation of Th17 cell migration is an attractive therapeutic option for reducing disease-related inflammation. However, the precise mechanism of Th17 cell accumulation in damaged SLE organs remains unclear.

A close relationship exists between SLE pathogenesis and deregulation of CD95 signaling already. Patients suffering from autoimmune lymphoproliferative syndrome (ALPS) type Ia harbor mutations in CD95 responsible for lymphoproliferation and SLE-like autoimmunity (Drappa et al., 1996; Fisher et al., 1995; Rieux-Laucat et al., 1995). These ALPS type Ia patients show heterozygous mutations (Straus et al., 2001) leading to the inhibition of the CD95-mediated apoptotic signal without affecting activation of non-apoptotic signaling pathways (Legembre et al., 2004). Accordingly, we hypothesize that aggravation of lupus symptoms is not only caused by a defective apoptotic process (Kuhtreiber et al., 2003) but also by induction of CD95-mediated non-apoptotic signaling pathways.

Herein, we demonstrated that high concentrations of cl-CD95L in SLE patients promoted Th17 cell migration across the endothelial barrier at the expense of regulatory T (Treg) cells in a Ca^{2+}-dependent manner. This CD95-mediated Ca^{2+} signaling occurred independently of the CD95-DD and exploiting this result, we designed a therapeutic molecule that selectively neutralized the CD95-mediated non-apoptotic signaling pathways. Moreover in a murine model of SLE, this treatment halted the pro-inflammatory actions of cl-CD95L, alleviating both immune and pathological hallmarks of SLE.

RESULTS

CD95L in SLE serum promotes endothelial transmigration of activated Th17 cells

Soluble CD95L concentrations in serum obtained from SLE patients were higher than those from age-matched healthy donors (Fig. 1A). SLE serum was fractionated by size-exclusion chromatography (Fig. 1B). By ELISA, CD95L was mainly detected in fractions 76–78; the proteins in these fractions showed molecular masses ranging from 75 to 80 kDa under native conditions. Next, CD95L was immunoprecipitated from these fractions, revealing under denaturing conditions, a polypeptide band of 26 kDa (Fig. 1B). These results do not rule out the possibility that soluble CD95L is associated with another partner but strongly suggest that serum CD95L in SLE patients corresponds to a homotrimeric ligand.

We next hypothesized that if serum CD95L contributes to inflammatory processes in SLE patients by promoting extravasation of Th17 cells in inflamed tissues, then CD95L-expressing cells should be detected in these tissues and surrounded by IL-17-expressing cells. Therefore, we performed an immunohistochemical analysis of skin biopsies obtained from SLE patients to examine the distribution of CD95L- and IL-17-expressing cells. Skin biopsies from SLE patients, but not from healthy controls, showed positive staining for CD95L and IL-17 (Figs. 1C and S1). CD95L expression was mainly restricted to blood vessel endothelial cells, and these cells were surrounded by infiltrating immune cells (Figs. 1C and S1). Serial slices of skin biopsies from SLE patient revealed that IL17 was co-expressed by $CD4^+$ T cells (Fig.1D), indicating that CD95L-expressing blood vessels were surrounded by infiltrating Th17 cells. Moreover, a densitometric analysis of stained tissues from lupus patients (n = 10) revealed a correlation between CD95L concentrations and the number of tissue-infiltrating, IL-17-expressing immune cells (Fig. 1E). This suggested that CD95L may behave as a chemoattractant for Th17 cells.

To examine whether after cleavage by metalloproteases, soluble CD95L had a

chemoattractive effect on all T cells or was selective for distinct Th cell subsets, we next evaluated transmigration of undifferentiated (Th0) and differentiated (Th1 and Th17) $CD4^+$ T-cells with or without serum from SLE patients. Compared with healthy serum, SLE serum triggered a moderate increase in Th1 cell transmigration and a marked increase in Th17 cell transmigration (Fig. 1F). Pre-incubation of SLE serum with a decoy CD95 receptor (CD95-Fc) dose-dependently inhibited Th17 cell migration, indicating that transmigration of these cells relied on CD95 signaling (Fig. 1G).

We produced a homotrimeric, metalloprotease-cleaved version of human CD95L (cl-CD95L)(Tauzin et al., 2011). Similarly to CD95L in SLE serum, cl-CD95L more efficiently promoted the transmigration of Th1 and Th17 lymphocytes relative to undifferentiated Th0 and differentiated Th2 cells (Fig. 1H). Because an imbalance between the Th17/Treg cell ratio in inflamed organs has been previously reported in the pathogenesis of SLE and other autoimmune disorders (Yang et al., 2009), we also examined the effect of cl-CD95L on Treg cell transmigration. Cl-CD95L increased the endothelial transmigration of in vitro-differentiated Th17 cells, but not that of Treg cells (Fig. 1I). These results support that high concentrations of serum CD95L in SLE patients can cause pro-inflammatory Th17 cell accumulation and destabilize Th17/Treg cell balance in diseased organs.

To determine the mechanism responsible for this preferential transmigration of Th17 cells, we examined the expression of adhesion molecules known to promote endothelial transmigration. Cl-CD95L had no effect on the expression concentrations of adhesion molecules expressed by human umbilical vein endothelial cells (HUVECs) (Fig. S1B). On the other hand, while stimulation of Th17 cells with cl-CD95L had no effect on the amount of lymphocyte function-associated antigen-1 (LFA-1, the ICAM-1 binding partner), it led to upregulation of P-selectin glycoprotein-1 (PSGL-1, an E-/P-selectin ligand) (Fig. S1C). The concentration of PSGL-1 was also up-regulated in Th1 cells but to a lesser extent as compared to Th17 cells, and tended

to be downregulated in Treg cells (Fig. S1C). As HUVECs used in our transmigration assay expressed E-selectin but not P-selectin (Fig. S1B), we next examined whether blocking these E-selectin-PSGL-1 interactions could abrogate the CD95-mediated Th17 transmigration. An E-selectin-neutralizing monoclonal antibody (mAb) inhibited Th17 cell transmigration while it did not affect the weak endothelial transmigration observed in Treg cells exposed to cl-CD95L (Fig. S1D). This antibody was more effective in preventing the CD95-mediated endothelial transmigration of Th17 cells when compared to Th1 cells (Fig. S1D). To understand why Th1 cells responded less efficiently to cl-CD95L than Th17 cells, we compared the quantity of CD95 in different Th subsets from 20 blood donors. While the amount of CD95 was not lower in Treg cells compared to Th17 cells (Fig.S1E), Th1 cells exhibited a reduced concentration of CD95 as compared to Th17 cells (Fig.S1E). This finding may then explain why Th1 cells migrated with a lower intensity in the presence of cl-CD95L when compared to Th17 cells.

To address how cl-CD95L selectively promoted the endothelial transmigration of Th17 cells to the detriment of Treg cells, we investigated how cl-CD95L stimulation affected the gene expression profile of Th17 and Treg cells. Human Th17 cells ($CD4^+CXCR3^-CCR6^+CD45RA^-$) and Treg cells ($CD4^+CD127^{low}CD25^+$) were sorted from the blood of two different donors (Fig. S1F) and stimulated in the presence or absence of cl-CD95L. Transcriptomic signatures of Treg and Th17 cells stimulated with cl-CD95L were analyzed (Fig. 2A-B and Tables S1 and S2). Gene ontology analysis revealed that the sphingosine 1 phosphate (S1P) signaling pathway was modulated in Th17 cells stimulated with cl-CD95L (Fig. 2C) while Treg cells exposed to cl-CD95L showed over-expression of genes responsible for the implementation of cell death (Fig. 2C). The S1P signaling pathway (Fig. S1G) can promote endothelial transmigration of activated T and B lymphocytes leading to extra- or intravasation. Using Th17 and Treg cells sorted as aforementioned, we confirmed that cl-CD95L promoted

endothelial transmigration of Th17 cells but not Tregs (Fig.2D). Pre-incubation of Th17 cells with FTY720, a chemical that induces internalization of four S1P receptors (S1P-1, -3, -4 and -5) (Brinkmann et al., 2002) indicated that cl-CD95L selectively promoted endothelial transmigration of Th17 cells by stimulating the S1P signaling pathway (Fig. 2D). To evaluate the role of S1PR3 in the CD95-mediated Th17 transmigration, we next tested the effect of additional antagonist molecules, namely TY-52156 (Murakami et al., 2010), CAY-1044, VPC-23019, and W-146 (Li et al., 2015) (Fig. 2D) on Th17 cell migration. While the selective S1PR3 inhibitors, TY-52156 and CAY-1044, and the S1PR1 and S1PR3 inhibitor VPC-23019 efficiently inhibited the passage of Th17 cells across endothelial cells (Fig. 2D), the S1PR1 antagonist W146 did not prevent CD95-mediated Th17 transmigration (Fig. 2D). Overall, these findings established that cl-CD95L promotes a selective Th17 cell transmigration that partially relies on the increased PSGL-1-E-selectin interactions, the production of S1P and the implemention of the S1PR3-driven signaling pathway.

Cl-CD95L recruits Th17 cells in vivo

To demonstrate *in vivo* that cl-CD95L is a chemoattractant for Th17 cells, C57BL/6 mice were injected intraperitoneally with cl-CD95L, and infiltrating cells in the peritoneal cavity, the spleen and mesenteric lymph nodes (MLN) were examined 12, 24 and 48h later. The number of activated $CD4^+$ T-cells recruited to these organs was evaluated in cl-CD95L-injected mice by using loss of CD62L as an indication of T-cell activation. While the total number of Th1 and Treg cells did not change in the peritoneal cavity, spleen and MLNs of mice injected with cl-CD95L as compared to control medium-administrated mice (Fig. 3A), there was an accumulation of Th17 cells in the peritoneal cavity of cl-CD95L-injected mice and to a lesser extent in peripheral secondary lymphatic organs such as spleen and MLN (Fig. 3A,B). Real-time quantitative polymerase chain reaction (qPCR) analysis of key Th17 lineage

markers (IL-17, IL-23R, and C-C chemokine receptor type 6 (CCR6)) of activated $CD4^+$ T-cells confirmed that cl-CD95L recruited Th17 cells to these tissues (Fig. S2A-C). No increase was observed in the number of cells expressing IFN-γ (indicative of Th1 cells) or FoxP3 (indicative of Treg cells) (Fig. S2D & E), confirming that injection of cl-CD95L in the peritoneal cavity of immune-competent mice creates a gradient of cl-CD95L promoting the endothelial transmigration of Th17 cells.

CD95 triggers a DD-independent Ca^{2+} response

We previously showed that engagement of CD95 evoked a Ca^{2+} response in activated T lymphocytes, resulting in transient inhibition of cellular apoptosis (Khadra et al., 2011) and cell migration (Malleter et al., 2013; Tauzin et al., 2011). Due to the instrumental role of the CD95-mediated apoptotic signal in anti-infectious and anti-tumor responses, we assumed that the inhibition of the CD95 non-apoptotic responses while conserving the apoptotic signal could be an attractive therapeutic option to prevent Th17 recruitment in inflamed organs without altering immune surveillance. We then wondered whether it was possible to selectively inhibit the CD95-mediated Ca^{2+} response and whether this blockade could inhibit cell migration without blocking the apoptotic signal. Human T-cells exposed to cl-CD95L rapidly formed a transient molecular complex containing phospholipase Cγ1 (PLCγ1) (Fig. 4A). Using proximity ligation assay (PLA), we confirmed that this interaction was selective of CD95 and occurred in a transient and rapid manner (Fig. S3A). CD95-PLCγ1 interaction was not detected in CEM-IRC cells, which express a faint amount of endogenous CD95 (Beneteau et al., 2008) and the peak of interaction in parent CEM T cells was reached 5 minutes after addition of cl-CD95L (Fig. S3A). Moreover, the lack of PLCγ1 in T-cells resulted in a loss of CD95-mediated Ca^{2+} response (Fig. S3B). PLA experiments also revealed that CD95 rapidly recruited PLCγ1 in Th17 cells exposed to cl-CD95L (Fig.4B). We next

investigated whether the predominant DISC components, FADD and caspase-8, might contribute to CD95-mediated Ca^{2+} signaling. FADD and caspase-8-deficient Jurkat T cells (Juo et al., 1998; Juo et al., 1999) exposed to the cytotoxic CD95L showed no apoptotic signaling (Fig. S3C), but the CD95-mediated Ca^{2+} signaling pathway remained unaffected in these cells (Fig. S3D) suggesting that PLCγ1 activation occurs independently of CD95-DISC and cell death signaling. To further investigate whether the death domain (DD) of CD95 was involved in the Ca^{2+} response, we generated CD95 constructs devoid of the entire intracellular domain of CD95 ($CD95^{1–175}$), the DD ($CD95^{1–210}$), or the last 15 aa involved in FAP-1 protein tyrosine phosphatase recruitment ($CD95^{1–303}$) (Sato et al., 1995) (Fig. 4C). These constructs were expressed in the CEM-IRC T-cell line, which was selected for its low CD95 expression (Fig. S3E).

A CD95-deficient CEM cell designated CEM-IRC (described in (Beneteau et al., 2007)) cells showed minimal cell death in response to a multimeric (dodecamer) and cytotoxic CD95L (IgCD95L, Fig. S3F); however, expression of $CD95^{1–303}$ or wild-type CD95 restored cell death levels to those observed for parental CEM cells (Fig. S3F). Contrarily, introduction of $CD95^{1–175}$ or $CD95^{1–210}$ failed to induce apoptosis and, as previously observed, these constructs behaved as dominant-negative receptors (Fig. S3F)(Siegel et al., 2000). Furthermore, reconstituting CEM-IRC cells with wild type CD95 or $CD95^{1–303}$ restored CD95-mediated Ca^{2+} signaling (Fig. 4D).

Whereas the loss of the DD from the $CD95^{1–210}$ construct prevented apoptotic signaling, CD95-DD deletion did not affect induction of Ca^{2+} signaling (Fig. 4D). Given that a CD95 construct devoid of the entire intracellular region ($CD95^{1–175}$) failed to evoke a Ca^{2+} response, we concluded that Ca^{2+} signaling was triggered by CD95 aa 175–210.

We next examined whether $CD95^{1–210}$ was capable of recruiting PLCγ1. To this end, we transiently co-transfected HEK cells with green fluorescent protein (GFP)-fused CD95

constructs and wild-type PLCγ1. Although the transfected cells expressed similar quantity of CD95-GFP chimeric constructs at the cell surface (Fig. S3G), PLCγ1 was absent only from the $CD95^{1–175}$ immunoprecipitate (Fig. 4E). To demonstrate that amino acid residues 175-210 of CD95 contributes to PLCγ1 recruitment, we generated a construct comprising $CD95_{175–210}$ (termed the calcium-inducing domain (CID)) fused to the fluorescent protein mCherry. Unlike mCherry alone, $CD95^{175–210}$-mCherry interacted with PLCγ1 and inhibited its recruitment to CD95 (Fig. S3H), suggesting that interference with this juxtamembrane domain may prevent CD95-mediated Ca^{2+} signaling.

To confirm this hypothesis, we synthesized a cell-penetrating peptide, TAT-CID, by linking CID to the nine-aa human immunodeficiency virus (HIV)-TAT sequence (Fig. S4A), which serves as a carrier for protein translocation across the plasma membrane (Vives et al., 1997). Pre-incubation of activated peripheral blood lymphocytes (PBLs) with TAT-CID impaired the recruitment of PLCγ1 (Fig. 4F) and abolished the induction of CD95-mediated Ca^{2+} signaling (Fig. 4G). Similarly, pre-incubation of CEM cells with TAT-CID inhibited PLCγ1 binding to CD95 (Fig. S4B) and abrogated the CD95-induced Ca^{2+} response in Jurkat and CEM T-cell lines (Fig. S4C). TAT-CID also reduced Akt phosphorylation at serine 473 (a hallmark of PI3K signaling activation) in cl-CD95L-exposed PBLs (Fig. S4D) confirming a role of calcium in the modulation of the PI3K signaling pathway (Malleter et al., 2013). Nevertheless, although TAT-CID impeded CD95-mediated Ca^{2+} and PI3K signaling, the peptide did not affect the apoptotic signaling pathway (Fig. S4E). Hence, we mapped a domain in CD95 receptor, namely CID, which recruits PLCγ1 and elicits Ca^{2+} responses.

CID interacts with the SH3 domain of FLCγ1

To address whether CD95 directly interacts with PLCγ1, we performed a Renilla luciferase-based protein fragment complementation assay (RLuc-PCA) (Stefan et al., 2007). The Renilla

luciferase enzyme was divided into two fragments. Each fragment (F1 and F2) was fused to various CD95 and PLCγ1 domains and co-transfected in HEK cells (Figs. S5A-D). Only PLCγ1-SH3 interacted with the whole CD95 intracellular region and CD95-CID, but failed to reconstitute enzyme activity when combined with CD95-DD (Fig. 5A,B). To strengthen this result, we evaluated whether the cell-penetrating TAT-CID peptide could inhibit the interaction of PLCγ1-SH3 with CD95-CID. While TAT-control peptide did not alter luciferase activity in cells co-expressing PLCγ1-SH3-F1 and CD95-CID-F2, TAT-CID efficiently blocked this activity in a dose-dependent manner (Fig. 5C), supporting the hypothesis that CD95 directly associates with PLCγ1 through the CD95-CID domain. Intriguingly, SH3 domains primary bind to peptides containing a consensus PxxP sequence that is not present in CID; however, many examples of unconventional SH3-binding peptides have previously been described (Saksela and Permi, 2012).

To understand how CD95 CID might interact with PLCγ1-SH3, we undertook two computational peptide screenings. First, we performed homology modeling by using the crystal structure of PLCγ1-SH3 in association with the SLP-76 heptapeptide complex (PDB:1YWO) (Deng et al., 2005). This structure served as a template, and the SLP-76 peptide was replaced by each heptapeptide combination present in CD95-CID. Second, a protein-peptide docking approach was carried out by using each aforementioned CID heptapeptide alternatively docked within the PLCγ1-SH3 domain. Both methods predicted that aa 182–188 (TCRKHRK) would have the highest affinity for PLCγ1-SH3, and the calculated binding energy of the complex consisting of PLCγ1-SH3 and TCRKHRK was similar to that of the PLCγ1-SH3 interaction with SLP-76 (Fig. 5D and Table S3). To prove that the TCRKHRK amino acid sequence corresponded to the minimal domain interacting with PLCγ1, we first used RLuc-PCA and performed an alanine-scanning experiment. This confirmed that amino acid residues R184, K185, K188 were instrumental in the interaction of

CD95 with PLCγ1 (Fig. S5E). In agreement with this cell-based assay, our computer model identified an interaction between R184 guanidine and SH3-PLCγ1 through a hydrogen bond network involving amino acids Y845 and Q805 side-chains and K803 backbone. K185 amine function forms hydrogen bonds, in an intramolecular manner, with H186 backbone and with G826 backbone of SH3-PLCγ1. A salt bridge occurred between K188 and E825. Furthermore, the positioning of K188 in the SH3 cavity required the displacement of a water molecule (H_2O105 observed in the crystal structure), an entropically favourable process. For this solvent exposed interface, the methylene chain of these basic residues form extensive van der Waals contacts with the SH3 hydrophobic shallow pockets. Overall, these observations indicated that even if the CID sequence is not related to a typical class II ligand of SH3, it complies with its properties in terms of van der Waals interactions (Deng et al., 2005). Of note, RLuc-PCA also revealed that glutamic acid 189, localized outside the minimal TAT-CID domain, participated in the binding of CD95 with PLCγ1 (Fig. S5E). This amino acid may play a role of "compass residue" evoked for typical proline-rich SH3 ligands (Musacchio, 2002). Indeed, the canonical PxxP motif-containing peptides could be docked in two opposite orientations regarding the relative positioning of a positively charged residue (+xxPxxP or xPxxPx+) interacting with a negatively charged cleft on the SH3 surface (Saksela and Permi, 2012). Similarly to this basic amino acid in the PXXP motif, E189 could contribute to the positioning of the minimal CD95-CID peptide in the PLCγ1 SH3 domain. Secondly, we generated two constructs, a CD95 in which R184 and K185 were replaced by alanine (double mutant or DM) and a CD95 in which R184, K185 and K188 (triple mutant or TM) were replaced by alanine. These two constructs and a wild type CD95 were transfected into HEK cells and the CD95-mediated Ca^{2+} response was evaluated in these cells. HEK cells express endogenous wild type CD95 and thereby expression of our constructs was expected to create heterotrimeric complexes consisting of wild type and mutated CD95, which could

inhibit PLCγ1 recruitment in a dominant negative fashion. Both double and triple mutants abrogated the CD95-mediated Ca^{2+} signaling pathway (Fig. S5F). For each amino acid, we also generated single mutation. Strikingly, these mutants when expressed in HEK cells, did not alter the CD95-mediated calcium signaling pathway (data not shown) suggesting that unlike double and triple mutants, PLCγ1 recruitment could accommodate to a single mutation inside the minimal CID. As CID corresponds to a disorganized domain, we surmised that to increase PLCγ1 binding affinity, a larger zone of contact is mandatory and that elimination of only one amino acid may not be sufficient to impair this recruitment in a heterotrimeric complex containing wild type CD95. Overall, these findings indicated that the CD95-CID amino-terminal region corresponded to an unconventional SH3-binding peptide.

To confirm our *in silico* result, we synthesized two cell-penetrating peptides consisting of the amino- and carboxyl-terminal regions of CD95 CID (CID-N, corresponding to aa 175–192, and CID-C, corresponding to aa 193–210) (Fig. S5G). We then evaluated their effects on the CD95-mediated Ca^{2+} response (Fig. 5E), and showed that only CID-N abrogated CD95-mediated Ca^{2+} signaling in Jurkat cells and activated PBLs (Fig. 5E). Taken together, these findings demonstrated that the juxtamembrane region of CD95 directly interacts with PLCγ1-SH3 to evoke Ca^{2+} signaling.

Lastly, we examined whether the inhibitory actions of TAT-CID were selective for CD95-mediated Ca^{2+} signaling. Although T-cell receptor (TCR) stimulation led to a PLCγ1-dependent Ca^{2+} response in Jurkat cells (Fig. S5H), pre-treatment with the TAT-CID peptide had no such effect (Fig. S5I). Similarly, TAT-CID did not influence the PLCβ-driven Ca^{2+} response stimulated by carbachol, a cholinergic agonist that activates G-protein-coupled receptors to release calcium (Fig. S5J). Therefore, TAT-CID selectively inhibits CD95-mediated Ca^{2+} signaling.

Inhibition of CD95-mediated Ca^{2+} signaling prevents Th17 cell transmigration in vivo

To assess the potential of TAT-CID as a therapeutic agent for SLE patients, we first examined its effect on Th17 cell transmigration. Figure 6A shows that TAT-human CID (TAT-hCID) dose-dependently inhibited CD95-mediated endothelial transmigration of human Th17 cells. Alignment of the human and mouse CD95 protein sequences highlighted differences in the CID region (21.2% sequence identity) (Fig. S6A). We reconstituted human CEM-IRC cells with mouse CD95 (Fig. S6B). CD95-mediated apoptotic signaling was restored in the mouse CD95-expressing cells, but not in the parental CEM-IRC cells (Fig. S6B). TAT-mouse CID (TAT-mCID), but not TAT-hCID, inhibited the mouse CD95-mediated Ca^{2+} response (Fig. S6C,D). Similarly, TAT-mCID also inhibited the CD95-mediated Ca^{2+} response in mouse T lymphocytes (Fig. S6E), indicating that despite differences in the human and mouse CD95-CID sequences, both domains trigger Ca^{2+} signaling.

We next injected C57Bl/6 mice with TAT-control or TAT-mCID prior to the intraperitoneal injection of cl-CD95L, and then determined the number of T-cells infiltrating the peritoneal cavity 24 h later. TAT-mCID treatment reduced the CD95-mediated accumulation of peritoneal exudate cells (PECs) (Fig. 6B) and $CD4^+$ lymphocytes (Fig. 6C). In agreement with the data shown in Figure 3, cl-CD95L injection increased IL-17 levels in the peritoneal cavity, but the increase was overturned by TAT-mCID pre-treatment (Fig. 6D). These findings indicated that TAT-CID inhibits cl-CD95L-mediated recruitment of IL-17-secreting $CD4^+$ T-cells *in vivo*.

TAT-CID alleviates clinical outcomes in lupus-prone MRL/lpr mice

Patients suffering from ALPS type Ia exhibit CD95 mutations that cause SLE-like autoimmunity (Drappa et al., 1996; Fisher et al., 1995; Rieux-Laucat et al., 1995). Heterozygous $Lpr^{+/-}$ mice express reduced levels of CD95 due to insertion of a

retrotransposon into intron 2 of the CD95 gene and develop lupus (Adachi et al., 1993). T cells from both ALPS type Ia patients and MRL/lpr$^{+/-}$ mice show loss of sensitivity to CD95-mediated apoptosis, but retain normal activation of non-apoptotic signaling pathways (Legembre et al., 2004). We asked whether the implementation of CD95-mediated non-apoptotic signaling pathways in lupus mice contributed to symptom severity. Because TAT-CID inhibited CD95-mediated Ca^{2+} response without affecting apoptotic signaling (Fig. S4C–E), this peptide allowed us to address this question.

TAT-mCID and TAT-control peptides were administered to lpr$^{+/-}$ heterozygote mice. After completion of the trial, animals were sacrificed, revealing an alleviation of splenomegaly in TAT-CID-treated mice relative to controls (Fig. 6E), without any negative effect on whole-body weight (Fig. S6F). Likewise, TAT-CID significantly reduced the weights of the inflamed kidneys and the mesenteric lymph nodes (Fig. S6G). Examination of the cellular composition of the spleen in lpr$^{+/-}$ mice revealed a significant decrease in total spleen cell number (Fig. 6F) and activated CD4$^+$ T-cells (Fig. 6G), but not B-cells (Fig. S6H). Additionally, TAT-CID significantly decreased Th17 cell infiltration in the spleen of TAT-CID- vs. TAT-control-treated mice, as indicated by reduced expression levels of *Ccr6* and *Il23r*, and to a lesser extent *Rorc*, three key molecular markers of Th17 cells (Fig. 6H). Re-stimulation of spleen-infiltrating CD4$^+$ T-cells confirmed that the immune cells failed to produce IL-17A in TAT-CID-treated mice (Fig. 6I).

Examination of the kidneys in lpr$^{+/-}$ mice demonstrated that TAT-CID vs. TAT-control decreased cell infiltration (Fig. 7A–C). The reduction in cellular infiltration in TAT-CID-treated lpr$^{+/-}$ mice was translated into a reduction of glomerulus damage (Fig. 7D–F). The number of cells infiltrating the glomeruli was significantly lower in TAT-CID-treated mice as compared to TAT-control mice, resulting in significant swelling and loss of shape of the glomeruli in these latter mice (Fig.7D *vs* 7E). Moreover, improvement of the kidney

architecture in TAT-CID-treated mice (Fig. 7F) was associated with a decreased deposition of C3 activation fragments as compared to TAT-control mice (Fig.7G). Accordingly, organ function was restored in mice treated with repeated injections of TAT-CID as compared to TAT-control-treated mice with reduction of blood concentrations of creatinine and urea (Fig. 7H). In parallel, serum concentrations of anti-dsDNA IgG1 were lower in TAT-CID mice than in TAT-control treated MRL/Lpr$^{+/-}$ mice (Fig.7I). When kidneys of TAT-CID and TAT-control treated Lpr+/- mice were analyzed, we found a lower number of CD4^{+}IL17^{+} cells in the TAT-CID group as compared to TAT-control treated mice (Fig.7J). While CD4^{+}IFN-γ^{+} cell number tended to be lower in TAT-CID treated mice than in control mice, this effect was non-significant (Fig.7J). Treatment efficiency supported our prediction that CD95-induced non-apoptotic signaling pathways contribute to lupus severity and progression.

DISCUSSION

An initial study showing that activated T cells transmigrated in the presence of cl-CD95L through the implementation of PI3K and Ca^{2+} signaling pathways (Tauzin et al., 2011), raised the question of whether all T-cells responded similarly to cl-CD95L and whether it was possible to selectively inhibit the CD95-mediated pro-inflammatory signaling pathway without affecting the apoptotic cues. While the death domain of CD95 is instrumental in the induction of the PI3K signaling pathway (Tauzin et al., 2011), we here provided evidence that the Ca^{2+} response stemmed from a different region within CD95 that we identified and designated calcium inducing domain (CID).

$CD95L^{+}$ blood vessels in skin of SLE patients were surrounded by infiltrating immune cells, suggesting that these structures could serve as "gateways" for inflammatory leukocytes and the ensuing recruitment of Th17 cells. By contrast, a recent study showed that CD95L expressed on endothelial cells functions to eliminate $CD8^{+}$ T-cells and in doing so, prevents effective anti-tumor immunity (Motz et al., 2014). Examination of the $CD8^{+}$ T cell infiltrate surrounding $CD95L^{+}$ blood vessels in SLE patients revealed no inverse correlation between CD95L expression and the number of infiltrating $CD8^{+}$ T-cells (Fig. S7A,B). Given that CD95L exerts its chemoattractant activity only after cleavage by metalloproteases (Tauzin et al., 2011), the observed discrepancy between the amount of immune infiltrate surrounding $CD95^{+}$ blood vessels in cancer subjects and SLE patients may be explained by the absence or presence of an as yet unidentified CD95L-processing metalloprotease.

The aggravation of SLE by cl-CD95L thus appears to involve a two-step mechanism. First, selective recruitment of Th17 and Th1-cell, conserved in both mouse and humans, occurs at the expense of Treg cell recruitment and may advance inflammation in damaged SLE organs. Second, Th17 cells exposed to cl-CD95L upregulate their expression of the PSGL-1 adhesion

molecule. PSGL-1 not only promotes tethering of lymphocytes to endothelial cells and subsequent rolling, but also its high expression levels in T-cells provoke the secretion of effector cytokines (Baaten et al., 2013).

Of interest, the cellular balance between ceramide (apoptotic) and S1P (survival) is crucial for cell fate (Cuvillier et al., 1996) and although the interplay between CD95 and ceramide synthesis is well-known and contributes to the induction of the cell death program (Cifone et al., 1994), our findings provide evidence that a molecular link also exists between CD95 stimulation and activation of the S1P signaling pathway. Furthermore, activation of the S1P signaling pathway by cl-CD95L furnishes a molecular mechanism that can explain how T-cells and more specifically Th17 cells migrate in presence of this naturally-processed ligand. Based on our study and recent data from Yosef and colleagues that showed using transcriptional profiling, a role for CD95 in Th17 differentiation (Yosef et al., 2013), we conclude that CD95L/CD95 signals play a pivotal role in autoimmunity and not only through its canonical apoptotic role.

We employed complementary approaches to reveal that CD95-CID directly interacts with the PLCγ1-SH3 domain to implement a Ca^{2+} signal. Linker for activation of T-cells (LAT) is a critical adaptor molecule required for TCR-mediated Ca^{2+} responses. Upon TCR engagement, LAT recruits PLCγ1 via its SH2 domains (Zhang et al., 2000). CD95 and TCR therefore recruit PLCγ1 through different domains, and TAT-CID failed to inhibit TCR-mediated Ca^{2+} signaling in the current study. Moreover, blockade of CD95-mediated Ca^{2+} signaling by TAT-CID not only prevented selective recruitment of Th17 cells to the peritoneal cavity of cl-CD95-injected mice, but also lessened clinical symptoms in heterozygous lpr mice. These observations implicate TAT-CID as an attractive therapeutic molecule with high selectivity toward the CD95-mediated Ca^{2+} signaling pathway.

Cl-CD95L induces the transient (within minutes) recruitment of PLCγ1. The CD95 domain encompassing aa 175–210 has never been crystallized, probably because this region corresponds to an intrinsically disordered region (IDR) that lacks a unique three-dimensional structure. We conducted several molecular dynamics experiments to confirm that this peptide has very low propensity, if any, for folding (Fig. S7C-D). Numerous examples are now documented of transient protein/protein interactions involving IDRs, indicating the importance of IDRs in allowing proteins to briefly associate with a large number of partners so as to dynamically modulate cell signaling (Cumberworth et al., 2013). This molecular feature is consistent with the CD95-CID-mediated induction of a rapid and transient Ca^{2+} response to promote cell migration via the MISC formation.

A recent phase I/II clinical trial demonstrated that a decoy CD95 receptor, APG101, could impede CD95/CD95L interaction and benefited patients suffering from glioblastoma (Tuettenberg et al., 2012). Although APG101 may be of short-term therapeutic benefit to lupus patients, its inability to discriminate between the anti-tumor/infectious (i.e., apoptotic signaling) and pro-inflammatory actions of CD95 may lead to unexpected adverse events.

As we have found that inhibiting the CD95-mediated Ca^{2+} response does not interfere with apoptotic signaling, we propose that selective blockade of CD95-mediated Ca^{2+} signaling might open new therapeutic avenues for SLE treatment in the future. Moreover, given the selective effect of cl-CD95L on Th17 cell recruitment, we also propose that downregulating Ca^{2+} signaling may lessen the inflammatory activity of Th17 cells in other chronic inflammatory disorders.

MATERIALS & METHODS

Antibodies and other reagents

See supporting materials and methods.

Plasmids and Constructs

All constructs and primer pairs used are described in supporting materials and methods.

T Cell subset isolation

Peripheral blood mononuclear cells (PBMC) were isolated from buffy-coat by density gradient using lymphocyte separation medium (Eurobio, Les Ulis, France). PBMCs were then subjected to selection using a cocktail of antibody-coated magnetic beads: $CCR6^{+}CXCR3^{-}CD4^{+}$ cells (Th17 cells) were sorted with Human Th17 Enrichment kit (STEMCELL Technologies, Grenoble, France) and $CD4^{+}CD25^{+}CD127^{-}$ Treg cells were isolated with MACS column (Miltenyi Biotec, Paris, France).

Transcriptomic analysis

Isolated Th17 and Treg cells from two healthy donors were treated with or without 100ng/ml of cl-CD95L for 8h. Total RNA was extracted using the Nucleospin RNA XS kit (Macherey-Nagel, Hoerdt, France), quality was assessed using the RNA6000 nano chip (Agilent, Les Ulis, France). For each condition, 9 ng of RNA was reverse transcribed using the Ovation PicoSL WTA System V2 (Nugen, Leek, The Netherlands). Fragmented cDNAs were hybridized to GeneChip Human Gene 2.0 ST microarrays (Affymetrix, High Wycombe, UK). Then chips were scanned on a GeneChip Scanner 3000 7G (Affymetrix). Raw data and

quality controls metrics were generated from scanned images using the Expression Console software (Affymetrix).

Probes were mapped using Brainarray V20 CDF files (http://brainarray.mbni.med.umich.edu/) and RMA normalized using R software. Raw and normalized data are deposited to the GEO database (accession id GSE78909). Statistical analyses were performed with Partek Genomics Suite (Partek Inc., St. Louis, MO, USA), a p-value ≤0,05 was considered significant. Pathway enrichment analyses were generated with Ingenuity Pathway Analysis (QIAGEN, Redwood City, CA, USA).

MRL/lpr mouse treatment

MRL/lpr were obtained from the Jackson Laboratory and backcrossed onto a MRL background. Females mice (n=8/group) were intraperitoneally administrated with either TAT-CID or TAT-Ctrl peptides (40mg/kg) starting at 8 weeks of age, twice weekly for 5 weeks. After re-stimulation of $CD4^+$ cell populations with anti-CD3, cell culture supernatants were dosed for IL-17A and IFN-γ by ELISA, qPCR analysis of purified cell population was also performed as above mentioned. Kidneys were fixed into 4% PFA o/n prior to moving to ethanol, sectioning and staining. Scoring was conducted by an individual blind to the objective/treatments within the study as per (Kikawada et al., 2003). FITC-conjugated rabbit anti-C3 polyclonal antibody (Dako) and nuclei (DAPI, sigma-aldrich) staining were performed on frozen kidney sections and analyzed using NIKON Ni-E (magnification ×200). C3 accumulation in kidneys was assessed by densitometric analysis of ten different fields using NIS-Elements AR Analysis software.

Transendothelial migration of activated T lymphocytes

Membranes (3 pm pore size) of a Boyden chamber were hydrated in sterile D-PBS (Millipore, Molsheim, France). Activated T-lymphocytes (10^6) were added to the top chamber on a confluent monolayer of HUVEC in a low serum (1%)-containing medium. The bottom chamber was filled with low serum (1%)-containing medium in presence or absence of 100 ng/ml of cl-CD95L. In experiments using human sera, 500pl of serum from either healthy donors or SLE patients was added to the lower chamber. Cells were cultured for 24 h at 37°C in a 5% CO2, humidified incubator. Transmigrated cells were counted in the lower reservoir by flow cytometry using a standard of $2.5x10^4$ fluorescent beads (Flow-count, Beckman Coulter).

Additional information in supporting Materials and Methods

Author Contribution

AP, DS, MLG, MM, RV, LM, AP, AF, FJ, EF, TD, AMV, PAB, RJF and PV conducted the experiments**.** NL developed computer analyses. PB, AD, FP, JS, JR, NR and CC provided reagents. RJF, PV and PL designed the experiments, analyzed data and wrote the paper. PL supervised the project.

Acknowledgments

We are grateful to H2P2 facility of Biosit (Rennes) for its technical assistance. This work was supported by INCa PLBIO, Ligue Contre le Cancer, INSERM Transfert, Fondation ARC, Région Bretagne, Rennes Métropole. We would like to thank the University of Nottingham Faculty of Medicine BSU Pump priming for funding. RJF was supported by the Biotechnology and Biological Sciences Research Council award BB/M018369/1. AP was supported by ANR (ANR-12-JSV2-0004-001).

The authors declare that there are no conflicts of interest.

REFERENCES

Adachi, M., Watanabe-Fukunaga, R., and Nagata, S. (1993). Aberrant transcription caused by the insertion of an early transposable element in an intron of the Fas antigen gene of lpr mice. Proc Natl Acad Sci U S A *90*, 1756-1760.

Baaten, B.J., Cooper, A.M., Swain, S.L., and Bradley, L.M. (2013). Location, Location, Location: The Impact of Migratory Heterogeneity on T Cell Function. Frontiers in immunology *4*, 311.

Beneteau, M., Daburon, S., Moreau, J.F., Taupin, J.L., and Legembre, P. (2007). Dominant-negative Fas mutation is reversed by down-expression of c-FLIP. Cancer Res *67*, 108-115.

Beneteau, M., Pizon, M., Chaigne-Delalande, B., Daburon, S., Moreau, P., De Giorgi, F., Ichas, F., Rebillard, A., Dimanche-Boitrel, M.T., Taupin, J.L., *et al.* (2008). Localization of Fas/CD95 into the lipid rafts on down-modulation of the phosphatidylinositol 3-kinase signaling pathway. Mol Cancer Res *6*, 604-613.

Brinkmann, V., Davis, M.D., Heise, C.E., Albert, R., Cottens, S., Hof, R., Bruns, C., Prieschl, E., Baumruker, T., Hiestand, P., *et al.* (2002). The immune modulator FTY720 targets sphingosine 1-phosphate receptors. J Biol Chem *277*, 21453-21457.

Cifone, M.G., De Maria, R., Roncaioli, P., Rippo, M.R., Azuma, M., Lanier, L.L., Santoni, A., and Testi, R. (1994). Apoptotic signaling through CD95 (Fas/Apo-1) activates an acidic sphingomyelinase. J Exp Med *180*, 1547-1552.

Cumberworth, A., Lamour, G., Babu, M.M., and Gsponer, J. (2013). Promiscuity as a functional trait: intrinsically disordered regions as central players of interactomes. Biochem J *454*, 361-369.

Cuvillier, O., Pirianov, G., Kleuser, B., Vanek, P.G., Coso, O.A., Gutkind, S., and Spiegel, S. (1996). Suppression of ceramide-mediated programmed cell death by sphingosine-1-phosphate. Nature *381*, 800-803.

Deng, L., Velikovsky, C.A., Swaminathan, C.P., Cho, S., and Mariuzza, R.A. (2005). Structural basis for recognition of the T cell adaptor protein SLP-76 by the SH3 domain of phospholipase Cgamma1. Journal of molecular biology *352*, 1-10.

Drappa, J., Vaishnaw, A.K., Sullivan, K.E., Chu, J.L., and Elkon, K.B. (1996). Fas gene mutations in the Canale-Smith syndrome, an inherited lymphoproliferative disorder associated with autoimmunity. N Engl J Med *335*, 1643-1649.

Fisher, G.H., Rosenberg, F.J., Straus, S.E., Dale, J.K., Middleton, L.A., Lin, A.Y., Strober, W., Lenardo, M.J., and Puck, J.M. (1995). Dominant interfering Fas gene mutations impair apoptosis in a human autoimmune lymphoproliferative syndrome. Cell *81*, 935-946.

Fouque, A., Debure, L., and Legembre, P. (2014). The CD95/CD95L signaling pathway: A role in carcinogenesis. Biochim Biophys Acta.

Juo, P., Kuo, C.J., Yuan, J., and Blenis, J. (1998). Essential requirement for caspase-8/FLICE in the initiation of the Fas-induced apoptotic cascade. Curr Biol *8*, 1001-1008.

Juo, P., Woo, M.S., Kuo, C.J., Signorelli, P., Biemann, H.P., Hannun, Y.A., and Blenis, J. (1999). FADD is required for multiple signaling events downstream of the receptor Fas. Cell Growth Differ *10*, 797-804.

Khadra, N., Bresson-Bepoldin, L., Penna, A., Chaigne-Delalande, B., Segui, B., Levade, T., Vacher, A.M., Reiffers, J., Ducret, T., Moreau, J.F., *et al.* (2011). CD95 triggers Orai1-mediated localized Ca2+ entry, regulates recruitment of protein kinase C (PKC) beta2, and prevents death-inducing signaling complex formation. Proc Natl Acad Sci U S A *108*, 19072-19077.

Kikawada, E., Lenda, D.M., and Kelley, V.R. (2003). IL-12 deficiency in MRL-Fas(lpr) mice delays nephritis and intrarenal IFN-gamma expression, and diminishes systemic pathology. J Immunol *170*, 3915-3925.

Kischkel, F.C., Hellbardt, S., Behrmann, I., Germer, M., Pawlita, M., Krammer, P.H., and Peter, M.E. (1995). Cytotoxicity-dependent APO-1 (Fas/CD95)-associated proteins form a death-inducing signaling complex (DISC) with the receptor. Embo J *14*, 5579-5588.
Kleber, S., Sancho-Martinez, I., Wiestler, B., Beisel, A., Gieffers, C., Hill, O., Thiemann, M., Mueller, W., Sykora, J., Kuhn, A., *et al.* (2008). Yes and PI3K bind CD95 to signal invasion of glioblastoma. Cancer Cell *13*, 235-248.
Kuhtreiber, W.M., Hayashi, T., Dale, E.A., and Faustman, D.L. (2003). Central role of defective apoptosis in autoimmunity. J Mol Endocrinol *31*, 373-399.
Legembre, P., Barnhart, B.C., Zheng, L., Vijayan, S., Straus, S.E., Puck, J., Dale, J.K., Lenardo, M., and Peter, M.E. (2004). Induction of apoptosis and activation of NF-kappaB by CD95 require different signalling thresholds. EMBO Rep *5*, 1084-1089.
Li, C., Li, J.N., Kays, J., Guerrero, M., and Nicol, G.D. (2015). Sphingosine 1-phosphate enhances the excitability of rat sensory neurons through activation of sphingosine 1-phosphate receptors 1 and/or 3. J Neuroinflammation *12*, 70.
Malleter, M., Tauzin, S., Bessede, A., Castellano, R., Goubard, A., Godey, F., Leveque, J., Jezequel, P., Campion, L., Campone, M., *et al.* (2013). CD95L cell surface cleavage triggers a prometastatic signaling pathway in triple-negative breast cancer. Cancer Res *73*, 6711-6721.
Motz, G.T., Santoro, S.P., Wang, L.P., Garrabrant, T., Lastra, R.R., Hagemann, I.S., Lal, P., Feldman, M.D., Benencia, F., and Coukos, G. (2014). Tumor endothelium FasL establishes a selective immune barrier promoting tolerance in tumors. Nat Med.
Murakami, A., Takasugi, H., Ohnuma, S., Koide, Y., Sakurai, A., Takeda, S., Hasegawa, T., Sasamori, J., Konno, T., Hayashi, K., *et al.* (2010). Sphingosine 1-phosphate (S1P) regulates vascular contraction via S1P3 receptor: investigation based on a new S1P3 receptor antagonist. Mol Pharmacol *77*, 704-713.
Musacchio, A. (2002). How SH3 domains recognize proline. Adv Protein Chem *61*, 211-268.
Orlinick, J.R., Elkon, K.B., and Chao, M.V. (1997). Separate domains of the human fas ligand dictate self-association and receptor binding. J Biol Chem *272*, 32221-32229.
Peter, M.E., Hadji, A., Murmann, A.E., Brockway, S., Putzbach, W., Pattanayak, A., and Ceppi, P. (2015). The role of CD95 and CD95 ligand in cancer. Cell Death Differ *22*, 549-559.
Rieux-Laucat, F., Le Deist, F., Hivroz, C., Roberts, I.A., Debatin, K.M., Fischer, A., and de Villartay, J.P. (1995). Mutations in Fas associated with human lymphoproliferative syndrome and autoimmunity. Science *268*, 1347-1349.
Saksela, K., and Permi, P. (2012). SH3 domain ligand binding: What's the consensus and where's the specificity? FEBS Lett *586*, 2609-2614.
Sato, T., Irie, S., Kitada, S., and Reed, J.C. (1995). FAP-1: a protein tyrosine phosphatase that associates with Fas. Science *268*, 411-415.
Shin, M.S., Lee, N., and Kang, I. (2011). Effector T-cell subsets in systemic lupus erythematosus: update focusing on Th17 cells. Curr Opin Rheumatol *23*, 444-448.
Siegel, R.M., Frederiksen, J.K., Zacharias, D.A., Chan, F.K., Johnson, M., Lynch, D., Tsien, R.Y., and Lenardo, M.J. (2000). Fas preassociation required for apoptosis signaling and dominant inhibition by pathogenic mutations. Science *288*, 2354-2357.
Stefan, E., Aquin, S., Berger, N., Landry, C.R., Nyfeler, B., Bouvier, M., and Michnick, S.W. (2007). Quantification of dynamic protein complexes using Renilla luciferase fragment complementation applied to protein kinase A activities in vivo. Proc Natl Acad Sci U S A *104*, 16916-16921.
Steinmetz, O.M., Turner, J.E., Paust, H.J., Lindner, M., Peters, A., Heiss, K., Velden, J., Hopfer, H., Fehr, S., Krieger, T., *et al.* (2009). CXCR3 mediates renal Th1 and Th17 immune response in murine lupus nephritis. J Immunol *183*, 4693-4704.

Straus, S.E., Jaffe, E.S., Puck, J.M., Dale, J.K., Elkon, K.B., Rosen-Wolff, A., Peters, A.M., Sneller, M.C., Hallahan, C.W., Wang, J., *et al.* (2001). The development of lymphomas in families with autoimmune lymphoproliferative syndrome with germline Fas mutations and defective lymphocyte apoptosis. Blood *98*, 194-200.
Suda, T., Takahashi, T., Golstein, P., and Nagata, S. (1993). Molecular cloning and expression of the Fas ligand, a novel member of the tumor necrosis factor family. Cell *75*, 1169-1178.
Tauzin, S., Chaigne-Delalande, B., Selva, E., Khadra, N., Daburon, S., Contin-Bordes, C., Blanco, P., Le Seyec, J., Ducret, T., Counillon, L., *et al.* (2011). The naturally processed CD95L elicits a c-yes/calcium/PI3K-driven cell migration pathway. PLoS Biol *9*, e1001090.
Tuettenberg, J., Seiz, M., Debatin, K.M., Hollburg, W., von Staden, M., Thiemann, M., Hareng, B., Fricke, H., and Kunz, C. (2012). Pharmacokinetics, pharmacodynamics, safety and tolerability of APG101, a CD95-Fc fusion protein, in healthy volunteers and two glioma patients. International immunopharmacology *13*, 93-100.
Vives, E., Brodin, P., and Lebleu, B. (1997). A truncated HIV-1 Tat protein basic domain rapidly translocates through the plasma membrane and accumulates in the cell nucleus. J Biol Chem *272*, 16010-16017.
Yang, J., Chu, Y., Yang, X., Gao, D., Zhu, L., Yang, X., Wan, L., and Li, M. (2009). Th17 and natural Treg cell population dynamics in systemic lupus erythematosus. Arthritis Rheum *60*, 1472-1483.
Yosef, N., Shalek, A.K., Gaublomme, J.T., Jin, H., Lee, Y., Awasthi, A., Wu, C., Karwacz, K., Xiao, S., Jorgolli, M., *et al.* (2013). Dynamic regulatory network controlling TH17 cell differentiation. Nature *496*, 461-468.
Zhang, W., Trible, R.P., Zhu, M., Liu, S.K., McGlade, C.J., and Samelson, L.E. (2000). Association of Grb2, Gads, and phospholipase C-gamma 1 with phosphorylated LAT tyrosine residues. Effect of LAT tyrosine mutations on T cell angigen receptor-mediated signaling. J Biol Chem *275*, 23355-23361.

FIGURES

Figure 1. Serum CD95L in SLE patients induces transmigration of T lymphocytes. A. Soluble CD95L levels were measured in serum from newly diagnosed SLE patients (n=34) and healthy donors (n=8) via ELISA **(**Student's t-test). **B.** CD95L in SLE serum was fractionated by size-exclusion column chromatography and measured via ELISA. *Inset*: CD95L was immunoprecipitated from gel filtration fractions 40–46 and 76–78 and subjected to Western blotting. Image presented is representative of gel filtration analysis of four different patients. **C.** CD95L and IL-17 staining in inflamed skin samples from lupus patients or healthy mastectomy subjects. Numbers represent different patients. Space bar = 100 μm. **D.** CD95L, CD31, CD4 and IL-17 staining in inflamed skin samples from a SLE patient. V, represents endothelial vessel, arrowheads identify marker-expressing cells. **E.** Densitometric analysis of CD95L and IL-17 staining in different patients. **F.** Transmigration of human T-cell subpopulations in the presence of serum from SLE patients or healthy donors. **G.** Th17 T-cell transmigration in the presence of SLE serum containing the indicated concentrations of CD95-Fc. Undifferentiated Th0 T-cells served as controls. Data represent means ± the standard deviation (SD) of 5 individual serum donors. **H.** $CD4^+$ T-cell transmigration with or without cl-CD95L (100 ng/mL). Data represent means ± SD of three independent experiments. **I.** Treg and Th17 cell transmigration with or without cl-CD95L (100 ng/mL) Data represent means ± SD of three independent experiments. (two-way ANOVA).

Figure 2. Transcriptomic signature in human Th17 and Treg cells stimulated with cl-CD95L. A Venn diagram comparing the genes differentially expressed between untreated and cl-CD95L-treated T-cell subsets. **B.** Heatmap depicting the relative fold change in the amount of transcripts significantly ($p \leq 0.05$) and differentially expressed between Th17 and Treg cells stimulated with cl-CD95L (100 ng/mL). Data for each experimental group (n = 2 per

condition) are shown. The scale bar indicates fold change. **C.** Pathway enrichment analysis of genes whose expression is significantly modulated by cl-CD95L in Th17 and Treg cells, and associated P values. **D.** ***Left panel:*** endothelial transmigration of human Th17 and Treg cells was evaluated in presence or absence of cl-CD95L (100 ng/mL) using Boyden chamber. ***Right panel:*** Th17 cells were pre-treated with FTY720 (1 μM), TY-52156 (10 μM), VPC-23019 (10 μM), W146 (1 μM) or CAY-1044 (1 μM) and then exposed to cl-CD95L (100 ng/mL) and endothelial transmigration was evaluated using Boyden chamber. Data represent means ± SD of three independent experiments.

Figure 3. Cl-CD95L is a chemoattractant for Th17 cells *in vivo*. Mice received a single injection of cl-CD95L (200 ng/animal) or vehicle and were sequentially sampled. **A.** T cell populations were obtained from tissues or peritoneal cavity washes. Cells were then restimulated in the presence of PMA/Ionomycin for 4 hours and then analyzed by flow cytometry. Cells were identified as follows; Th1 ($CD4^+IFN\text{-}\gamma^+$), Th17 ($CD4^+IL\text{-}17^+$), and Treg ($CD4^+Foxp3^+$). Infiltrating cell numbers were calculated. **B.** 24 hours post injection, ratios of Th17/Th1 cells per organ were determined. Data represent two independent experiments, using 6 mice/group, displaying means ±SEM.

Figure 4. CD95 induces a DD-independent Ca^{2+} response. A. CEM T-cells were stimulated with cl-CD95L (100 ng/mL). Cells were lyzed and CD95 was immunoprecipitated. The protein complex was resolved by SDS-PAGE, and subjected to Western blotting. Total lysates served as controls. B indicates a treatment with beads alone. Data are representative of three independent experiments. **B.** ***Left panel:*** Th17 cells from peripheral blood were stimulated with cl-CD95L (100 ng/mL) for indicated times. PLA was performed using anti-CD95 and anti-PLCγ1 mAbs. Nuclei were stained in blue (DAPI). Red dots were observed when the

distance between anti-CD95 and anti-PLCγ1 mAbs was close (≈16 nm). ***Right panels:*** Red dots were counted in 200 cells taken from different fields. Data represent means ±SD of three independent experiments. **C.** Schematic diagram of CD95 constructs. **D.** CEM-IRC cells expressing GFP alone or the GFP-fused CD95 constructs shown in (C) were loaded with the Ca^{2+} probe, Fluo2-AM (1 μM). Cells were stimulated with cl-CD95L (100 ng/mL; arrow), and the intracellular calcium concentration ($[Ca^{2+}]_i$) was monitored. Data are given as means ± SD of three independently performed experiments on n=20 cells. **E.** HEK cells transfected with the indicated constructs were stimulated with CD95L (100 ng/mL) for indicated times. The CD95 protein complex was immunoprecipitated from cell lysates and subjected to Western blotting, as indicated. Total lysates served as controls. B indicates a treatment with beads alone. Data are representative of three independent experiments. **F.** Activated PBLs were pre-incubated for 1 h with TAT-control or TAT-CID (10 μM), and stimulated with cl-CD95L (100 ng/mL) for the indicated times. The CD95 protein complex was immunoprecipitated from cell lysates and subjected to Western blotting, as indicated. Total lysates served as controls. B indicates a treatment with beads alone. Data are representative of three independent experiments. **G.** Activated PBLs from healthy donors were loaded with FuraPE3-AM (1 μM) and pre-treated for 1 h with TAT-control or TAT-CID (10 μM). Cells were stimulated with cl-CD95L (100 ng/mL; arrow). Data represent means ± the SD.

Figure 5. CID interacts with the SH3 domain of PLCγ1. A. The intracellular region of CD95 (aa 175–319) fused to F2 was co-transfected into HEK cells with the indicated domains of PLCγ1 fused to F1. Refolding of the luciferase and reconstitution of enzyme activity revealed protein/protein interactions. Data represent means ± SD of three independent experiments. **B.** The PLCγ1-SH3 domain (aa 790–851) fused to F1 was co-transfected into HEK cells with the indicated regions of CD95 fused to F2, and luminescence was assessed.

Data represent means ± SD of three independent experiments. **C.** CD95-CID-F2 and PLCγ1-SH3-F1 were co-transfected into HEK cells. Transfected cells were pre-incubated for 1 h with TAT-control (50 μM) or TAT-CID (50 and 10 μM), and luminescence was measured. **D.** Predicted interaction between CID and PLCγ1. TCRKHRK is the optimal aa sequence within CD95-CID for interaction with PLCγ1-SH3. **E.** Indicated cells were pre-incubated for 1 h with TAT-control, TAT-CID, TAT-CID-N, or TAT-CID-C (10 μM) and then stimulated with cl-CD95L (100 ng/mL). $[Ca^{2+}]_{CYT}$ was assessed in FuraPE3-AM (1 μM)-loaded cells. Data represent means ± the SD of 3 independent experiments.

Figure 6. TAT-CID alters immunological parameters in lupus-prone mice. A. Transmigration of mouse Th17 cells was monitored with the indicated concentrations of TAT-CID. **B–D.** C57BL/6 mice were injected with TAT-control or TAT-CID (40 mg/kg) 2 hours prior to intraperitoneal injection of cl-CD95L (200 ng) or vehicle. Animals were examined 24 hours after cl-CD95L injection. **B.** Total cell counts are shown in the peritoneal cavity. **C.** PECs were subjected to magnetic bead separation to identify the percentage of infiltrating $CD4^+CD62L^-$ (activated) T-cells. **D.** IL-17A concentrations in the peritoneal cavity were measured via ELISA (two-way ANOVA). Data in B-D represent two independent experiments performed with 6 mice/group. Data are means ±SEM. **E–I.** MRL/$lpr^{+/-}$ mice received either TAT-CID or TAT-control for 5 weeks. **E.** Ratios spleen/body weights of individual animals were measured upon completion of the experimental protocol and compared to those of age matched MRL and homozygous MRL/Lpr mice. **F.** Total cell number in the spleen is shown. **G.** Cellular composition of the spleen was determined in regard to $CD4^+CD62L^-$ T-cell number. **H.** mRNA expression levels of *il-23r*, *ccr6*, and *ror-γt* in cells from (C). **I.** Isolated T-cells from (G) were re-stimulated with anti-CD3 mAb for 72 h. IL-17A was then quantified by ELISA (unpaired Student's t-test).

Figure 7. TAT-CID alleviates clinical disease in lupus-prone mice. MRL/lpr$^{+/-}$ mice received either TAT-CID or TAT-control twice weekly for 5 weeks. Kidneys were fixed, sectioned, and stained with hematoxylin and eosin. All images were captured at 40× magnification. **A.** Representative section of the vasculature (V) in a TAT-CID-treated mouse, with no obvious cellular infiltrate surrounding the border (delineated by the dashed black line). **B.** Cellular infiltrate surrounding the vasculature (V) in a TAT-control-treated mouse, with multiple cell layers observed adjacent to the vasculature border (dashed black line). **C.** Vascular infiltrate scores were calculated for the kidneys in TAT-CID- and TAT-control-treated mice. Data represent means ± SD (n = 8 mice/group; one-way ANOVA). **D.** Kidney tissue showing normal glomeruli (arrow) and an adjacent tubule in TAT-CID-treated mice. **E.** Kidney tissue showing pathological modifications (arrows) to the glomeruli in TAT-control-treated mice. All images were captured at 20X (B; scale bar = 250μm) or 40X (A, D, E; scale bar = 150μm) magnification. **F.** Glomerular damage scores were calculated for each kidney in TAT-CID- and TAT-control-treated mice. Data represent means ± SD (n = 8 mice/group; *** $P < 0.001$; t-Test). **G.** C3 complement accumulation in kidneys of TAT-CID and TAT-control-treated MRL/Lpr$^{+/-}$ mice was assessed by microscopy. *Inset:* pictures of nucleus (DAPI) and C3 staining in mouse kidneys. **H.** Serum creatinine (upper panel) and urea (lower panel) were measured. **I.** Anti-dsDNA IgG1 levels were determined by ELISA. Data represent means ± SD (n = 8 mice/group; t-Test). **J.** Immunohistochemistry staining of IFN-y or IL-17. Cytokine positive cells were counted in treated kidneys.

Figure 1

Click here to download Figure Diapositive) .tiff

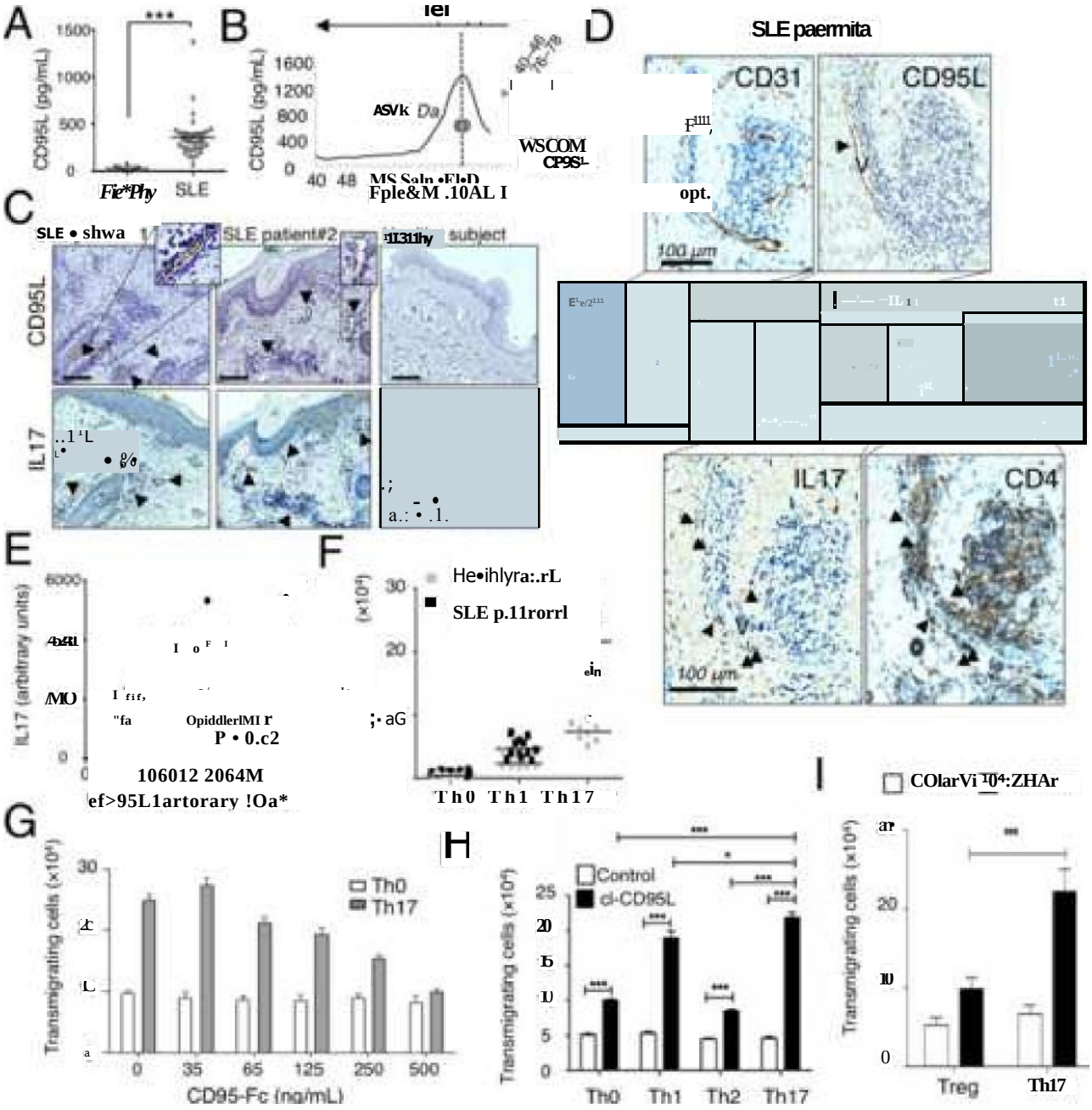

Figure 2

Click here to download Figure Diapositive2.tiff

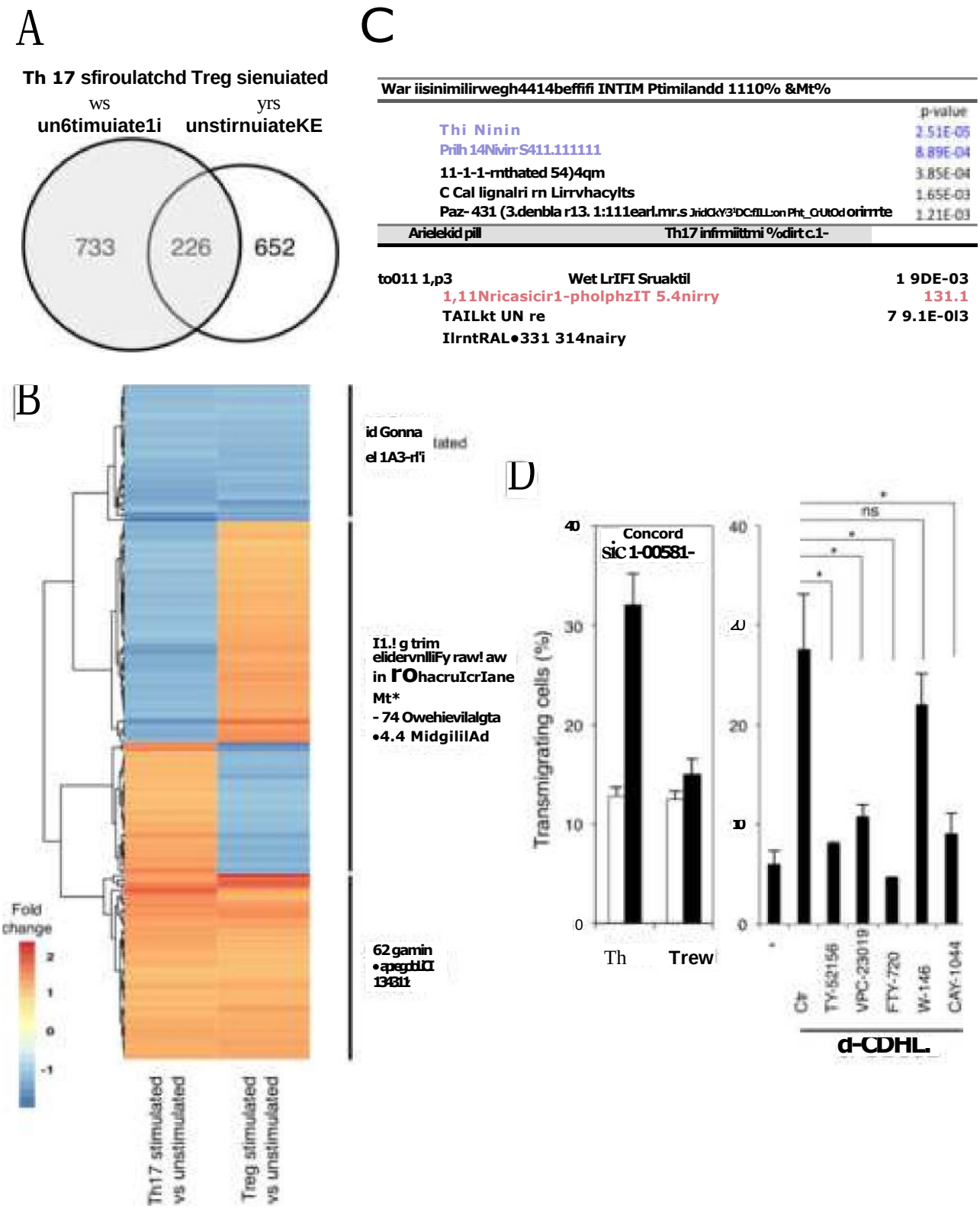

Figure 3

Click here to download Figure Diapositive3.tiff

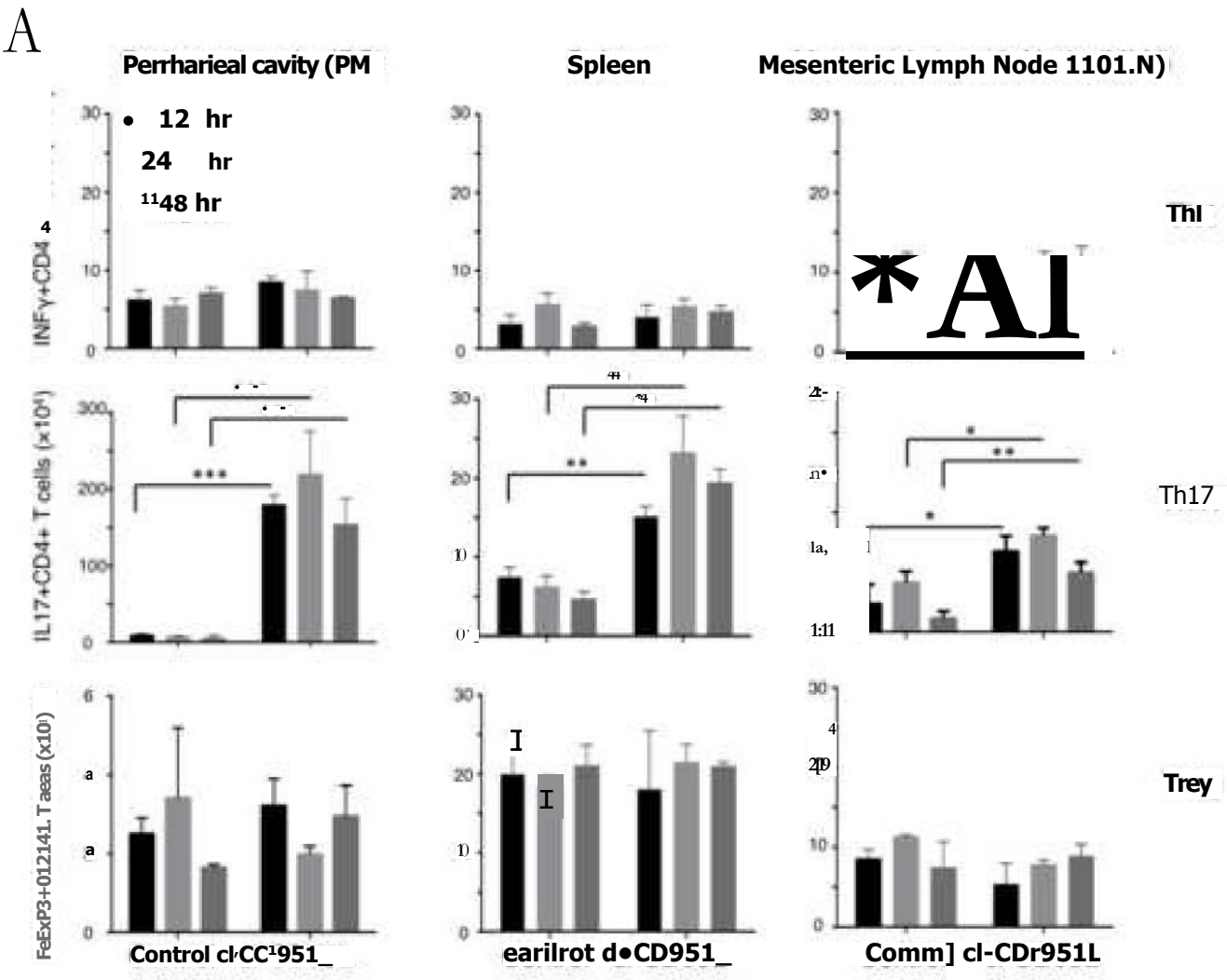

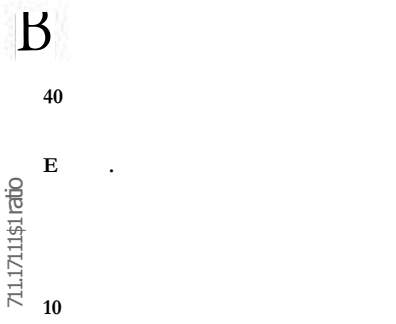

Figure 4

Click here to download Figure Diapositive4.tiff

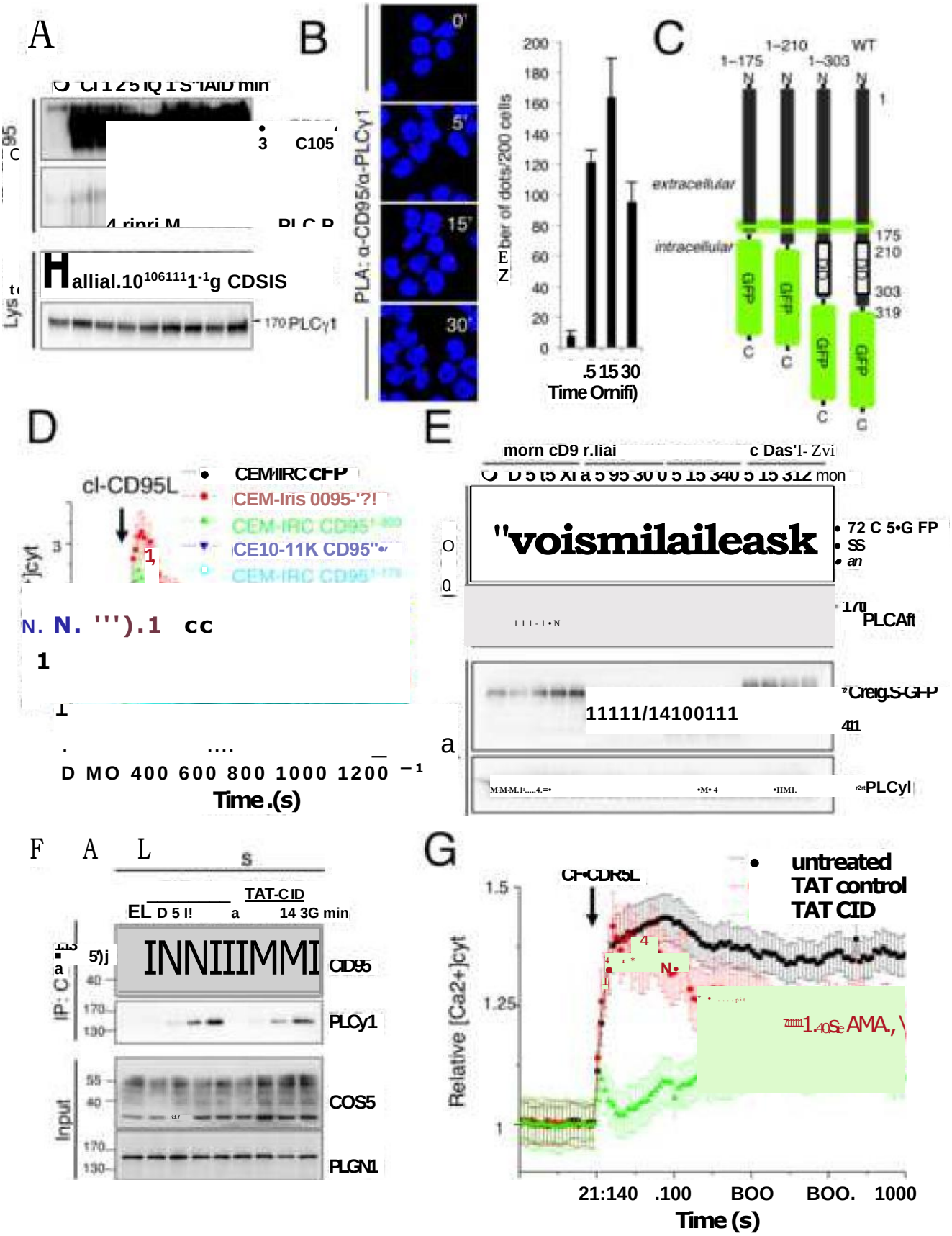

Figure

Click here to download Figure Diapositive5.tiff

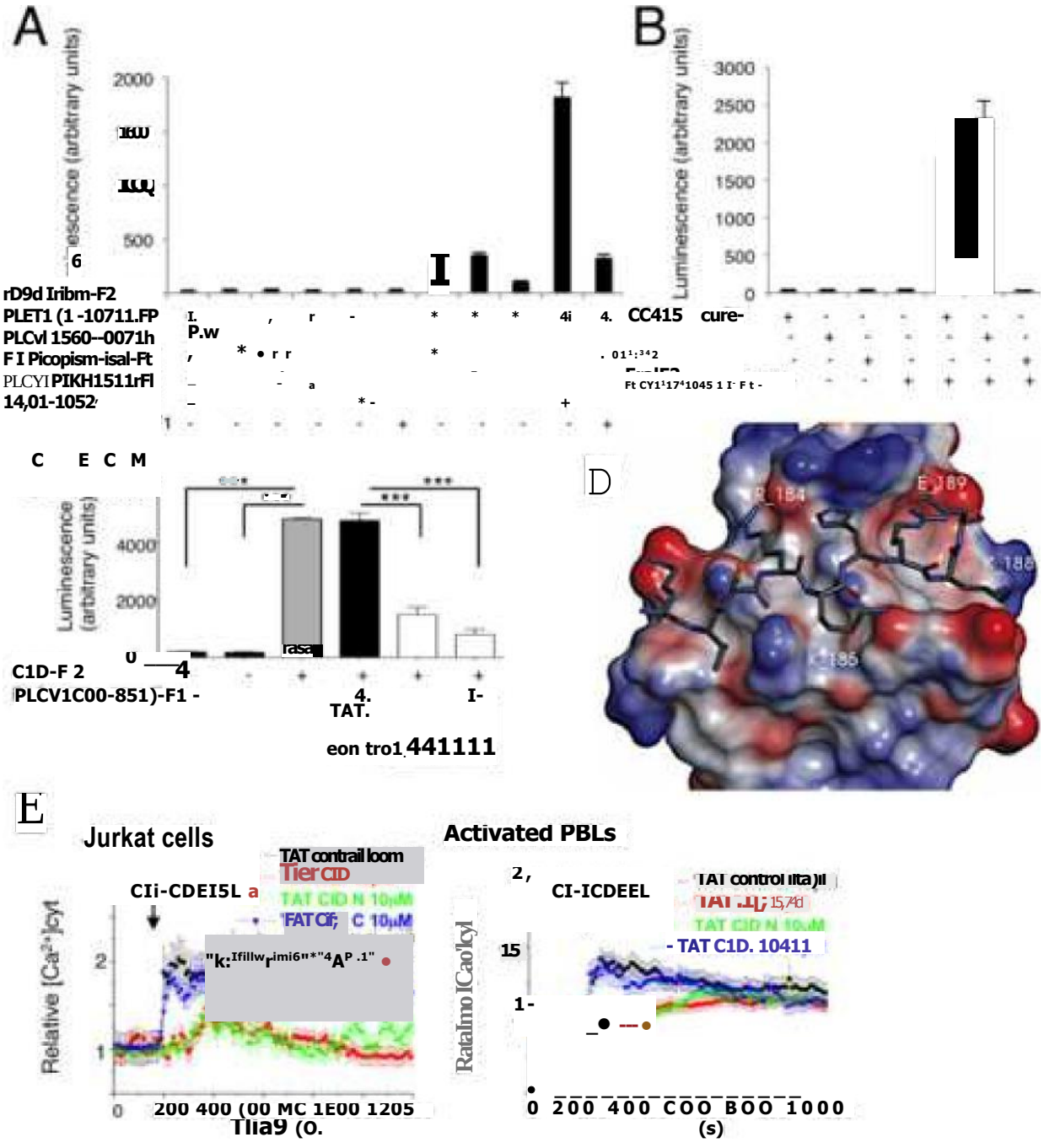

Figure

Click here to download Figure Diapositive6.tiff

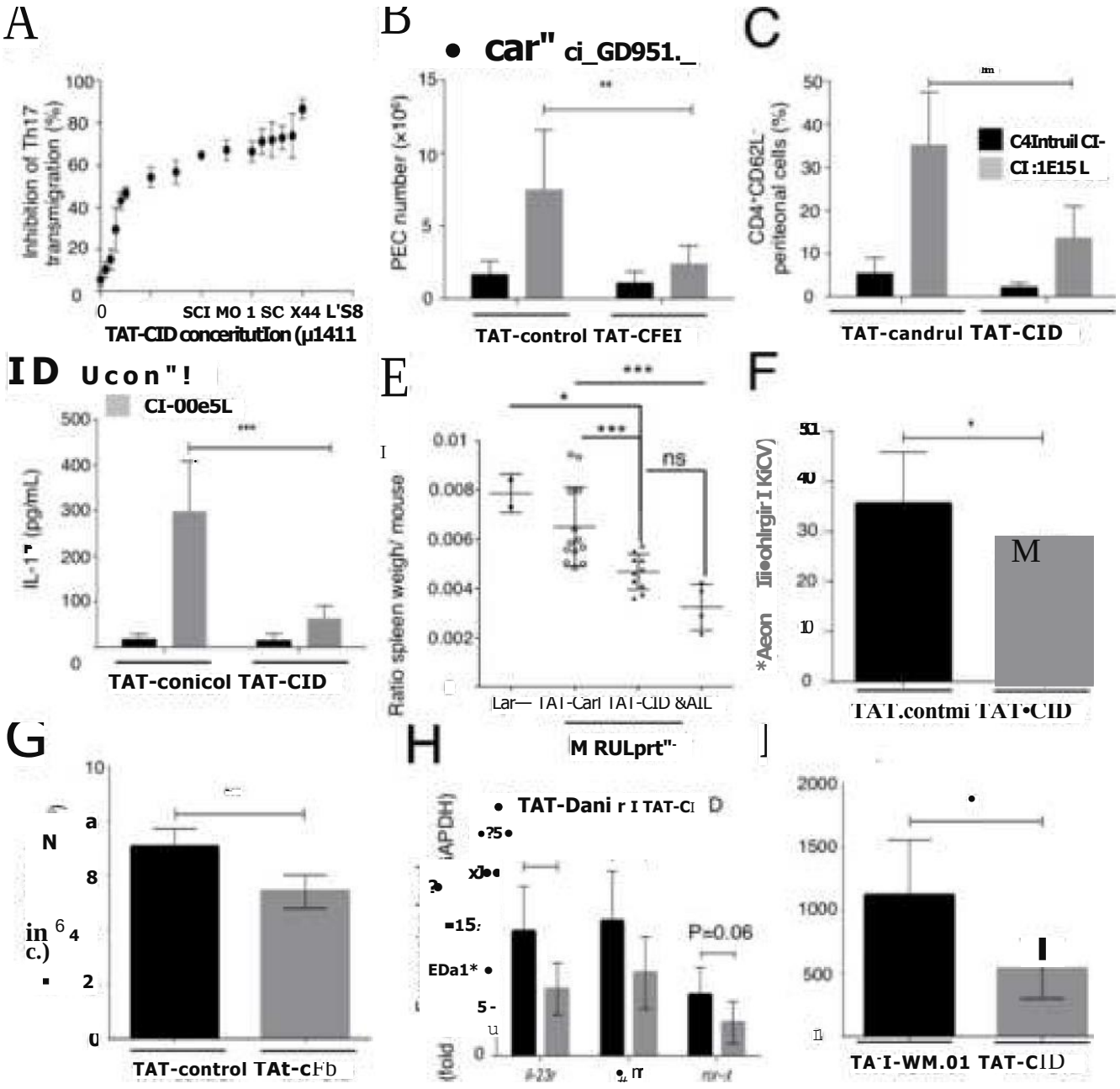

Figure

Click here to download Figure Diapositive7.tiff

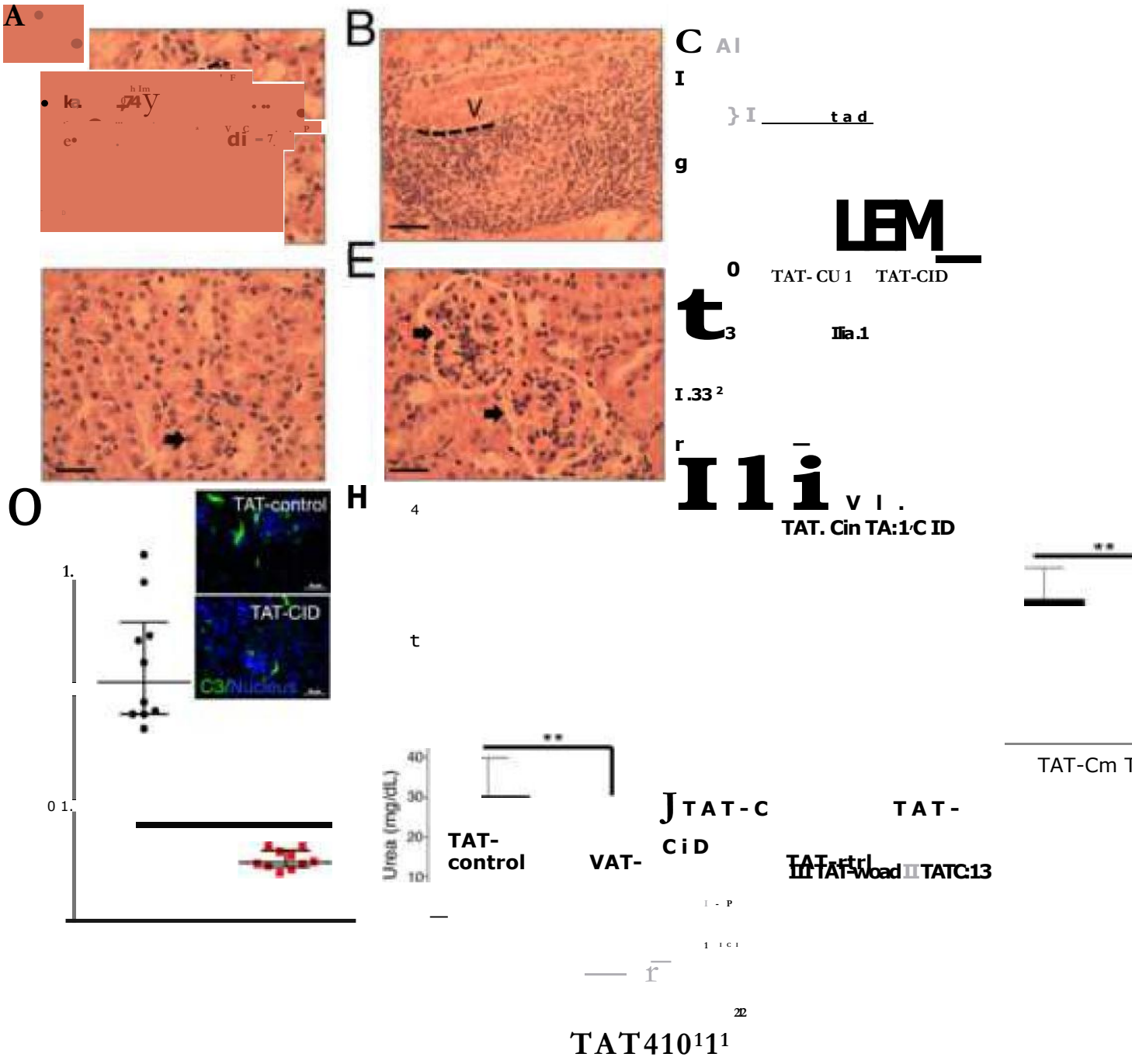

SUPPORTING FIGURE LEGENDS

Supporting Figure 1. Endothelial transmigration of Th17 CD4$^+$ T lymphocytes. A. The expression of CD95L or IL17 was analyzed by immunohistochemistry in inflamed skin from patients affected by lupus. Numbers represent different patients. **B.** HUVECs were incubated in the presence or absence of cl-CD95L (100 ng/mL) for 24 h. Next, the cells were detached using an EDTA-containing solution and stained with the indicated mAbs. The presence of the different proteins was detected by flow cytometry using a PE-conjugated secondary anti-mouse antibody. The histogram is representative of four independent experiments. **C.** The values for each indicated marker (*upper panels*: PSGL1 and *lower panel*: LFA-1) represent the mean fluorescence intensity (MFI) (± SD) measured by flow cytometry. For each Th subset, between 6 and 10 independent experiments were performed. **D.** Endothelial transmigration of human Th1, Th17, or Treg cells was assessed in the presence of neutralizing anti-E-selectin (10 µg/mL) antibody. Data were analyzed using two-way ANOVA. *P < 0.05 and ***P < 0.001. **E.** *Left panel:* Treg and Th17 cells were sorted from peripheral blood of healthy donors and the CD95 expression level at the surface of these cells was evaluated by flow cytometry. *Intermediate panel:* Comparison of CD95 Expression in different CD4$^+$T cell subsets: Naive CD4+ (CD45RA$^+$CD4$^+$), Memory CD4$^+$ (CD4$^+$CD45RA$^-$), Th1 (CD4$^+$CXCR3$^+$CCR6$^-$CD45RA$^-$), Th17 (CD4$^+$CXCR3$^-$CCR6$^+$CD45RA$^-$), Treg cells (CD4$^+$CD25^{high}FoxP3$^+$). *Right panel:* CD95 expression was normalized as follows: CD95 MFI in Th subset or Treg divided by CD95 in naive CD4+T. Wilcoxon paired analysis was performed in a set of 20 healthy donors. Histogram plots represent mean ±SD. **F.** Flow cytometry analyses demonstrating the efficiency of Treg (*left panels*) and Th17 cell (*right panels*) sorting from human peripheral blood. **G.** Schema of the S1P signaling pathway. In red, genes upregulated in Th17 cells stimulated with cl-CD95L.

Supporting Figure 2. Cl-CD95L is a chemo-attractant for Th17 cells *in vivo*. Mice received a single injection of cl-CD95L (200 ng) or vehicle prior to sacrifice 24 h later. All experiments were repeated three times. **A, B, C, D, E.** $CD4^+CD62L$ PECs were purified by AutoMACS separation, and RNA was prepared prior to real-time qPCR to assess expression levels of (A) IL-17A, (B) IL-23R, (C) CCR6, (D) IFN-y, and (E) FoxP3 mRNA**.** Data represent means ± the SD (n = 6 mice per group; *P < 0.05, **P < 0.01, and ***P < 0.001; Student's t-test). GAPDH, glyceraldehyde 3-phosphate dehydrogenase.

Supporting Figure 3. Amino acid residues 175–210 of CD95 induce the Ca^{2+} signaling pathway. A. Parental CEM T-cells and their low CD95-expressing counterpart, namely CEM-IRC (for Ig-CD95L resistant cell) were stimulated with cl-CD95L (100 ng/mL) for indicated time points. PLA was performed using anti-CD95 and anti-PLCy1 mAbs. Nuclei are stained in blue (DAPI). Red dots were observed when the distance between anti-CD95 and anti-PLCy1 mAbs was close (≈16 nm). *Inset:* The expression level of CD95 was evaluated in Parental CEM and CEM-IRC cells by flow cytometry. **B.** Parental Jurkat T-cells and their PLC-y1-deficient and PLC-y1-reconstituted counterparts were loaded with the Ca^{2+} probe, FuraPE3-AM (1 tM), prior to stimulation with cl-CD95L (100 ng/mL; black arrow). Ratio images (F340/F380, R) were taken every 10 s and normalized against pre-stimulated values (R_0). Data represent the mean ± SD of R/R_0. *Inset:* PLCy1-deficient Jurkat cells or their reconstituted counterparts were lysed, and the expression of PLCy1 and CD95 was evaluated by immunoblotting. Tubulin was used as a loading control. **C.** Parental Jurkat cells (A3) and their counterparts lacking FADD or caspase-8 were treated with the indicated concentrations of cytotoxic IgCD95L for 20 h. Cell death was assessed using MTT assay. **D.** Indicated cells were loaded with the Ca^{2+} probe FuraPE3-AM (1 tM) and then stimulated with cl-CD95L

(100 ng/mL). Data were analyzed as described in B. *Inset:* Parental Jurkat cells (A3) or their counterparts lacking either FADD or caspase-8 were lysed, and the expression levels of CD95, FADD, and caspase-8 were examined by immunoblotting. **E.** The levels of CD95 expression at the cell surface of CEM-IRC clones reconstituted with the indicated CD95 constructs were evaluated by flow cytometry. Data are representative of three independent experiments. **F.** Cells described in E were treated with the indicated concentrations of IgCD95L for 20 h. Cell death was assessed using MTT assay. **G.** HEK cells were co-transfected with the GFP-fused CD95 constructs and wild-type PLCγ1. Twenty-four hours after transfection, the levels of CD95 expression were evaluated by flow cytometry. **H.** *Left panel:* HEK cells were co-transfected with PLCγ1 and mCherry or mCherry-CID. After 24 h, cells were lysed and PLCγ1 was immunoprecipitated. The immune complex was resolved by SDS-PAGE and subjected to immunoblot analysis as indicated. Total lysates were loaded as a control. *Right panel:* HEK cells were co-transfected with PLCγ1 and CID-mCherry or mCherry alone. After 24 h, cells were stimulated in the presence or absence of CD95L (100 ng/mL), and CD95 was immunoprecipitated. The immune complex was resolved by SDS-PAGE and immunoblotted as indicated. Total lysates were loaded as a control.

Supporting Figure 4. Cell-penetrating TAT-CID peptide inhibits the CD95-induced Ca^{2+} response without affecting the apoptotic signaling pathway. A. Protein sequences of TAT-CID and TAT-control. **B.** The leukemic T-cell line CEM was pre-incubated for 1 h with 10 µM of TAT-control or TAT-CID and then stimulated in the presence or absence of cl-CD95L (100 ng/mL) for the indicated times. Cells were lysed and CD95 was immunoprecipitated. The immune complex was resolved by SDS-PAGE and immunoblotted as indicated. Total lysates were loaded as a control. **C.** Jurkat and CEM cells were loaded with FuraPE3-AM (1 µM), pre-treated for 1 h with 10 µM TAT-control or TAT-CID, and then stimulated with 100

ng/mL of cl-CD95L (black arrow). Ratio images were taken every 10 s and normalized against pre-stimulated values. **D.** Activated PBLs were pre-incubated for 1 h with 10 jiM TAT-control or TAT-CID and then stimulated in the presence or absence of cl-CD95L (100 ng/mL) for the indicated times. Cells were then lysed, and 100 jig of protein was resolved by SDS-PAGE and immunoblotted as indicated. Total Akt served as a loading control. **E.** The indicated cells were pre-incubated for 1 h with a non-toxic dose of TAT-control or TAT-CID (10 jiM), and cell death was assessed in an MTT assay.

Supporting Figure 5. CID-CD95 directly interacts with SH3-PLCγ1 domain. A. The Renilla luciferase enzyme was divided into amino-terminal and carboxy-terminal fragments (F1 and F2, respectively). **B.** Human PLC71 domains. PH, pleckstrin homology domain; cat, catalytic domain; and SH, src homology domain. **C.** HEK cells were transfected with indicated constructs. After 24 h, cells were lysed, and the expression levels of the different constructs were examined by immunoblotting using an anti-luciferase mAb recognizing the amino-terminal region of luciferase (MAB4410, Millipore, France). **D.** HEK cells were treated as in **C** and the expression levels of the indicated constructs were examined by immunoblotting using an anti-luciferase mAb recognizing the carboxy-terminal region of luciferase (MAB4400, Millipore). **E.** Each amino acid in CID sequence was replaced by alanine (alanine scanning) and all constructs were co-transfected with SH3-PLC71 in HEK cells. For each co-transfection, luminescence was assessed and a ratio was calculated as follows: (luminescence for mutated construct/ luminescence for wild type CID) x 100). For each condition, this value was next multiplied by the relative expression level of CID-F2 and SH3-PLC71-F1, evaluated by densitometric analysis of proteins as follows: ((densitometric value of mutated CID-F2 construct/ densitometric value of wild type CID-F2) x (densitometric value of co-transfected SH3-PLC71-F1/ densitometric value of SH3-PLC71-F1

co-transfected with wild type CID)). **F.** CID sequence of wild type CD95 (TCRKHRK) underwent double (TC**AA**HRK) or triple (TC**AA**HR**A**) mutations and these constructs were transiently transfected in HEK cells. Calcium signal was assessed using fluo2-AM (1 µM). Cells were stimulated with cl-CD95L (100 ng/mL; arrow), and the intracellular calcium concentration ($[Ca^{2+}]_i$) was monitored by measuring the F/F_0 ratio (relative cytoplasmic calcium concentration ($[Ca^{2+}]_{CYT}$)). **G.** Sequences of cell-penetrating peptides CID-N and CID-C. **H-I-J.** Indicated cells were loaded with the Ca^{2+} probe FuraPE3-AM (1 µM). Ratio images were taken every 10 s and normalized against pre-stimulated values**. H.** The anti-CD3 mAb OKT3 (1 µg/mL) evokes a PLCγ1-dependent Ca^{2+} response in Jurkat cells. **I.** Pre-incubation of Jurkat T-cells for 1 h with 10 µM TAT-CID or TAT-control had no effect on the CD3-induced Ca^{2+} response. **J.** The PLCβ-driven Ca^{2+} response induced by carbachol (10 µM) in Jurkat cells was not affected by TAT-CID pre-treatment (10 µM for 1 h).

Supporting Figure 6. A cell-penetrating murine CID inhibits the CD95-mediated Ca^{2+} response in murine T-cells. A. Mouse and human CD95 sequences were aligned using ClustalW2 (Larkin et al., 2007). **B.** *Inset:* CEM-IRC cells were reconstituted with murine CD95, a clone was selected, and its CD95 expression level was evaluated by flow cytometry. The sensitivity of murine CD95-expressing CEM-IRC to the cytotoxic CD95L, IgCD95L, was assessed using MTT assay. **C.** The cells were loaded with the Ca^{2+} probe FuraPE3-AM (1 µM). Ratio images were taken every 10 s and normalized against pre-stimulated values**.** Pre-incubation of murine CD95-expressing CEM-IRC T-cells with 10 µM TAT-mCID for 1 h inhibited the CD95-mediated Ca^{2+} response, whereas pre-incubation with TAT-hCID did not. **D.** The murine CID sequence fused to the cell-penetrating peptide TAT. **E.** Activated murine PBLs were loaded with the Ca^{2+} probe FuraPE3-AM (1 µM). Ratio images were taken every 10 s and normalized against pre-stimulated values**.** Pre-incubation of activated murine PBLs

with 10 µM TAT-mCID for 1 h inhibited the CD95-mediated Ca^{2+} response, whereas pre-incubation with TAT-hCID did not. **F-G-H.** 8-week old MRL/lpr+/- mice were administered with either TAT-CID or TAT-control peptide twice weekly for five weeks. Upon completion of the treatment, total body (**F**) and organ weight (**G**) were assessed. **H.** B-cell composition of the spleen was evaluated.

Supporting Figure 7. Infiltrating CD8 T-cells in skin lesions of lupus patients and computer modeling of CID. A. Expression of CD95L and CD8 was assessed by immunohistochemistry. The numbers represent the different patients. **B.** Densitometric analysis of the CD8 and CD95L staining depicted in **A** revealed no inverse correlation between CD8 and CD95L expression levels in skins of SLE patients. **C.** Observed backbone hydrogen bonds between pairs of residues (% as a function of the simulation time). Counting main chain hydrogen bonds during the 40 ns molecular dynamics analysis revealed that these interactions were rare. **D.** Dynamics of the peptide structures. RMSD and radius of gyration suggest that the system was stable, with no detectable compression of the peptide. This means that no stable secondary structures occurred. The presence of short structural elements was noticed from time-to-time, e.g., in the middle of the peptide at 5 ns and at the COOH-terminus at 13, 20, 30, and 37 ns. These folds correspond to discrete events, and the peptide did not adopt a stable 3D structure (the small α-helices have a short half-life and are quickly broken).

Reference

Larkin, M.A., Blackshields, G., Brown, N.P., Chenna, R., McGettigan, P.A., McWilliam, H., Valentin, F., Wallace, I.M., Wilm, A., Lopez, R., *et al.* (2007). Clustal W and Clustal X version 2.0. Bioinformatics *23*, 2947-2948.

Supplementary Figure 1

a

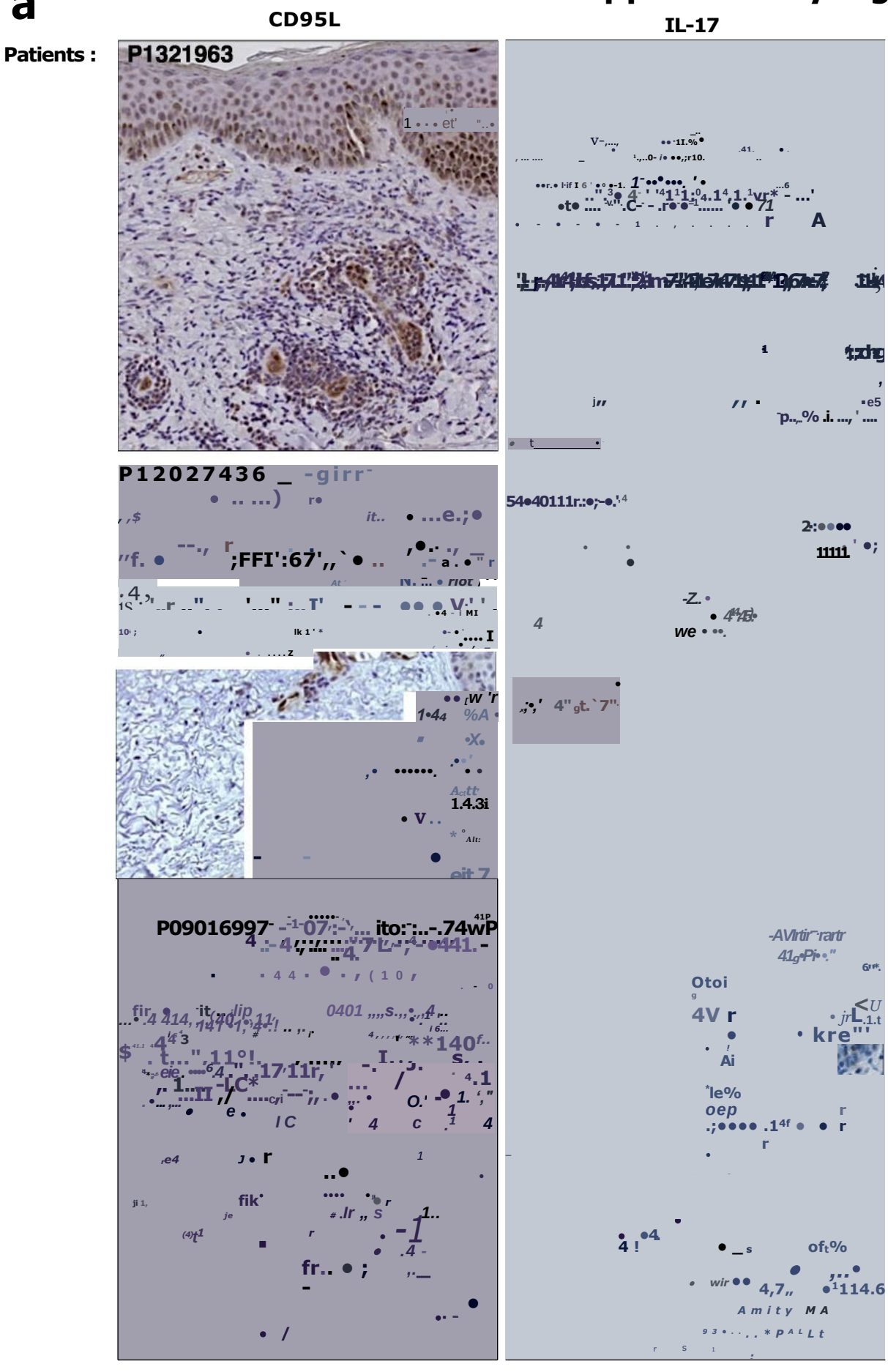

Supplementary Figure 1

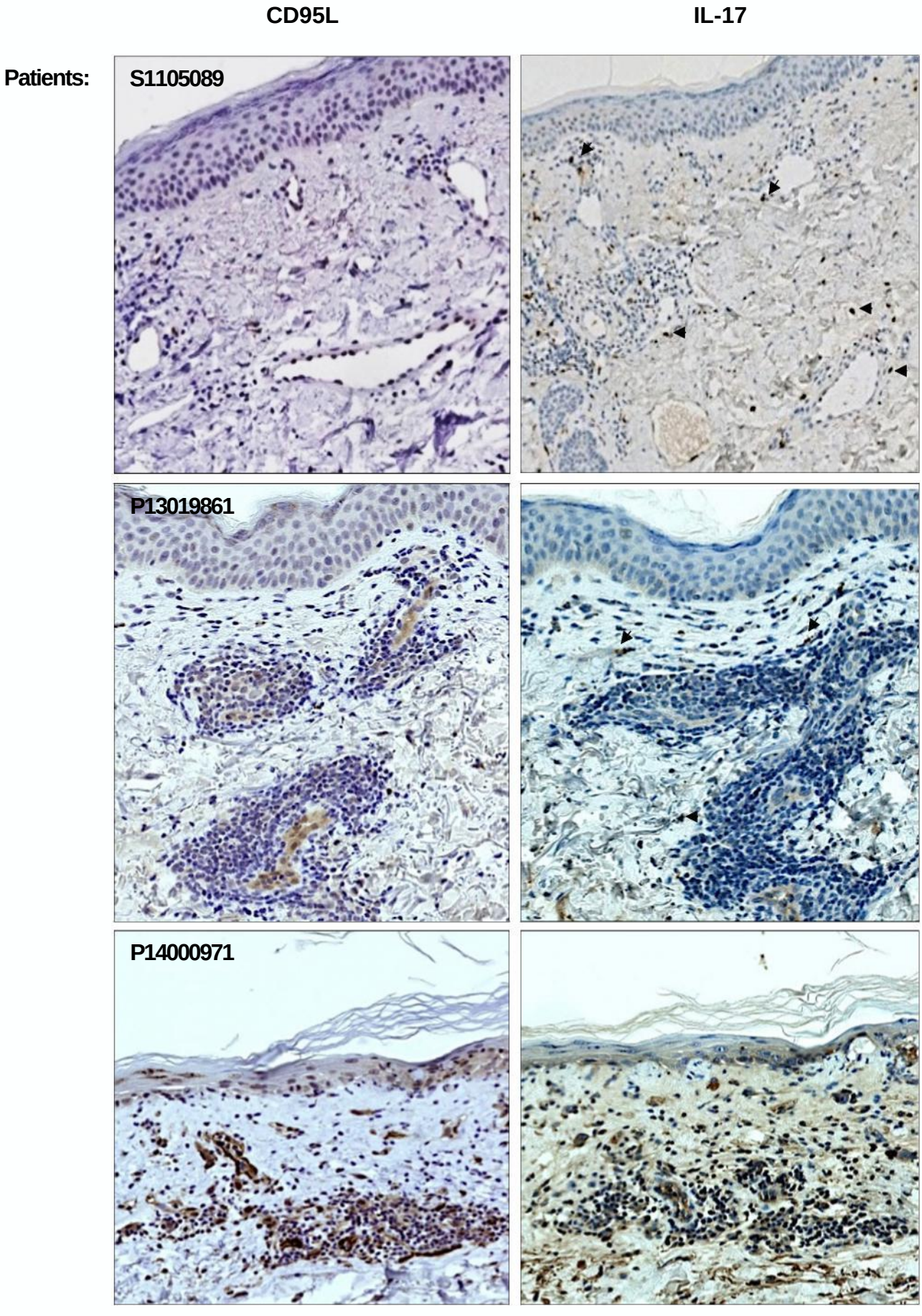

Supplementary Figure 1

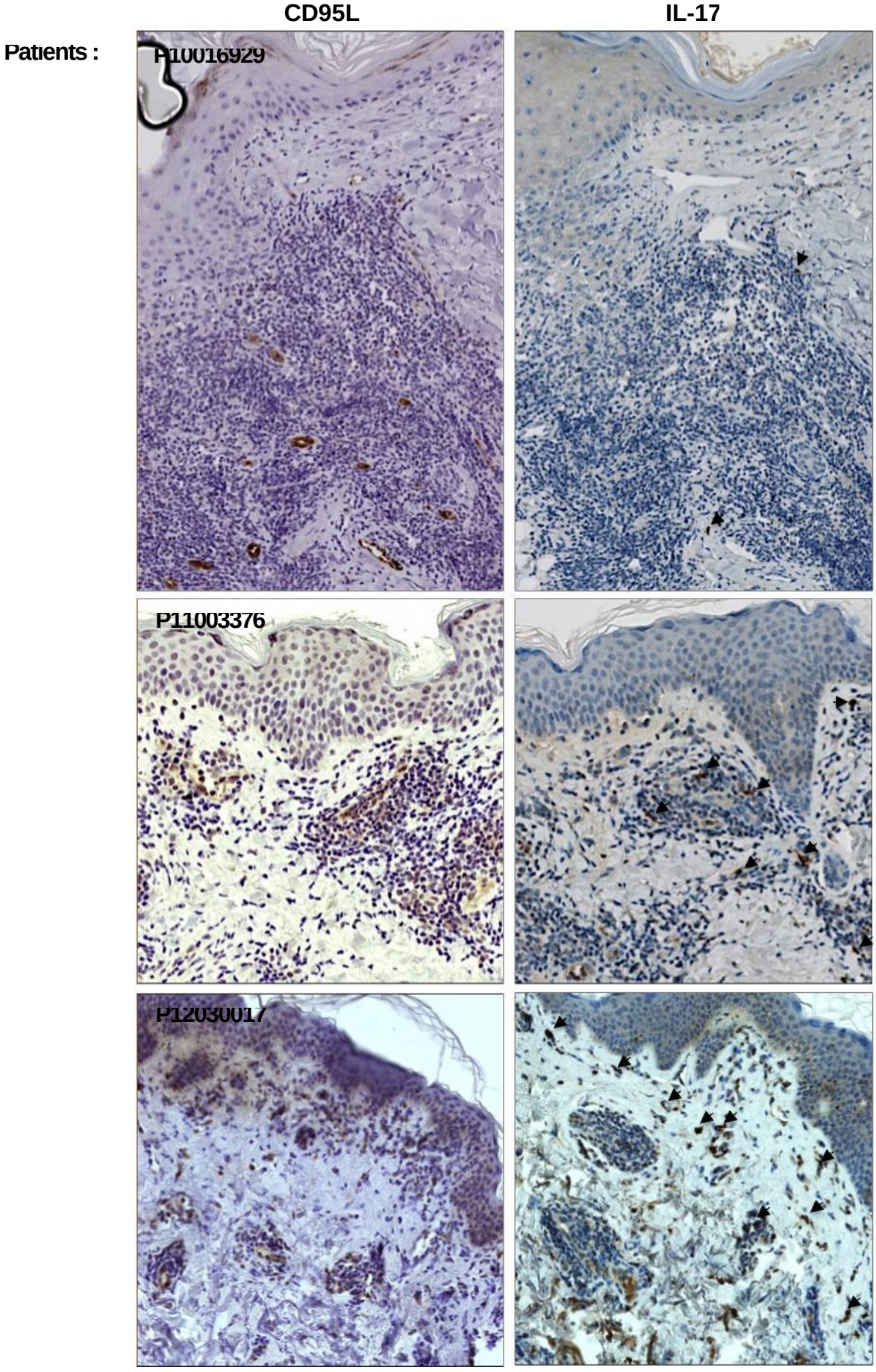

Supplementary Figure 1

CD95L

IL-17

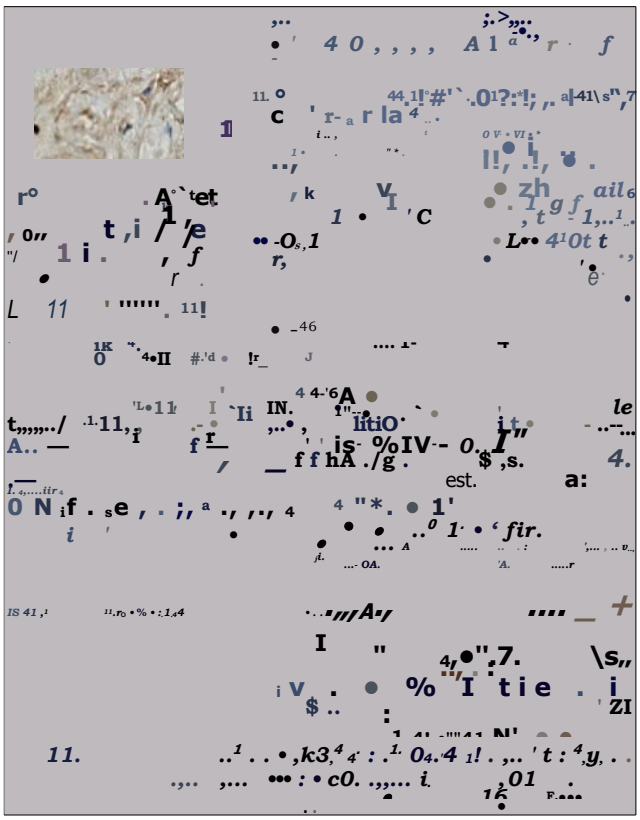

Supplementary Figure 1

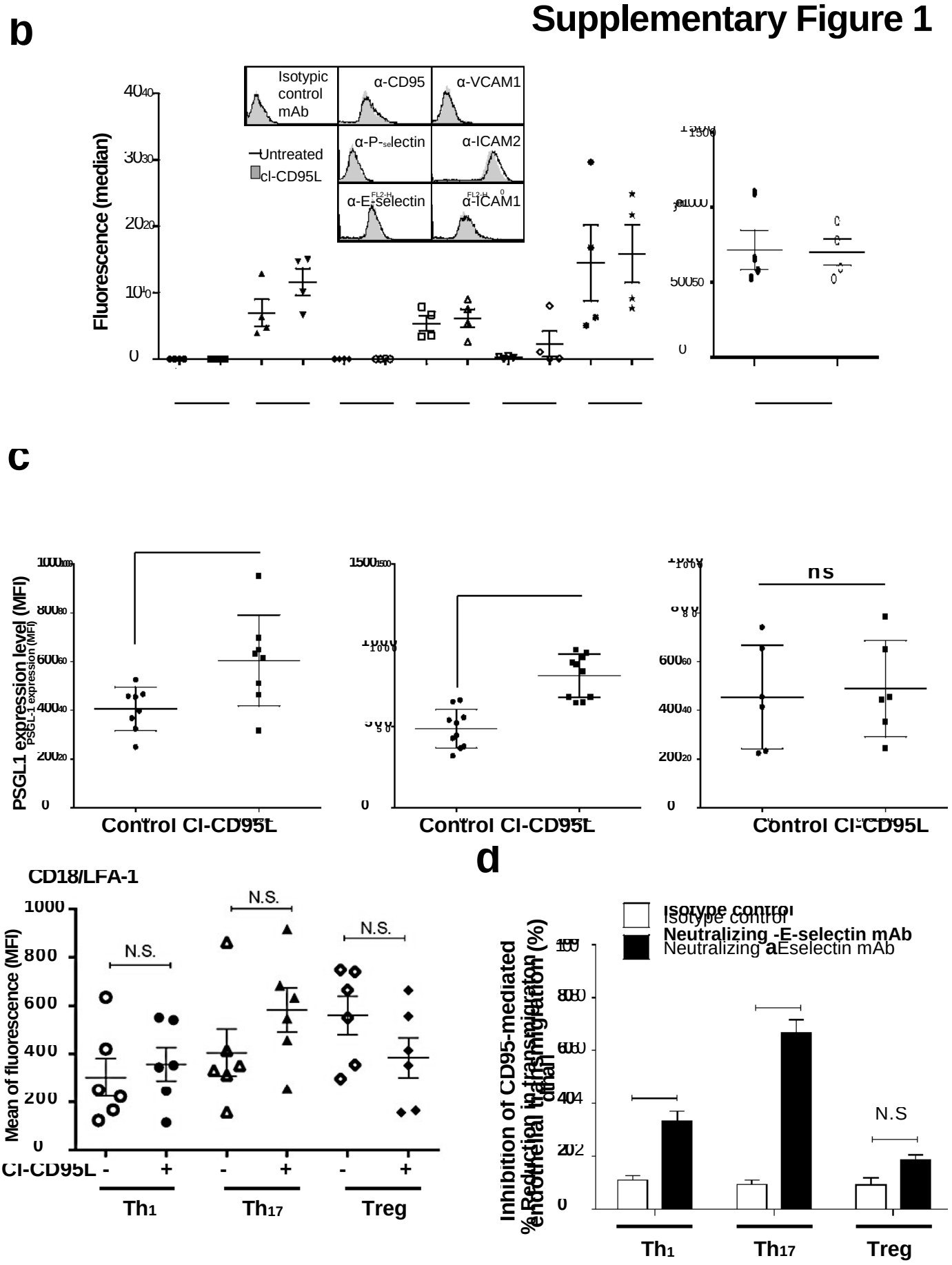

Supplementary Figure 1

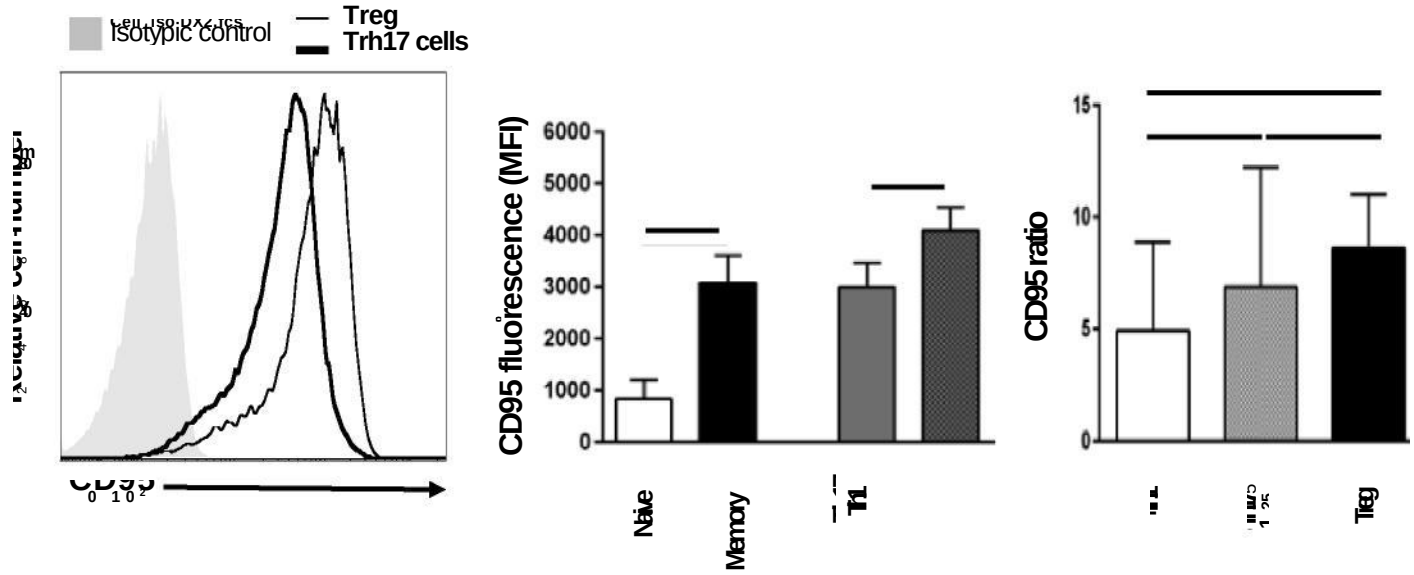

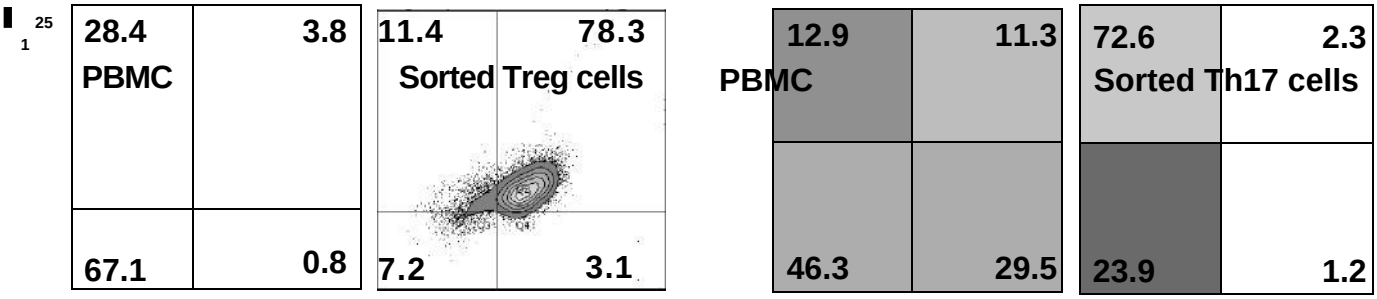

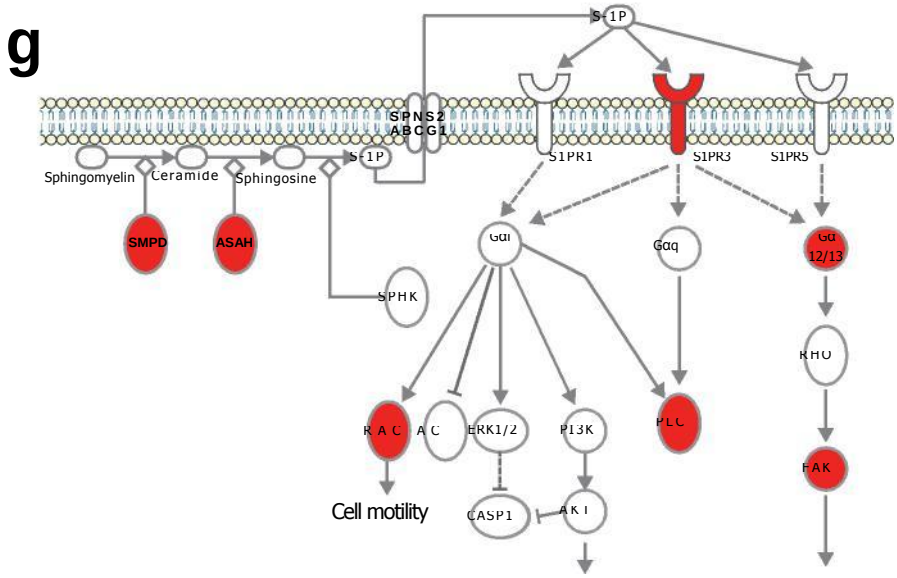

Supplementary Figure 2

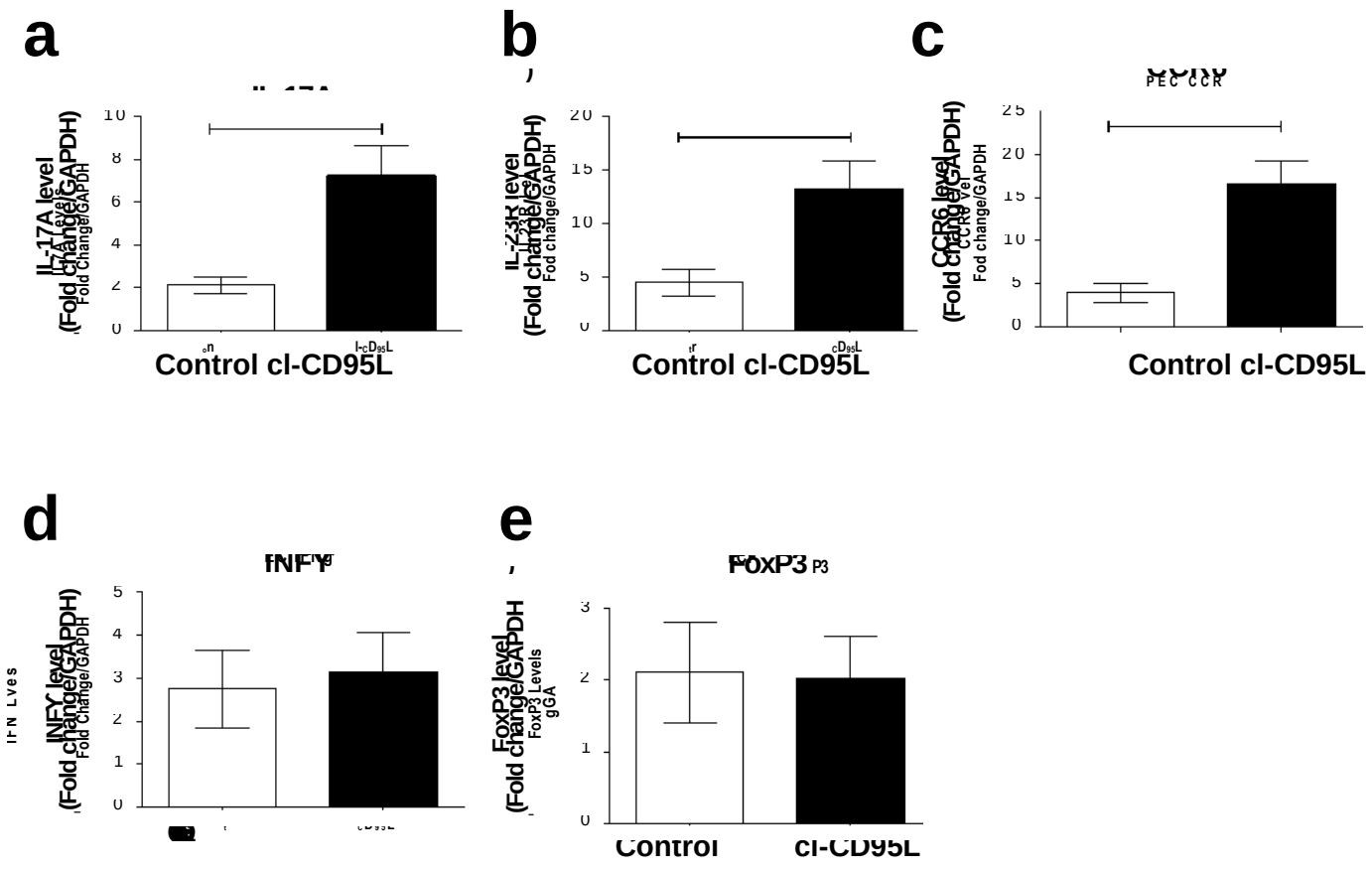

Supplementary Figure 3

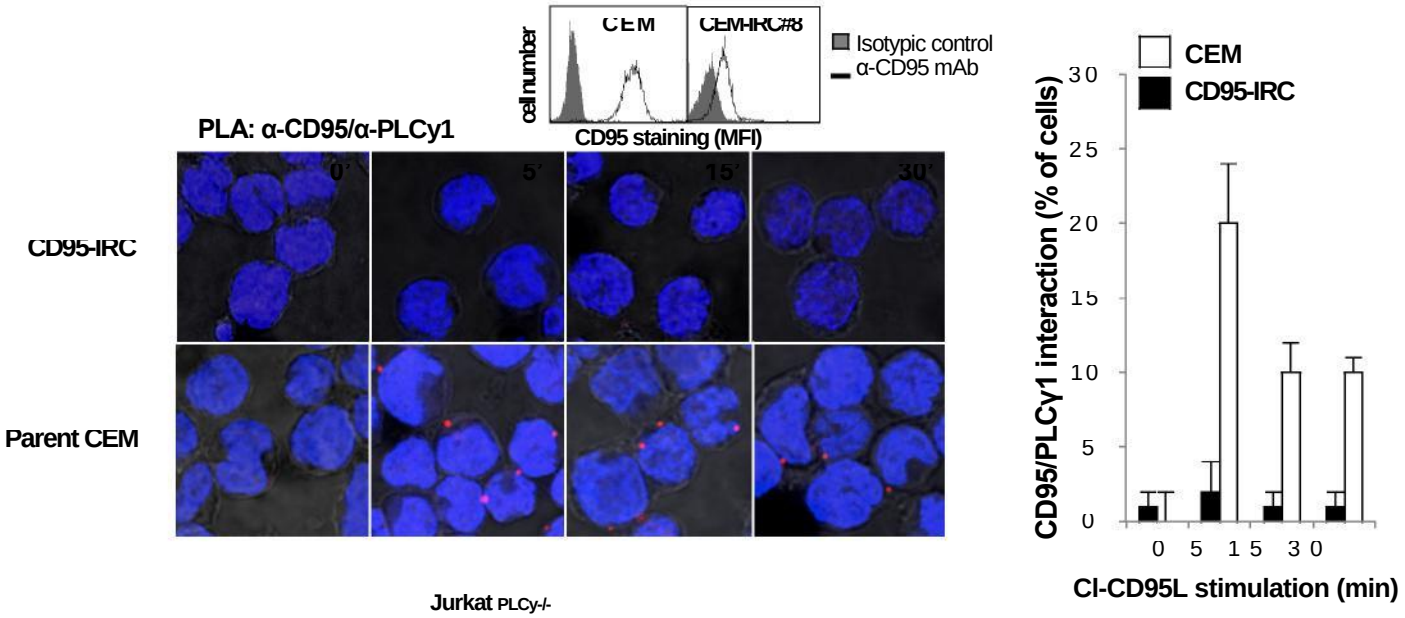

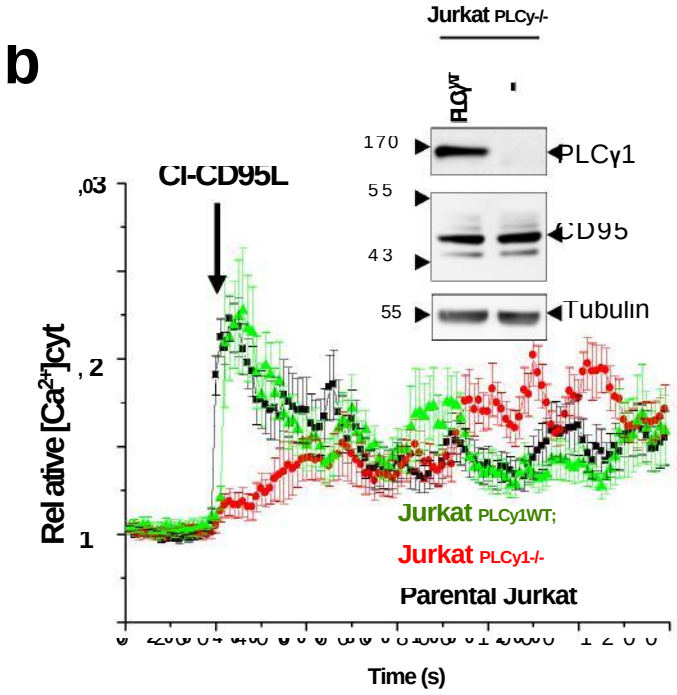

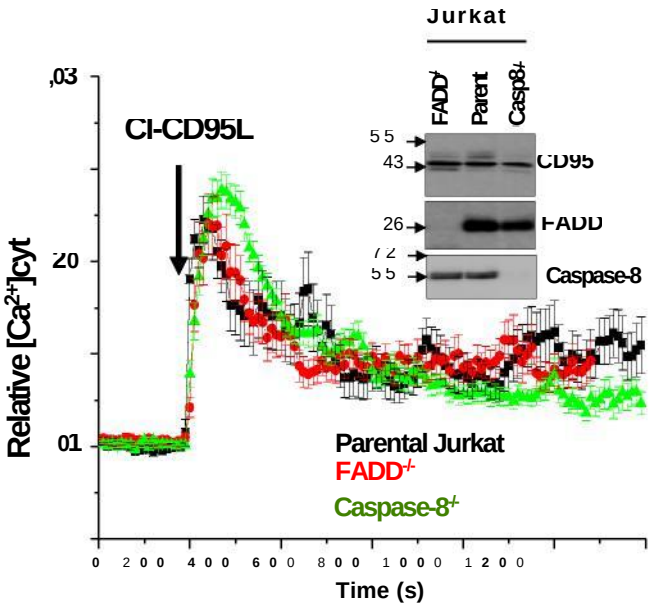

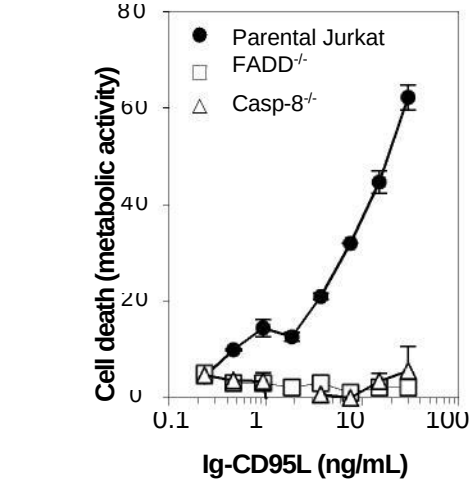

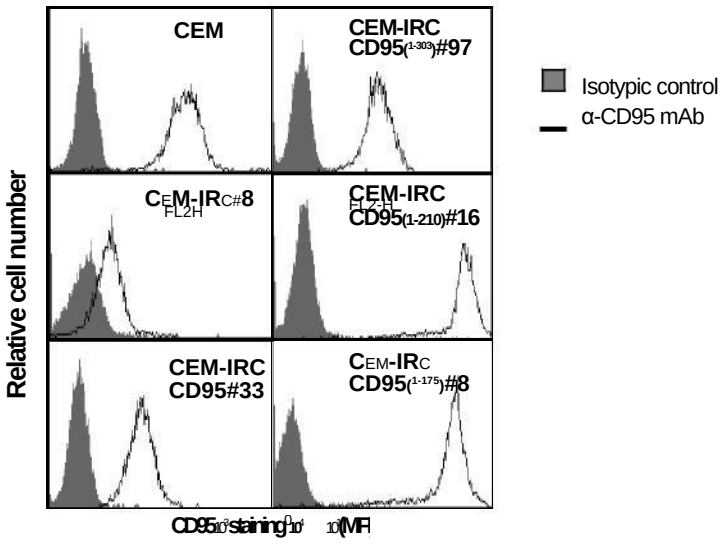

Supplementary Figure 3

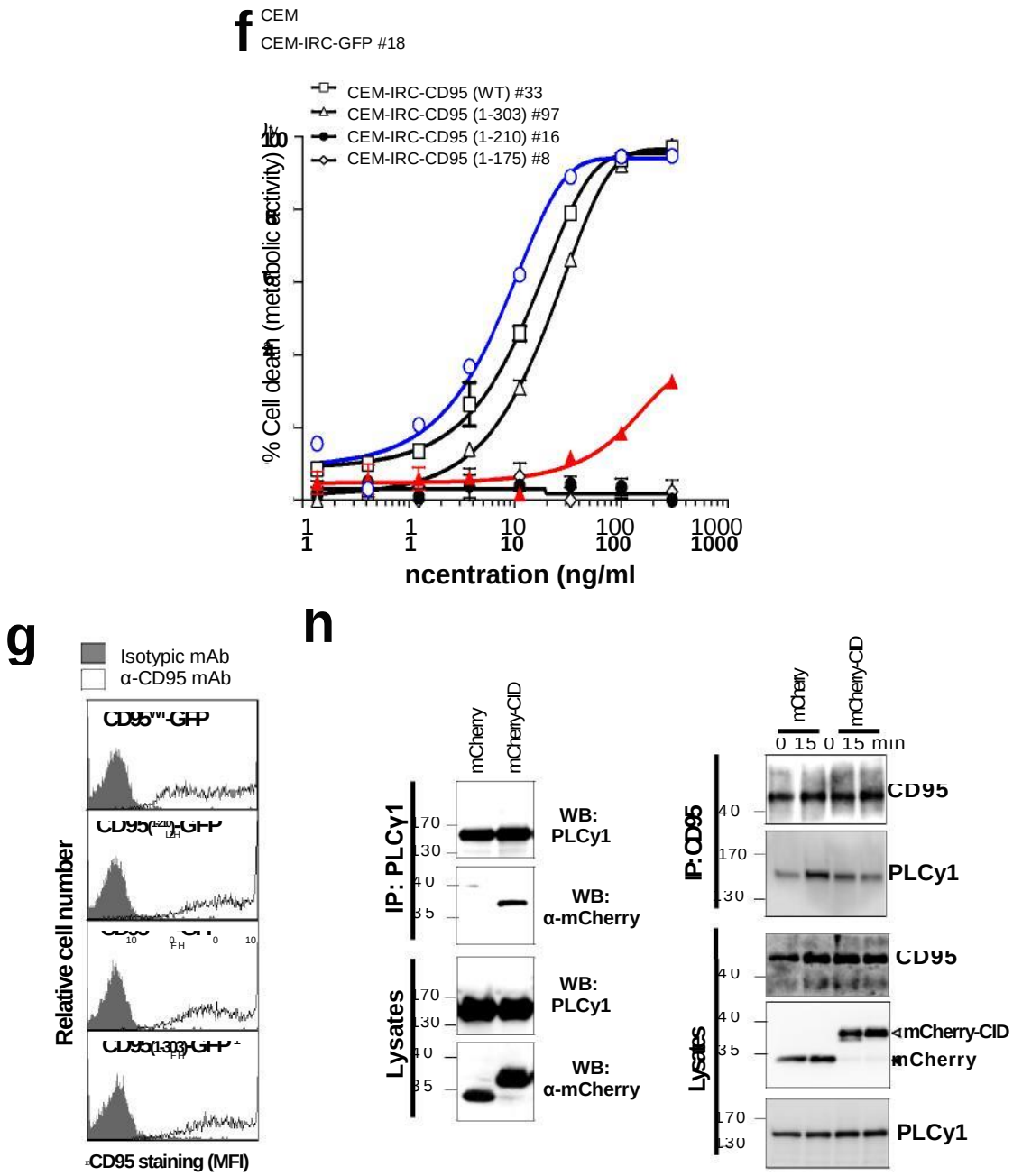

IgCD95L (ng/mL)

Supplementary Figure 4

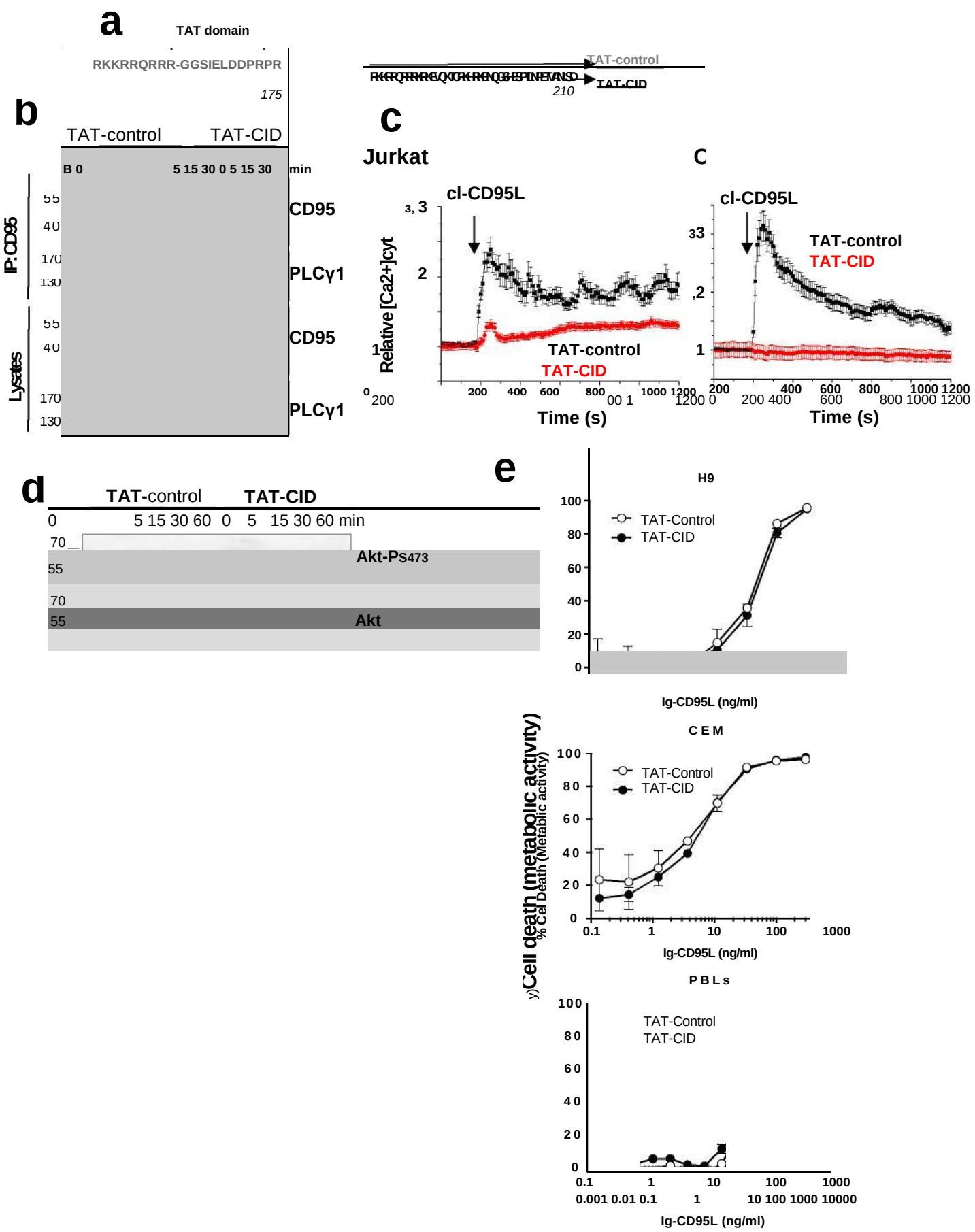

Supplementary Figure 5

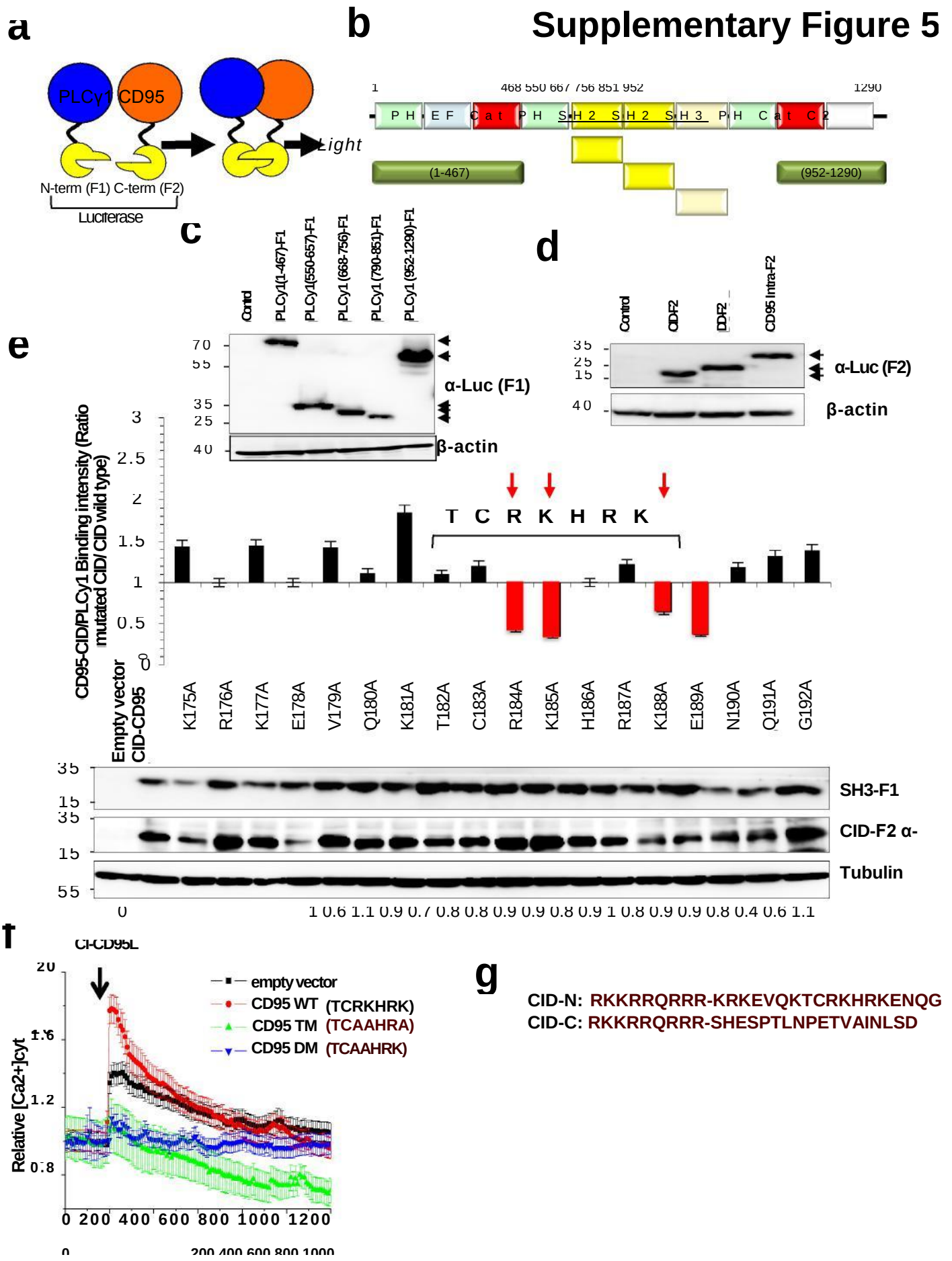

Supplementary Figure 5

h

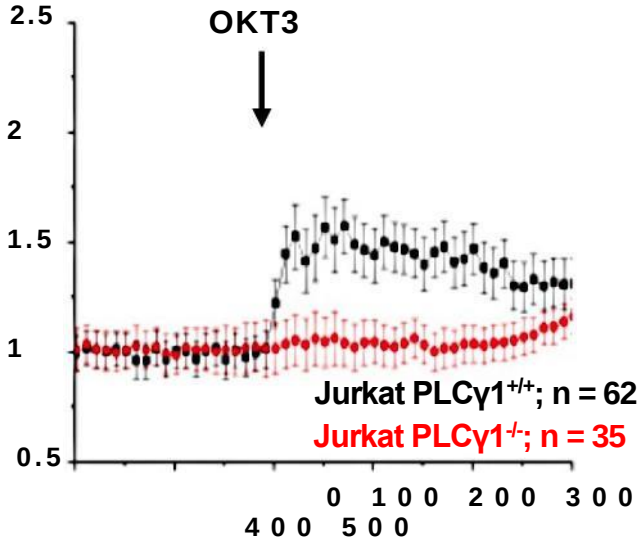

i

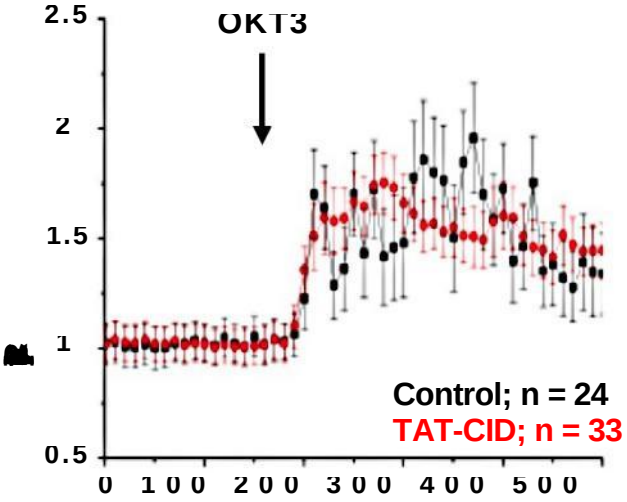

j

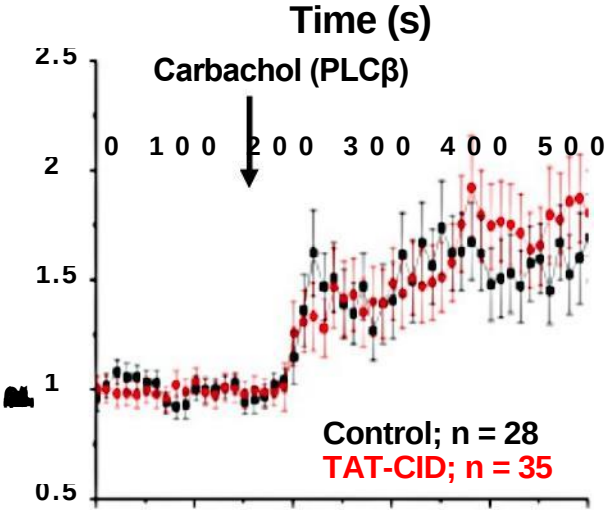

Time (s)

Supplementary Figure 6

a

```
HUMAN  MLGIWTLLPLVLTSVARLSSKSVNAQVTDINSKGLELRKTVTTVETQNLEGLHHDGQFCH 60
Mouse  MLWIWAVLPLVLAG----SQLRVHTQGTNSISESLKLRRRVRETDKNCSEGLYQGGPFCC 56
       ** **::*****:.    *.  *::* *:  *:.*:**: *  .:.:  ***::.* **

HUMAN  KPCPPGERKARDCTVNGDEPDCVPCQEGKEYTDKAHFSSKCRRCRLCDEGHGLEVEINCT 120
Mouse  QPCQPGKKKVEDCKMNGGTPTCAPCTEGKEYMDKNHYADKCRRCTLCDEEHGLEVETNCT 116
       :** **::*..**.:**. * *.** ***** ** *::.***** **** ****** ***

HUMAN  RTQNTKCRCKPNFFCNSTVCEHCDPCTKCEHGIIKECTLTSNTKCKEEGSRSNLGWLCLL 180
Mouse  LTQNTKCKCKPDFYCDSPGCEHCVRCASCEHGTLEPCTATSNTNCRKQSPRNRLWLLTIL 176
        ******:***:*:*:*. ****  *:.**** :: ** ****:*::::..*..*  * :*

HUMAN  LLPIPLIVWVKRKEVQKTCRKHRKENQGSHESPTLNPETVAINLSDVDLSKYITTIAGVM 240
Mouse  VLLIP-LVFIYRKYRKRKCWKRRQDDP---ESRTSSRETIPMNASNLSLSKYIPRIAEDM 232
       :* ** :*:: **  ::.* *:*:::    ** * . **:.:* *::.*****. **  *

HUMAN  TLSQVKGFVRKNGVNEAKIDEIKNDNVQDTAEQKVQLLRNWHQLHGKKEAYDTLIKDLKK 300
Mouse  TIQEAKKFARENNIKEGKIDEIMHDSIQDTAEQKVQLLLCWYQSHGKSDAYQDLIKGLKK 292
       *:.:.* *.*:*.::*.***** :*.:**********  *:* ***.:**: ***.***

HUMAN  ANLCTLAEKIQTIILKDITSDSENSNFRNEIQSLV 335
Mouse  AECRRTLDKFQDMVQKDLGKSTPDTGNENEGQCLE 327
       *:     :*:* :: **: ..: ::. .** *.*
```

b

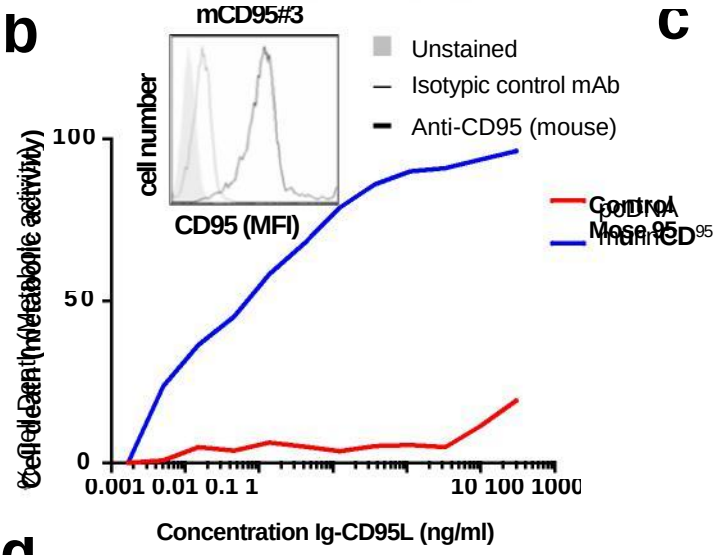

c

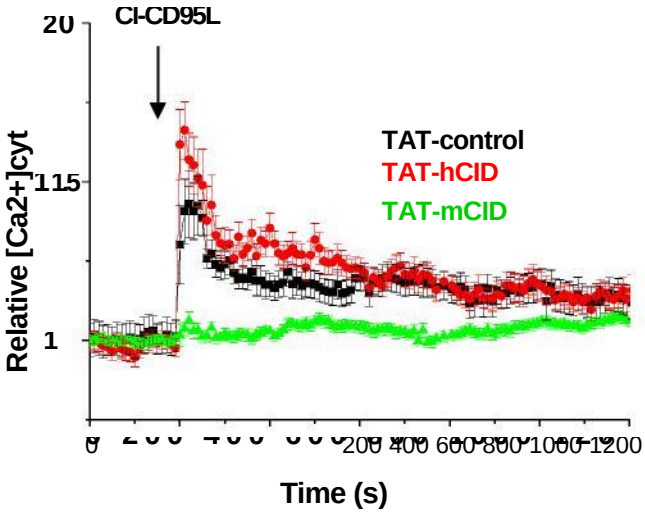

d

RKKRRQRRR-YRKYRKRKCWKRRQDDPESRTSSRETIPMNASN-TAT-mCID

e

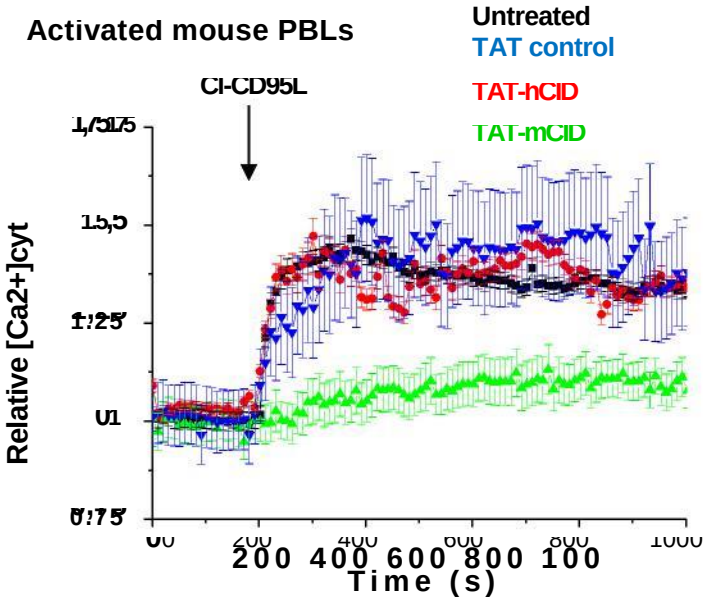

Supplementary Figure 6

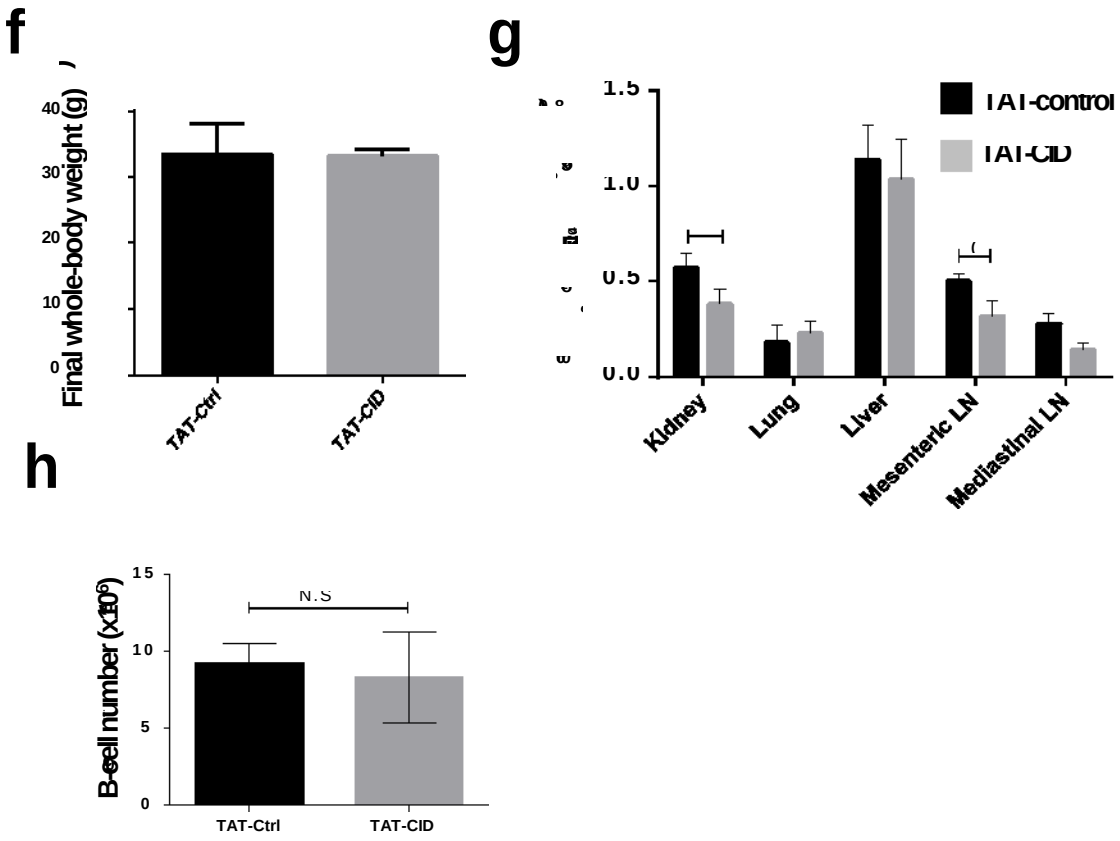

Supplementary Figure 7

a

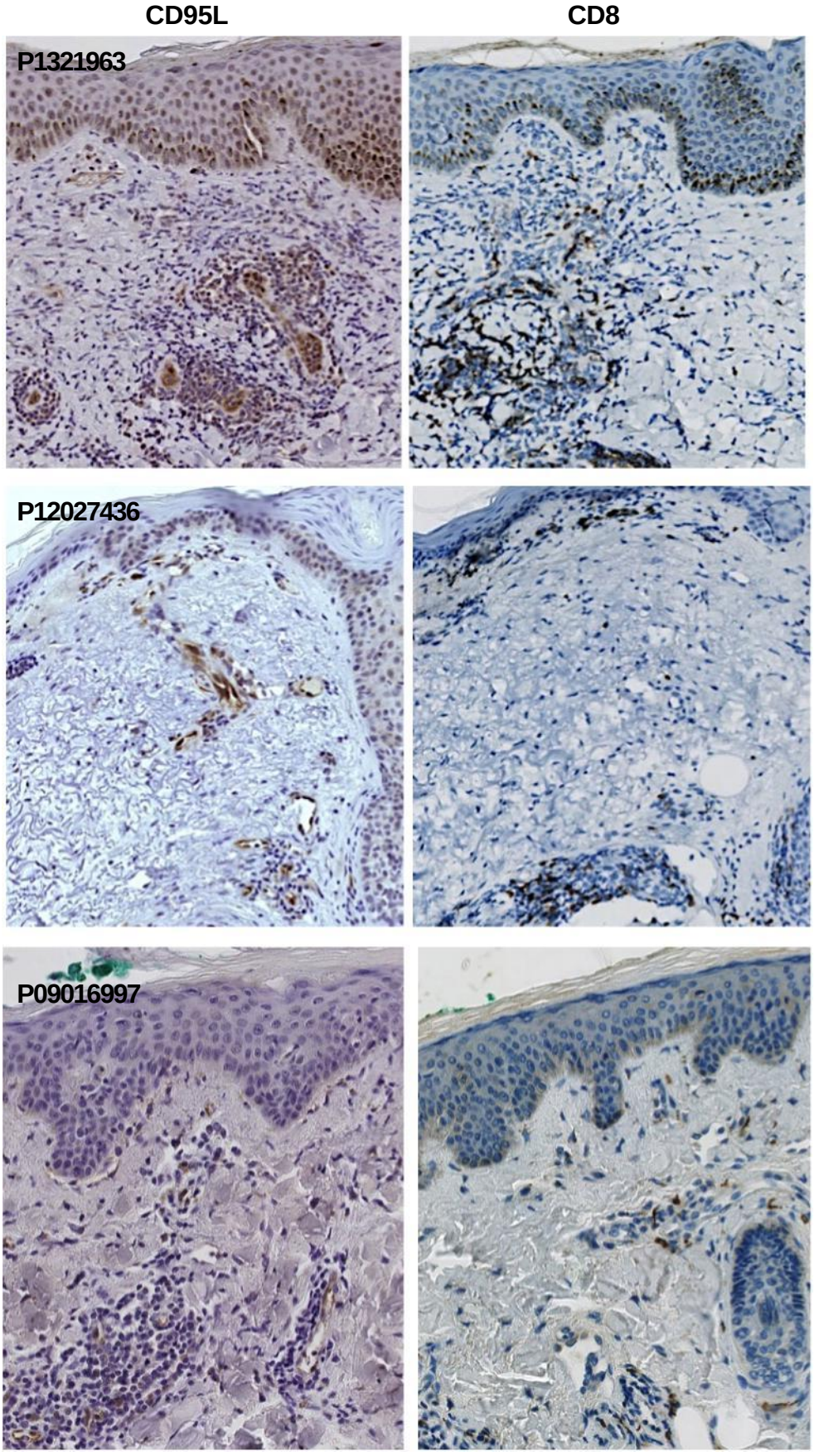

Supplementary Figure 7

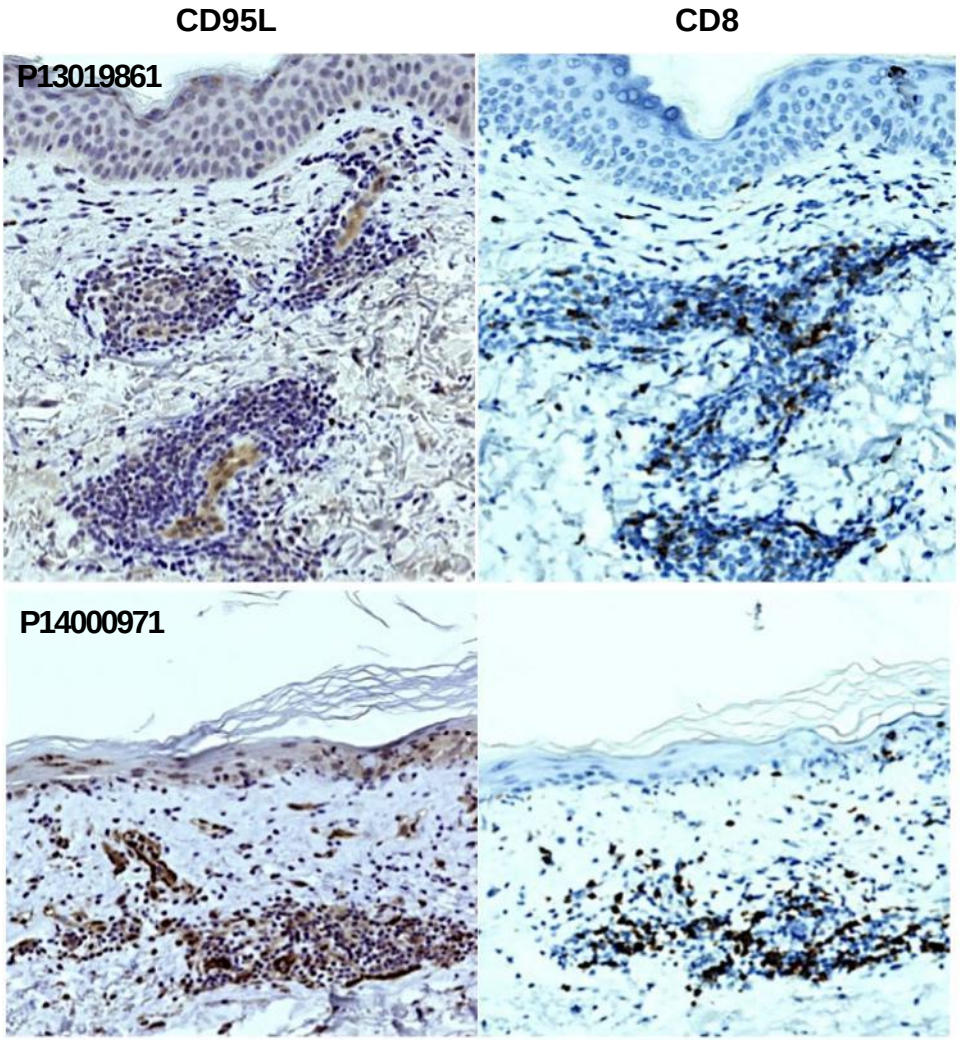

Supplementary Figure 7

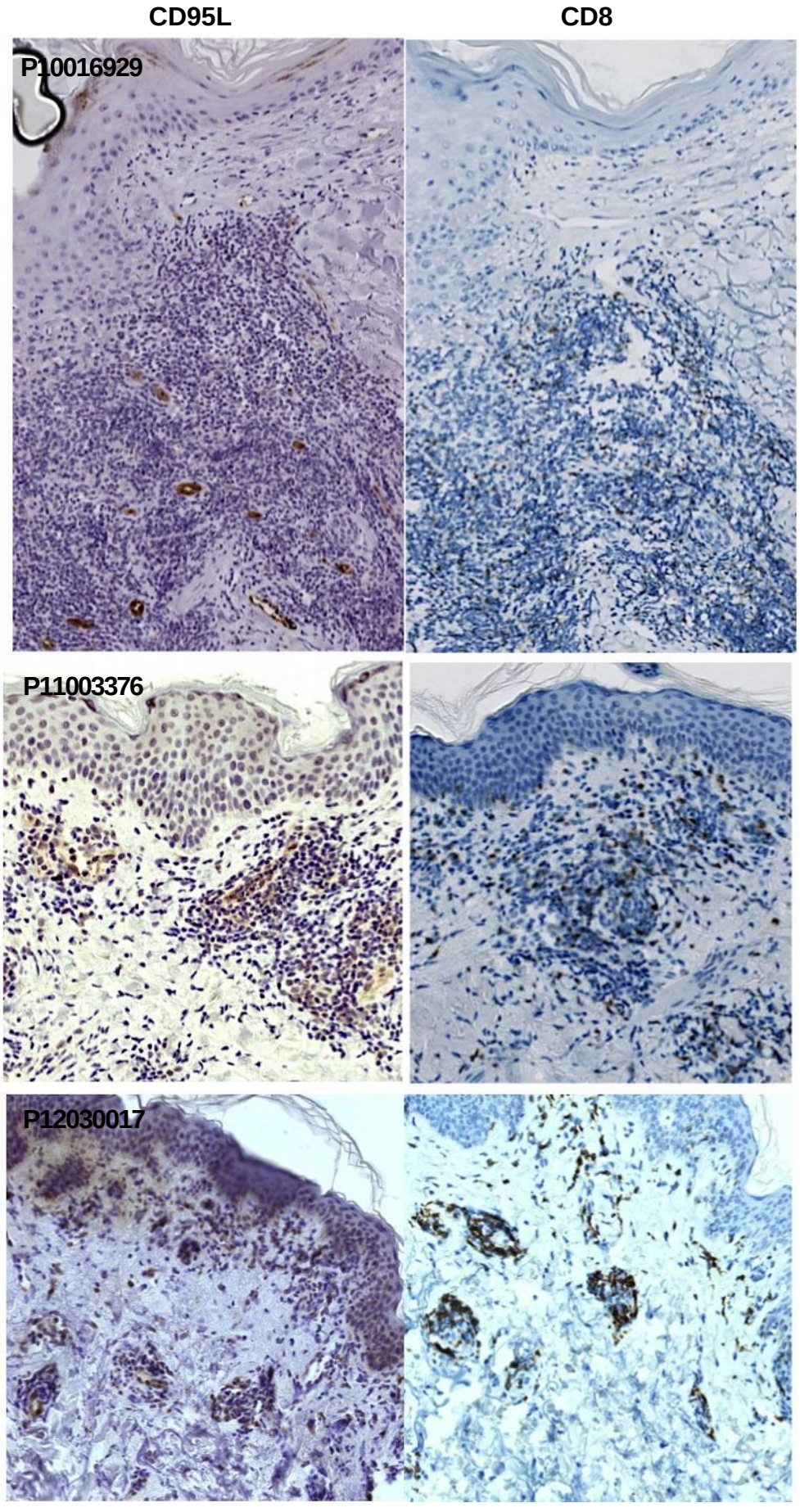

Supplementary Figure 7

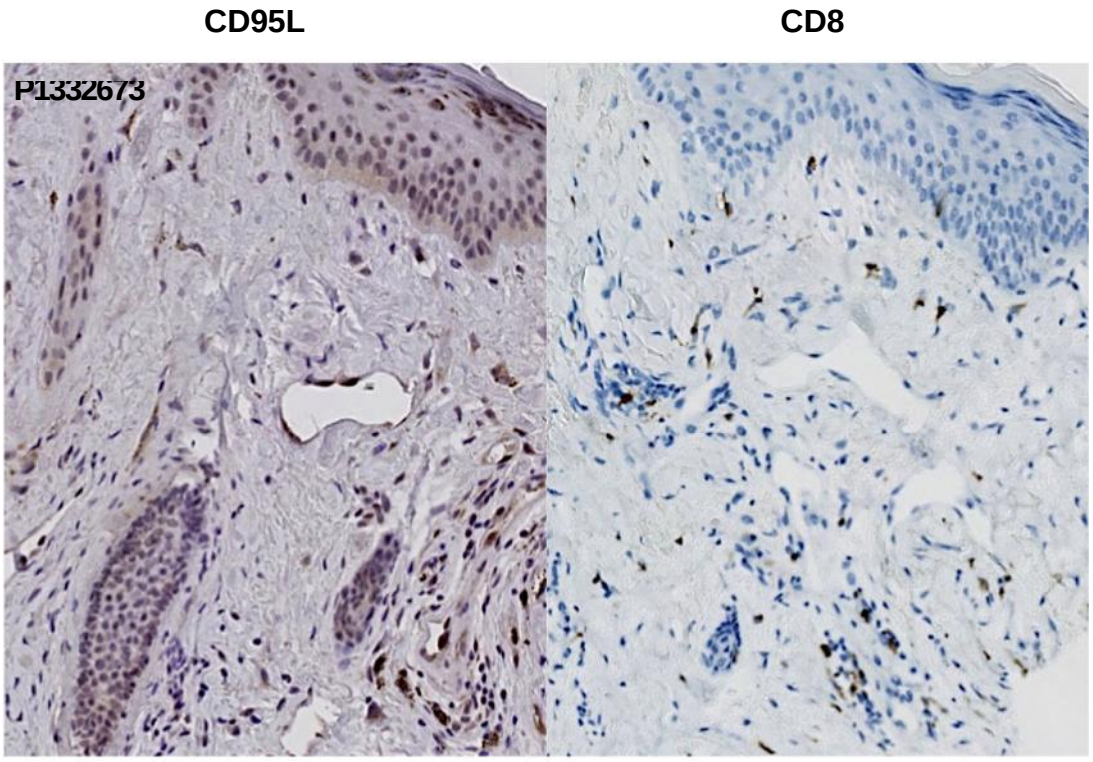

b

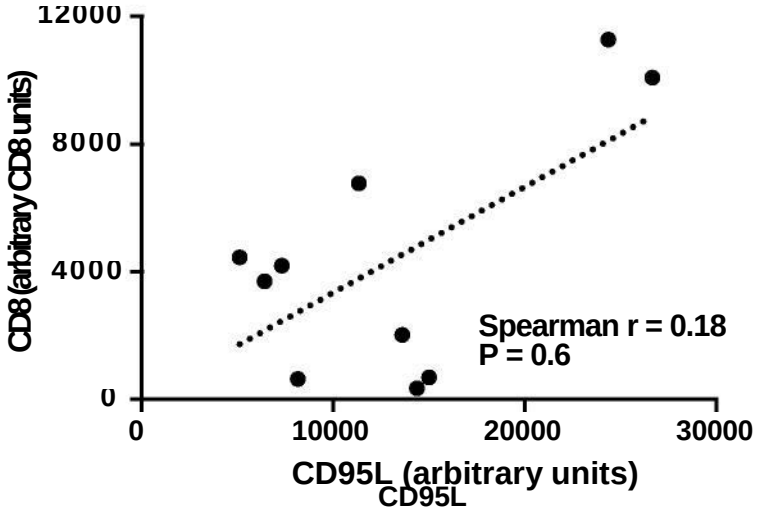

Supplementary Figure 7

c

Observed hydrogen bonds in back bone (presence per % simulation time)

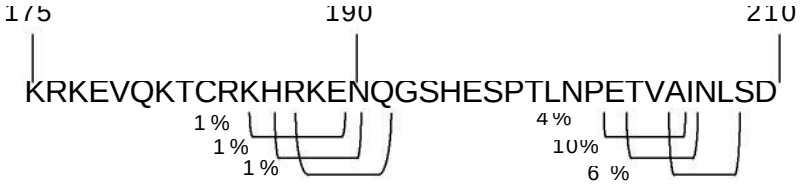

d

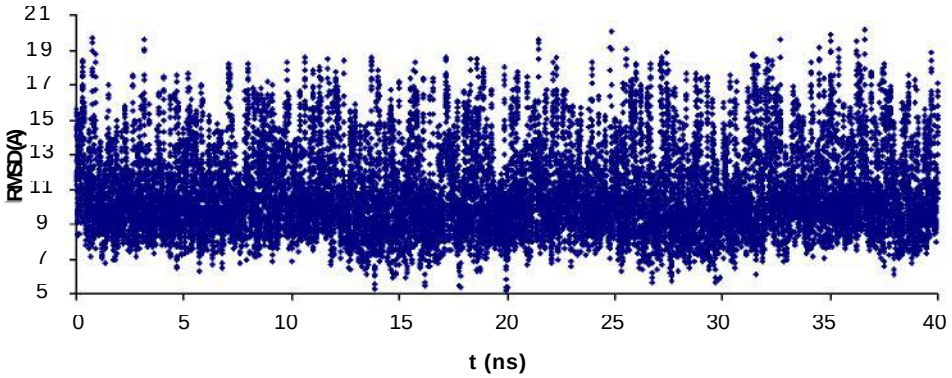

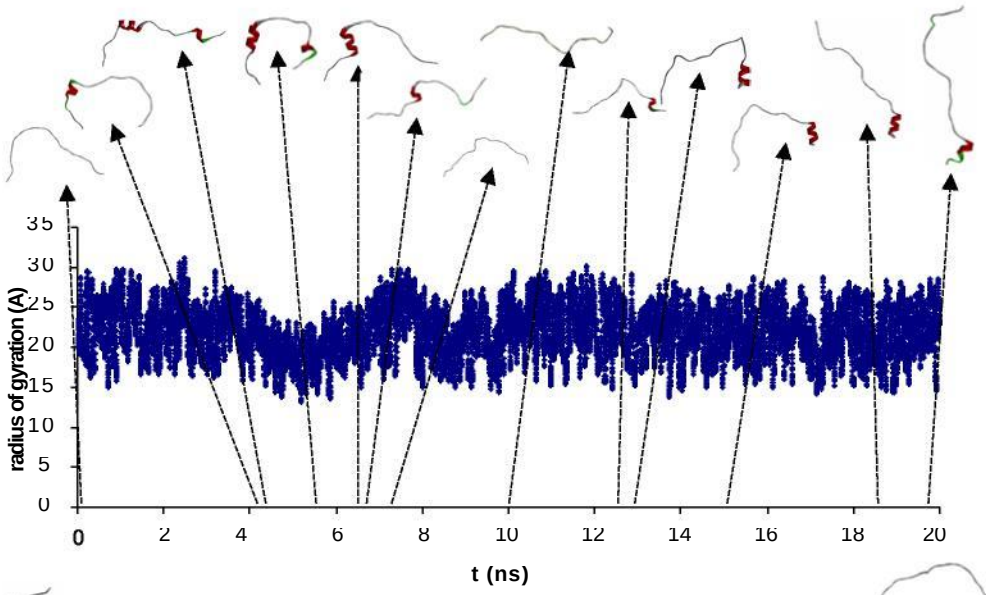

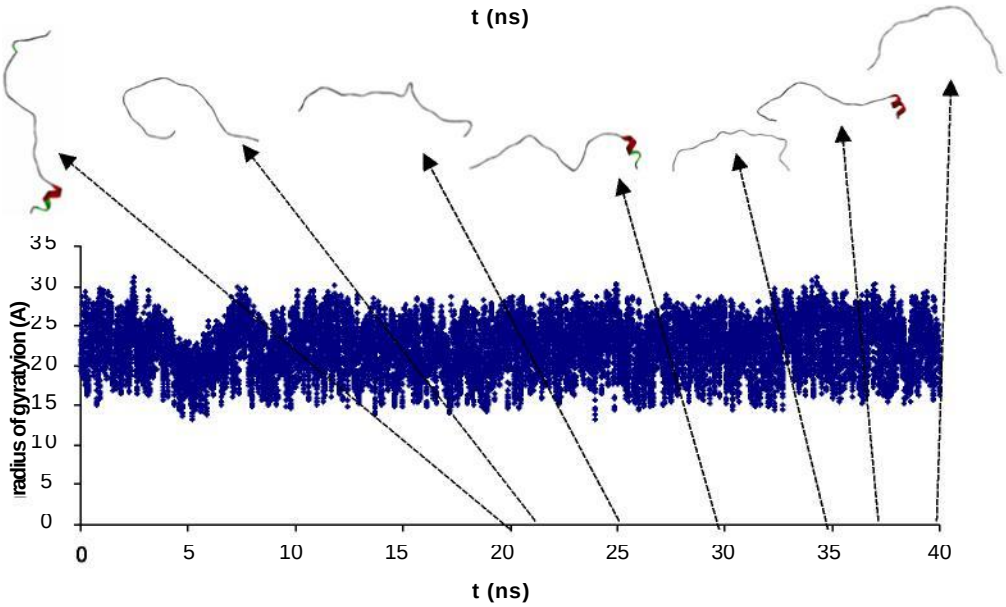

SUPPORTING MATERIALS AND METHODS

Patients and Ethics Statement

SLE patients fulfilled four or more of the 1982 revised ACR criteria for the disease. All clinical investigations were conducted according to the principles expressed in the Declaration of Helsinki. Blood was sampled from patients diagnosed with SLE after written consent was obtained from each individual. This study was approved by institutional review board at the Centre Hospitalier Universitaire de Bordeaux. Animal experiments were conducted under UK Home Office licence number 40/3412 at the University of Nottingham and subject to local ethical review.

Antibodies and other reagents

PHA, 3-[4,5-dimethylthiazol-2-yl]-2,5-diphenyltetrazolium bromide (MTT), protease and phosphatase inhibitors were purchased from Sigma-Aldrich (L'Isle-d'Abeau-Chesnes, France). Anti-CD95L mAb was from Cell Signaling Technology (Boston, MA, USA). Recombinant IL-2 was obtained from PeproTech Inc. (Rocky Hill, NJ, USA). Anti-PLCγ1 was purchased from Millipore (St Quentin en Yvelines, France). Anti-CD95 mAbs (APO1-3) came from Enzo Life Sciences (Villeurbanne). PE-conjugated anti-human CD95 (DX2) mAb, anti-human FADD mAb (clone1), neutralizing anti-CD95L mAb (Nok1) were provided by BD Biosciences (Le Pont de Claix, France). Anti-Fas (C-20) mAbs were from Santa Cruz Biotechnology (Heidelberg, Germany). CD95-Fc, neutralizing anti-ICAM-1 and E-selectin antibodies were from R&D Systems. Anti-CD4 (VIT4) and anti-CD25 (4E3) mAbs were from Miltenyi Biotec and anti-CCR6 (G034E3) and anti–CXCR3 (G025H7) were purchased from Biolegend. Anti-CD25 (4E3) and anti-Foxp3 (236AE7) mAbs were from eBiosciences (Paris, France).

Plasmids and Constructs

GFP-tagged human CD95 (hCD95) constructs were obtained by PCR and inserted in frame between the Nhe1 and EcoR1 restriction sites of the pEGFP-N1plasmid (Clontech). Note that for all CD95 constructs the numbering takes into consideration the subtraction of the 16 amino-acid signal peptide sequence The primer pairs used are as follow: forward GCTAGCGACGCTTCTGGGGAGTGA; reverse (1-319) CTCGAGGACCAAGCTTTGGATTTC; (1-303) CTCGAGAGTAATGTCCTTGAGGATGAT; (1-210) CTCGAGATCAGATAAATTTATTGCCACTGTTTC; (1-175) CTCGAGCTTCACCCAAACAATTAGTGG. Substitution of the cystein at position 183 by a valine in hCD95$^{(1-210)}$ was performed using the Quickchange Lightning Site-directed Mutagenesis kit (Agilent Technologies, Les Ulis, France) according to manufacturer instructions and using the primer pair forward GAGAAAGGAAGTACAGAAAACAGTGAGAAAGCACAGAAAGGAAAACC and reverse GGTTTTCCTTTCTGTGCTTTCTCACTGTTTTCTGTACTTCCTTTCTC. The CID-mCHERRY construct was obtained by PCR amplifying the hCD95 sequence coding for the residues 175 to 210 using a forward primer GAATTCATCGATATGAAGAGAAAGGAAGTACAGAAAACATGC adding in 5' an EcoR1 cloning site, an optimal Kozak sequence and a starting methionine in combination with the reverse primer CTCGAGAGCACCAGCACCAGCACCAGCACCATCAGATAAATTTATTGCCACTGTTTC coding for a 8 amino acid linker (GAGAGAGA) and a BamH1 cloning site. The resulting fragment was inserted between the EcoR1 and BamH1 restriction sites of a pmCHERRY-N1 vector. Mouse full length CD95 (mCD95) was kindly provided by Dr Pascal Schneider

(Universite de Lausanne, Lausanne, Switzerland). The mCD95 sequence lacking the signal peptide (SP - residues 1-21) was amplified by PCR using the following primer pair: forward GGATCCCAAGGTACTAATAGCATCTCCGAGAG and reverse GAATTCTCACTCCAGACATTGTCCTTCATTTTC. After digestion by BamHI/EcoRI, the amplicon was inserted into pcDNA3.1(+) vector in frame with SP sequence of the influenza virus hemagglutinin protein from (MAIIYLILLFTAVRG) followed by a flag tag sequence and a 6 amino acid linker (GPGQVQ). The pTriEx-4 vector encoding for Myc-tagged full-length human PLCγ1 was a gift from Dr. Matilda Katan (Chester Beatty Laboratories, The Institute of Cancer Research, London, United Kingdom). Plasmids coding for full length CD95L and the secreted IgCD95L have been described elsewhere (Tauzin et al., 2011). All constructs were validated by sequencing on both strands (GATC Biotech, Constance, Germany).

PKAReg.hRluc-F[1].pcDNA3.1(+) and PKACat.hRluc-F(2).pcDNA3.1(+) (Stefan et al., 2007) were a kind gift from Dr S. W. Michnick (Université de Montréal). PKAReg.hRluc-F[1].pcDNA3.1(+) was cleaved by EcoR1 and BspEI to eliminate the PKA sequence and insert the following linker GAATTCGCGGCCGCATCGATGGTGGCGGTGGCTCTGGAGGTGGTGGGTCCTCCGGA to generate hRluc-F[1].pcDNA3.1(+). The different PLCγ1 domains were amplified by PCR from the pTriEx-4 vector encoding Myc-tagged full-length human PLCγ1, with the following set of primers: PLCγ1 (1-467) (TAGTCCAGTGTGGTGGAATTCATGGCGGGCGCCGCGTCCCCT and TCCAGAGCCACCGCCACCATCGATAGCCAGCTTCTTGTGCTTGATG); PLCγ1 (550-667) (TAGTCCAGTGTGGTGGAATTCATGTGGTTCCATGGGAAGCTAGGGGC and TCCAGAGCCACCGCCACCATCGATGACAGGCTCTGAAAGTCGCATCTC); PLCγ1 (668-756) (TAGTCCAGTGTGGTGGAATTCATGTGGTACCACGCGAGCCTGACCAG

and TCCAGAGCCACCGCCACCATCGATGATGGGATAGCGCAGCTTCATCTTG); PLCγ1 (790-851) (TAGTCCAGTGTGGTGGAATTCATGCCAACTTTCAAGTGTGCAGTC and TCCAGAGCCACCGCCACCATCGATGTTGACCATCTCTTCCACGTAG); PLCγ1 (952-1290) (TAGTCCAGTGTGGTGGAATTCATGGAGCTCTCTGAACTTGTCGTCTAC- and TCCAGAGCCACCGCCACCATCGATGAGGCGGTTGTCTCCATTGAC) and inserted in hRluc-F[1].pcDNA3.1(+) using Gibson assembly protocol (NEB, Ipswich, MA, USA). In parallel, PKACat.hRluc-F(2).pcDNA3.1(+) was double digested by EcoRI/ClaI to eliminate the PKA sequence and replace it using Gibson assembly, by amplicons coding for CD95-CID (amino acid residues 175 to 210) (TAGTCCAGTGTGGTGGAATTCATGAAGAGAAAGGAAGTACAGAAAAC and TCCAGAGCCACCGCCACCATCGATATCAGATAAATTTATTGCCAC), CD95-DD (amino acid residues 211 to 303) (TAGTCCAGTGTGGTGGAATTCATGGTTGACTTGAGTAAATATATC and TCCAGAGCCACCGCCACCATCGATAGTAATGTCCTTGAGGATGAT) CD95 intracellular domain (amino acid residues 175 to 319) (TAGTCCAGTGTGGTGGAATTCATGAAGAGAAAGGAAGTACAGAAAAC and TCCAGAGCCACCGCCACC ATCGAT GACCAAGCTTTGGATTTCATT). All primers were purchased from Eurogentec (Liège, Belgium). Constructs were validated by DNA sequencing (GATC Biotech, Germany). Alanine scanning experiments were described in supporting materials and methods.

Renilla luciferase-based protein fragment complementation assay

HEK293T cells were electroporated with 5 jig of DNA using BTM-830 electroporation generator (BTX Instrument Division, Harvard Apparatus) with 10 jig of DNA. Transfected

cells were cultured for 24 hrs prior to protein complementation assay analyses as previously described (Stefan et al., 2007). Briefly, transfected cells (10^6) were washed, resuspended in 100 pl PBS and deposited in OptiPlate-96 (PerkinElmer, Waltham, MA, USA). Coelenterazine-h (5 µM, Sigma) was injected to each well and renilla luciferase activity was monitored for the first 10 seconds using Infinite200Pro (Tecan, Männedorf, Switzerland).

Cell lines and peripheral blood lymphocytes

All cells were purchased from ATCC (Molsheim Cedex, France). The T-cell lines CEM, H9 and Jurkat were cultured in RPMI supplemented with 8% heat-inactivated FCS (v/v) and 2 mM L-glutamine at 37 °C in a 5% CO2 incubator. CEM-IRC cells expressing a low amount of endogenous CD95 was described in (Beneteau et al., 2007; Beneteau et al., 2008). HEK293 cells were cultured in DMEM supplemented with 8% heat-inactivated FCS and 2 mM L-glutamine at 37°C in a 5% CO_2 incubator. PBMCs (peripheral blood mononuclear cells) from healthy donors were isolated by Ficoll centrifugation, washed twice in PBS. Monocytes were removed by a 2 hours adherence step and the naive PBLs (peripheral blood lymphocytes) were incubated overnight in RPMI supplemented with 1 pg/ml of PHA. Cells were washed extensively and incubated in the culture medium supplemented with 100 units/ml of recombinant IL-2 (R&D) for 5 days. Human umbilical vein endothelial cell (HUVEC) (Jaffe et al., 1973) were grown in human endothelial serum free medium 200 supplemented with LSGS (Low serum growth supplement) (Invitrogen, Cergy Pontoise, France). CEM-IRC cells were electroporated using BTM-830 electroporation generator with 10 pg of DNA. 24 hrs after electroporation, cells were treated for one week with 1 mg/mL of neomycin and then clones were isolated using standard limiting dilution procedures.

T Cell subset isolation (Th17 and Treg cells)

Peripheral blood mononuclear cells (PBMC) were isolated from buffy-coat by density gradient using lymphocyte separation medium (Eurobio, Les Ulis, France). PBMCs were then subjected to selection using a cocktail of antibody-coated magnetic beads: $CCR6^{+}CXCR3^{-}CD4^{+}$ cells (Th17 cells) were sorted with Human Th17 Enrichment kit (STEMCELL Technologies, Grenoble, France) and $CD4^{+}CD25^{+}CD127^{-}$ Treg cells were isolated with MACS column (Miltenyi Biotec, Paris, France). Cell sorting efficiency was evaluated by FACS.

Transcriptomic analysis

Isolated Th17 and Treg cells from two healthy donors were treated with or without 100ng/ml of cl-CD95L for 8h. Then, total RNA was extracted using the Nucleospin RNA XS isolation kit (Macherey-Nagel, Hoerdt, France) and RNA quality was assessed using the RNA6000 nano chip kit (Agilent, Les Ulis, France). For each condition, 9 ng of total RNA was reverse transcribed using the Ovation PicoSL WTA System V2 (Nugen, Leek, The Netherlands). Fragmented cDNAs were then hybridized to GeneChip® Human Gene 2.0 ST microarrays (Affymetrix, High Wycombe, UK). After overnight hybridization, chips were washed on the fluidic station FS450 and scanned using the GeneChip Scanner 3000 7G (Affymetrix). The scanned images were then analyzed with the Expression Console software (Affymetrix) to generate raw data and metrics for quality controls.

Probes were mapped using custom CDF files from Brainarray V20 (http://brainarray.mbni.med.umich.edu/Brainarray/Database/CustomCDF/CDF_download.asp) and RMA normalization was performed using R software. Raw data as well as RMA normalized data have been deposited to the Gene Expression Omnibus under the accession number GSE78909 (http://www.ncbi.nlm.nih.gov/geo/query/acc.cgi?acc=GSE78909). Statistical analyses were performed using Partek® Genomics Suite® software (Partek Inc., St.

Louis, MO, USA). Data was filtered based on p-value ($p<0,05$ was considered significant). Pathway enrichment analyses were generated using the Ingenuity Pathway Analysis software (QIAGEN Redwood City, CA, USA).

Immunohistochemistry analysis

Skin biopsies from lupus patients were embedded in paraffin and cut into 4 µm sections. For CD4, CD8 and IL-17 detection, immunohistochemical staining was performed on the Discovery Automated IHC stainer using the Ventana OmniMap detection kit (Ventana Medical Systems, Tucson, AZ, USA). The slides were rinsed with Ventana tris-based Reaction buffer (Roche). Following deparaffination with Ventana EZ Prep solution (Roche) at 75 °C for 8 min, antigen retrieval was performed using Ventana proprietary chemistry, tris-based buffer solution CC1 (pH8) antibody, at 95°C to 100°C for 48 min. Endogen peroxidase was blocked with Inhibitor-D in 3% H_2O_2 (Ventana) for 10 min at 37°C. After rinsing, slides were incubated at 37°C for 60 min with anti-human IL-17 (Bioss), anti-human CD4 and anti-human CD8 (Dako), and secondary antibody - OmniMap HRP for 32 min (Roche). Signal enhancement was performed using the Ventana ChromoMap Kit Slides (biotin free detection system). For CD95L (BD Pharmigen) detection, antigen retrieval was performed using antigen unmasking solution pH 9 (Vector) at 95°C for 40 min and endogenous peroxidase was blocked using 3% H_2O_2 in methanol for 15 min. Slides were incubated in 5% BSA for 30 min at RT and then stained overnight at 4°C. Tissue sections were incubated with Envision+ system HRP-conjugated secondary antibodies for 30 min at RT and labeling was visualized by adding liquid DAB+. Sections were counterstained with hematoxylin and mounted with DPX mounting medium. Using ImageJ software (IHC toolbox), densitometry analysis was undertaken on scanned slides to quantify the level of staining for each target. The mean area for each marker was determined.

Mouse and Human CD4$^+$ T-cell subset generation

For the generation of murine T-cell subsets, spleens were removed from C57Bl/6 mice and single cell suspensions prepared. CD4$^+$CD62L$^+$ naïve cells were isolated using Miltenyi Biotec microbeads. Naïve human CD4$^+$ T-cells were prepared using the Miltenyi Biotec naïve CD4$^+$ T-cell isolation kit II, which are sorted produced a 99% pure population of CD4$^+$CD45RA$^+$ cells. Purified T-cells were cultured in complete IMDM media all with α-CD3 (1 µg/ml), α-CD28 (2 µg/ml), and as follows; Th1 cells IL-12 (10 ng/ml) with α-IL-4 (10µg/ml), Th2 cells IL-4 (10 ng/ml) and α-IFN-y (10 µg/ml), Th17 cells Il-6 (10 ng/ml), TGF-β1 (2 ng/ml), α-IFN-y (10µg/ml) with α-IL-4 (10 µg/ml), and Tregs IL-2 (10ng/ml) TGF-β1 (5ng/ml), α-IFN-y (10µg/ml) and α-IL-4 (10µg/ml). Cells were converted to T-cell subsets over five days as outlined above. All cytokines were supplied by PeproTech (London, UK). Mouse CD3 (clone 2C11); human CD3 (UCHT1); mouse CD28 (37.51); human CD28 (CD28.2); mouse IL-4 (11B11); human IL-4 (MP4-25D2); mouse IFN-y (XMG1.2); human IFN-y B27 came from BD Pharmigen.

In vivo administration of cl-CD95L

Female C57BL/6 mice (Harlan UK) aged between 8-10 weeks were housed in groups of 6 and administered IP with 200ng recombinant cl-CD95L or vehicle. Twenty-four hours following injection, mice were sacrificed and periteonial cavities were washed with 5ml of 2% FCS in sterile D-PBS/, blood smears were prepared, and spleens aseptically collected. Blood smears and cytospins of periteonal cells (PECs) were stained with Giemsa and differential counts performed. Single cell suspensions of spleens and PECs were prepared, total cell counts performed, CD4$^+$CD62$^-$ T-cells were isolated with Miltenyi microbeads (as above) and number of cells determined by trypan blue exclusion. For experiments where

animals received TAT-mCID or control peptides, 800μg (40 mg/kg) was injected IP 2hrs prior to administration of cl-CD95L. Cell-free peritoneal cavity fluid was retained and used to determine the levels of IL-17 and IFN-γ by ELISA (eBiosciences).

MRL/lpr mouse treatment

MRL/lpr homozygotes were obtained from the Jackson Laboratory and backcrossed onto a MRL background. Females mice (n=8/group) were intraperitoneally administrated with either TAT-CID or TAT-Ctrl peptides (40mg/kg) starting at 8 weeks of age, twice weekly for 5 weeks. After 5 weeks, final body weight was recorded, organs weighed and total spleen and $CD4^+$ cell populations sorted as above. After re-stimulation with anti-CD3, cell culture supernatants were dosed for IL-17A and IFN-γ by ELISA, qPCR analysis of purified cell population was also performed as above mentioned. Total urine protein was measured using a BCA assay (Pierce) on bladder contents collected at PM. Briefly, bladder contents were collected throughout fine needle aspiration into individual tubes, tubes were centrifuged at 500 x g for 10 minutes to collect debris. Kidneys were fixed into 4% PFA o/n prior to moving to ethanol, sectioning and staining. Scoring was conducted by an individual blind to the objective/treatments within the study as per (Kikawada et al., 2003). C3 (rabbit polyclonal FITC-conjugated anti-C3 antibody, F0201, Dako) and nuclei (DAPI, sigma-aldrich) staining were performed on frozen sections of mouse kidneys and analyzed using fluorescence microscopy (NIKON NI-E, magnification × 200). C3 accumulation in kidneys of TAT-CID and TAT-control-treated MRL/$Lpr^{+/-}$ mice was assessed by densitometric analysis of ten different fields using NIS-Elements AR Analysis software.

Metalloprotease-cleaved and Ig-fused CD95L production

IgCD95L was generated as previously described (Tauzin et al., 2011). HEK 293 cells

maintained in an 8% FCS-containing medium were transfected using by the Calcium/Phosphate precipitation method with 3 jig of empty plasmid (as control) or wild type CD95L-containing vector. 16 hours after transfection, medium was replaced by OPTI-MEM (Invitrogen) supplemented with 2 mM L-glutamine and 5 days later, media containing cleaved CD95L and exosome-bound full length CD95L were harvested. Dead cells and debris were eliminated through two steps of centrifugation for 15mins at 4500 rpm followed by elimination of exosomes by ultracentrifugation at 100,000 x g for 2hrs.

Size Exclusion Chromatography

Sera from 4 different SLE patients were filtered through a 0.2 jim filter and then 5 ml was resolved using a mid range fractionation S300-HR Sephacryl column (GE Healthcare) equilibrated with PBS (pH 7.4). Using an AKTAprime purifier (GE Healthcare), fractions were harvested with a flow rate of 0.5 mL/min. Fifty fractions were harvested and analyzed by ELISA to quantify CD95L.

CD95L ELISA

CD95L ELISA (Diaclone, Besançon, France) was performed to quantify the levels of cleaved-CD95L present in sera following the manufacturer's recommendations.

Immunoprecipitation

T-cells (5×10^7 cells per condition) were stimulated with cl-CD95L (100 ng/mL) for indicated times at 37°C. Cells were lysed, incubated with 1 ug/mL of anti-CD95 (clone APO1.3) for 15 min at 4°C and CD95 was immunoprecipitated using protein A/G coated magnetic beads (Ademtech, Pessac, France) for 1h. After extensive washing, the immune complex was resolved by SDS-PAGE and immunoblotting was performed with indicated antibodies.

Immunoblot analysis

Cells were lyzed for 30 minutes at 4°C in lysis buffer (25 mM HEPES pH 7.4, 1% v/v Triton X-100, 150 mM NaCl, 2 mM EGTA supplemented with protease inhibitor cocktail (Sigma-Aldrich)). Protein concentration was determined by the BCA assay (PIERCE, Rockford, IL, USA) according to the manufacturer's protocol. Proteins were separated on a 12% SDS-PAGE and transferred to a nitrocellulose membrane (GE Healthcare, Buckinghamshire, England). The membrane was blocked 15 minutes with TBST (50 mM Tris, 160 mM NaCl, 0.05% v/v Tween 20, pH 7.8) containing 5% w/v dried skimmed milk (TBSTM). Membranes were incubated with primary antibodies, listed above, overnight at 4°C in TBSTM. The membrane was washed in TBST and then incubated in the presence of peroxidase-conjugated anti-rabbit or anti-mouse secondary antibodies (SouthernBiotech, Birmingham, Alabama, US) for 45 minutes. Proteins were visualized with an enhanced chemiluminescence substrate kit as per manufacturers instructions (ECL, GE Healthcare).

Transendothelial migration of activated T lymphocytes

Membranes (3 μm pore size) of a Boyden chamber were hydrated in sterile D-PBS (Millipore, Molsheim, France). Thereafter, activated T-lymphocytes (10^6) were added to the top chamber on a confluent monolayer of HUVEC in a low serum (1%)-containing medium. The bottom chamber was filled with low serum (1%)-containing medium in presence or absence of 100 ng/ml of cl-CD95L. In experiments using human sera, 500μl of serum from either healthy donors or SLE patients was added to the lower chamber. Cells were cultured for 24 h at 37°C in a 5% CO2, humidified incubator. Transmigrated cells were counted in the lower reservoir by flow cytometry using a standard of $2.5x10^4$ fluorescent beads (Flow-count, Beckman Coulter).

Endothelial cell adhesion assay

Blocking antibodies were used against E-selectin and ICAM-1 in the CHEMICON® endothelial cell adhesion assay (Millipore). Briefly, after activation of the endothelial cell layer with TNF-α, anti-mouse Ig controls, anti-E-selectin or anti-ICAM-1 were added at final concentrations of 10μg/ml. Thereafter calcein-AM-stained T-cell subsets were added to the monolayers for 24 hours and unbound cells are washed. Cell numbers attached to the endothelium were assessed using fluorescence readings of excitation at 405nm and emission at 516nm with reference to a standard curve of stained cells. Human Th17 and Treg cells (3×10^5 cells) were pre-treated for 30 min with the selective S1P3 antagonists TY-52156 (TOCRIS Biosciences, Lille, France) and CAY-1044, the S1PR1 and S1PR3 inhibitor VPC-23019, the S1PR1 antagonist W146 or the S1P1, -3, -4 and -5 agonist FTY-720 and then incubated for 24 hours with cl-CD95L (100ng/mL). CAY-1044, VPC-23019, W146 and FTY-720 were kindly provided by Prof. B. Ségui (Toulouse, France).

Real-time qPCR

Single cell suspensions of spleens and PECs were prepared as described above. RNA was extracted from CD4 T-cells using phenol/chloroform. cDNA was prepared using the Promega GO-Script Reverse Transcription Kit and used in Real-Time PCR. Briefly, cDNA samples were subject to Taqman assay performed on a Roche Lightcycler. Results are reported as expression levels were calculated using the Δct method relative to HPRT.

Video imaging of the calcium response in living cells

Experiments on parent cell lines

T-cells were loaded with Fura-PE3-AM (1 μM) at room temperature for 30 min in Hank's

Balanced Salt Solution (HBSS). After washing, the cells were incubated for 15 min in the absence of Fura-PE3-AM to complete de-esterification of the dye. Cells were placed in a temperature controlled chamber (37°C) of an inverted epifluorescence microscope (Olympus IX70) equipped with an x40 UApo/340–1.15 W water-immersion objective (Olympus), and fluorescence micrograph images were captured at 510 nm and 12-bit resolution by a fast-scan camera (CoolSNAP fx Monochrome, Photometrics). To minimize UV light exposure, a 4×4 binning function was used. Fura-PE3 was alternately excited at 340 and 380 nm, and the ratios of the resulting images (emission filter at 520 nm) were produced at constant intervals (10 seconds). The Fura-PE3 ratio $_{(Fratio}$ 340/380) images were analyzed offline with Universal Imaging software, including Metafluor and Metamorph. $_{Fratio}$ reflects the intracellular Ca^{2+} concentration changes. Each experiment was repeated at least 3 times, and the average of more than 20 single-cell traces per experiment was analyzed.

Experiments on GFP-expressing cell lines

Fluo2-AM was used, instead of Fura-PE3-AM for experiments with GFP-expressing cells, because GFP fluorescence interferes with Ca^{2+} measurement using Fura-PE3. As aforementioned, T cells were loaded with Fluo2-AM (1 μM) for 30 min in Hank's Balanced Salt Solution (HBSS) and then incubated for 15 min in the Fluo2-AM free HBSS to complete de-esterification of the dye. Ca^{2+} changes were evaluated by exciting Fluo2-AM-loaded cells at 535 ± 35 nm. The values of the emitted fluorescence (605 ± 50 nm) for each cell (F) were normalized to the starting fluorescence (F0) and reported as F/F0 (relative $Ca^{2+}{}_{[CYT]).}$ Only GFP-positive cells were included in the analysis as described above.

Modelling

In supporting Materials and Methods.

Statistical analysis

Data were tested for normality prior to analysis in Prism 6.04 (Graphpad), data were analyzed by a combination of students t-tests, Mann-Whitney U test, 1-way Anova or 2-way Anova's with a Bonferroni correction for multiple group comparisons. A $p<0.05$ was considered significant, specific tests and p values are indicated in the relevant graphs.

Alanine scanning.

Alanine scanning was performed on 18 amino acid residues of the CID N-terminus region of CD95. Using pcDNA3.1-HA-CD95 (WT), plasmid encoding the different human CD95 mutants were generated by QuikChange Site-directed mutagenesis (Agilent technologies) with the following set of primers: K175A-(GTCCAGTGTGGTGGAATTCATGGCGAGAAAGGAAGTACAG and CTGTACTTCCTTTCTCGCCATGAATTCCACCACACTGGAC); R176A-(GTGGTGGAATTCATGAAGGCAAAGGAAGTACAGAAAACATGCAG and CTGCATGTTTTCTGTACTTCCTTTGCCTTCATGAATTCCACCAC); K177A-(GGTGGAATTCATGAAGAGAGCGGAAGTACAGAAAACATGCAG and CTGCATGTTTTCTGTACTTCCGCTCTCTTCATGAATTCCACC); E178A-(GGAATTCATGAAGAGAAAGGCAGTACAGAAAACATGCAGAAAGC and GCTTTCTGCATGTTTTCTGTACTGCCTTTCTCTTCATGAATTCC); V179A-(GGTGGAATTCATGAAGAGAAAGGAAGCACAGAAAACATGCAG and CTGCATGTTTTCTGTGCTTCCTTTCTCTTCATGAATTCCACC); Q180A-(GTGTGGTGGAATTCATGAAGAGAAAGGAAGTAGCGAAAACATGC and GCATGTTTTCGCTACTTCCTTTCTCTTCATGAATTCCACCACAC); K181A-(GGAAGTACAGGCAACATGCAGAAAGCACAGAAAGGAAAACC and GGTTTTCCTTTCTGTGCTTTCTGCATGTTGCCTGTACTTCC); T182A-

(GGTGGAATTCATGAAGAGAAAGGAAGTACAGAAAGCATGCAG and CTGCATGCTTTCTGTACTTCCTTTCTCTTCATGAATTCCACC); C183A- (GGAAGTACAGAAAACAGCCAGAAAGCACAGAAAGGAAAACC and GGTTTTCCTTTCTGTGCTTTCTGGCTGTTTTCTGTACTTCC); R184A- (GTACAGAAAACATGCGCAAAGCACAGAAAGGAAAACCAAGG and CCTTGGTTTTCCTTTCTGTGCTTTGCGCATGTTTTCTGTAC); K185A- (GGAAGTACAGAAAACATGCAGAGCGCACAGAAAGGAAAACC and GGTTTTCCTTTCTGTGCGCTCTGCATGTTTTCTGTACTTCC); H186A- (GCAGAAAGGCCAGAAAGGAAAACCAAGGTTCTCATGAATCTCC and GGAGATTCATGAGAACCTTGGTTTTCCTTTCTGGCCTTTCTGC); R187A- (GCAGAAAGCACGCAAAGGAAAACCAAGGTTCTCATGAATCTCC and GGAGATTCATGAGAACCTTGGTTTTCCTTTGCGTGCTTTCTGC); K188A- (GCAGAAAGCACAGAGCGGAAAACCAAGGTTCTCATGAATCTCC and GGAGATTCATGAGAACCTTGGTTTTCCGCTCTGTGCTTTCTGC); E189A- (GCACAGAAAGGCAAACCAAGGTTCTCATGAATCTCCAACC and GGTTGGAGATTCATGAGAACCTTGGTTTGCCTTTCTGTGC); N190A- (GGAAGCCCAAGGTTCTCATGAATCTCCAACCTTAAATCC and GGATTTAAGGTTGGAGATTCATGAGAACCTTGGGCTTCC); Q191A- (GCAGAAAGCACAGAAAGGAAAACGCAGGTTCTCATGAATCTCC and GGAGATTCATGAGAACCTGCGTTTTCCTTTCTGTGCTTTCTGC); G192A- (GCACAGAAAGGAAAACCAAGCGTCTCATGAATCTCCAACC and GGTTGGAGATTCATGAGACGCTTGGTTTTCCTTTCTGTGC). R184A-K185A (GGAAGTACAGAAAACATGCGCAGCGCACAGAAAGGAAAACCAAGG and CCTTGGTTTTCCTTTCTGTGCGCTGCGCATGTTTTCTGTACTTCC). The double mutant CD95 (R184A-K185A - DM) was used as template to generate the triple mutant CD95

(R184A-K185A-K188A - TM) with the following set of primers: (GCGCAGCGCACAGAGCGGAAAACCAAGGTTCTCATG and CATGAGAACCTTGGTTTTCCGCTCTGTGCGCTGCGC).

Proximity Ligation Assay (PLA)

CEM, CEM-IRC (low CD95-expressing CEM cells) cell lines and Th17 cells isolated from human peripheral blood were let adhere to poly-L-lysine-coated slides for 15 min at 37°C. Then, cells were stimulated with or without cl-CD95L (100 ng/mL) for indicated times at 37°C. After 2 washes with PBS, cells were fixed and permeabilized with PFA (4%) for 20 min at RT. Cells were blocked with PBS-5% FCS for 20 min at RT, then incubated for 20 min at 4°C with a mix of primary antibodies containing rabbit anti-human CD95 (C-20) and mouse anti-PLCγ1 (05-163) diluted to 1:400 in PBS-5% FCS. The ligation and rolling circle amplification reactions (Olink Bioscience) were performed following the manufacturer's recommendations. Finally, nuclei were stained with DAPI and cells were mounted on slides with coverslips for confocal microscopy analysis.

Interaction of CID and PLCγ1

Homology modelling.

Side chains of co-crystallized peptide (PDB: 1YWO, (Deng et al., 2005)) were replaced by the CID amino acids. For the sequence alignment, we only postulated that a salt bridge involving Asp808 or Glu809 should be conserved, setting a basic residue in the COOH terminus of the CID peptide. Ten possible sequence alignments met this criterion. The corresponding crude homology models were then optimized through energy minimization

procedures. The modelled complex with the lowest free energy and the highest interaction energy was finally submitted to 30 cycles of simulated annealing (30 successive steps of heating to 700 K then cooling to 300 K).

Protein-protein docking.

The CID was truncated into all possible heptapeptides according to the prerequisite that they contained at least one basic residue. Before docking, the peptides were equilibrated by a short (50 ps) molecular dynamics at 300 K, using a generalized Born implicit solvent model. ZDock and ZRank were used for peptide protein docking. (Chen and Weng, 2002; Pierce and Weng, 2007). The 30 best predicted complexes were refined with RDock (Li et al., 2003). As above, the modelled complex with the lowest free energy and the highest interaction energy was finally submitted to 30 cycles of simulated annealing. Both methods predicted that the peptide TCRKHRK could have the highest affinity for PLCγ1 SH3 domain.

Protein-peptide interaction energy.

The binding free energy was calculated with CHARMm, using CHARMm force-field. A nonbond list radius of 20 Å was used, with distance-dependant dielectrics (E=1). The interaction energy is the difference between energy of the complex and that of its individual components (receptor and 'ligand'), dissected into van der Waals and electrostatic contributions.

Analysis of CID 3D structure

The structure of peptide KRKEVQKTCRKHRKENQGSHESPTLNPETVAINLSD was investigated by molecular dynamics to test its autonomous folding ability. The simulation started from an extended conformation of the peptide, immersed in a rectangular solvent box

of 25 x 46 x 129 Å, under periodic boundary conditions. The system was neutralized and brought to 145 mM ionic strength by addition of Na^+ and Cl^- ions (5597 water molecules, 15 Na+ and 18 Cl-). Using CHARMm force field implemented in Discovery Studio 4.1 (Accelrys, San Diego, CA) and NAMD 2.9, the system was prepared by 6000 steps of steepest descent energy minimization, followed by 6000 steps of adopted Newton-Raphson protocol. The system was heated up to 300 K over a period of 40 ps with a 1 fs time step, then equilibrated for 50 ps. A 12 ns production run was performed at 300 K and carried out under NPT conditions, with a 1 fs time step. Particle mash Ewald (PME) was employed to calculate the long-range electronic interactions. Trajectories were analyzed with Discovery Studio. No secondary structure formation was observed in this simulation.

To ensure that explicit solvent modeling did not restrict the folding propensity of the peptide, and that our simulation time was not too restrictive to see a slow-occurring event, a 40 ns simulation was also ran with implicit solvent representation (Generalized Born with a simple swithcing), under CHARMM 37.2. These parameters of molecular dynamics can be viewed as accelerated conditions.

Analysis of hydrogen bonds was performed with VMD1.9.1 (Humphrey et al., 1996). The following parameters were used to define hydrogen bonds: donnor-acceptor distance < 3 Å , and angle cutoff < 20°.

References:

Beneteau, M., Daburon, S., Moreau, J.F., Taupin, J.L., and Legembre, P. (2007). Dominant-negative Fas mutation is reversed by down-expression of c-FLIP. Cancer Res *67*, 108-115.

Beneteau, M., Pizon, M., Chaigne-Delalande, B., Daburon, S., Moreau, P., De Giorgi, F., Ichas, F., Rebillard, A., Dimanche-Boitrel, M.T., Taupin, J.L., *et al.* (2008). Localization of Fas/CD95 into the lipid rafts on down-modulation of the phosphatidylinositol 3-kinase signaling pathway. Mol Cancer Res *6*, 604-613.

Chen, R., and Weng, Z. (2002). Docking unbound proteins using shape complementarity, desolvation, and electrostatics. Proteins *47*, 281-294.

Deng, L., Velikovsky, C.A., Swaminathan, C.P., Cho, S., and Mariuzza, R.A. (2005). Structural basis for recognition of the T cell adaptor protein SLP-76 by the SH3 domain of phospholipase Cgamma1. Journal of molecular biology *352*, 1-10.

Humphrey, W., Dalke, A., and Schulten, K. (1996). VMD: visual molecular dynamics. Journal of molecular graphics *14*, 33-38, 27-38.

Jaffe, E.A., Nachman, R.L., Becker, C.G., and Minick, C.R. (1973). Culture of human endothelial cells derived from umbilical veins. Identification by morphologic and immunologic criteria. J Clin Invest *52*, 2745-2756.

Kikawada, E., Lenda, D.M., and Kelley, V.R. (2003). IL-12 deficiency in MRL-Fas(lpr) mice delays nephritis and intrarenal IFN-gamma expression, and diminishes systemic pathology. J Immunol *170*, 3915-3925.

Li, L., Chen, R., and Weng, Z. (2003). RDOCK: refinement of rigid-body protein docking predictions. Proteins *53*, 693-707.

Pierce, B., and Weng, Z. (2007). ZRANK: reranking protein docking predictions with an optimized energy function. Proteins *67*, 1078-1086.

Stefan, E., Aquin, S., Berger, N., Landry, C.R., Nyfeler, B., Bouvier, M., and Michnick, S.W. (2007). Quantification of dynamic protein complexes using Renilla luciferase fragment complementation applied to protein kinase A activities in vivo. Proc Natl Acad Sci U S A *104*, 16916-16921.

Tauzin, S., Chaigne-Delalande, B., Selva, E., Khadra, N., Daburon, S., Contin-Bordes, C., Blanco, P., Le Seyec, J., Ducret, T., Counillon, L., *et al.* (2011). The naturally processed CD95L elicits a c-yes/calcium/PI3K-driven cell migration pathway. PLoS Biol *9*, e1001090.

Table 2

	Relative fold change	
Gene symbol	Th17 stimulated vs. unstimulated	Treg stimulated vs. unstimulated
VPS37A	-1.2187	1.0262
DRP2	-1.10687	1.11192
EFCAB5	-1.12642	1.14751
COQ4	-1.04827	1.10438
ZNF320	1.61477	1.18599
PSMC2	1.15354	-1.05771
ARHGEF26-AS1	-1.07685	1.11781
OR10H2	-1.12673	1.11702
UNC45A	-1.14011	1.25001
EPAS1	1.08741	-1.34553
ANTXRLP1	-1.14168	1.08615
TMEM25	-1.24294	1.08011
ZNF593	-1.41109	1.32329
SERPINB4	-1.18064	1.56211
ABHD12B	1.09144	-1.07552
MAP3K9	-1.14526	1.24006
ZDHHC22	-1.27771	1.0938
CHD1L	-1.14274	1.13755
MDFIC	1.08706	-1.03476
TRIM34	1.45832	-1.546
LOC101928137	-1.1616	1.15176
PRSS41	-1.23148	1.25143
SNORD35A	-1.37603	1.14985
TMEM237	-1.29511	1.3264
TMCC1-AS1	1.28487	-1.15848
RPL27	-1.09928	1.0452
ZCCHC8	-1.10625	1.19871
FCRL5	-1.28279	1.24124
SSR2	-1.03722	1.02959
FMOD	1.05909	-1.20482
ACTA2	-1.31173	1.2085
LRRC8E	-1.22236	1.12693
LIPM	-1.25676	1.13371
HKDC1	-1.07502	-1.2326
WWOX	-1.26201	1.1755
TMEM87A	1.06298	-1.04883
ESRP1	-1.06348	1.19337

M1AP	-1.08421	1.2416
PPP1R3E	1.12114	-1.23311
PPIEL	1.45727	-1.67878
CSMD2	1.08532	-1.11359
SLC2A4RG	1.06634	1.16064
CASC4	-1.0574	1.15611
INGX	-1.45982	-1.16203
GPR35	1.25408	1.06576
SLC22A23	1.61737	-1.54163
KLK8	1.22631	-1.27387
RPL30	-1.06549	1.0249
C1orf127	-1.11039	1.13547
C10orf120	-1.13776	1.24363
FABP3	-1.19801	1.35184
CACNA1C	1.11104	-1.06552
RTF1	1.09766	-1.05759
SRD5A1	1.32915	2.31024
BAG4	-1.22314	1.0878
PKD2L2	-1.13438	1.18495
LOC100147773	-1.11951	1.2163
SH2D5	1.0991	-1.14987
TP53TG5	-1.12766	1.30732
POU1F1	-1.10557	1.13973
NEK11	1.13472	-1.12905
TMEM217	1.25413	-1.24333
TRMT2A	-1.32245	1.41185
INTS12	1.4251	-1.19657
SLC2A6	1.1417	-1.23887
CCDC115	1.24743	-1.24976
LY6G5B	1.13385	-1.1463
SPCS3	-1.11826	1.07262
DMRT1	1.2028	-1.14724
HAT1	1.08729	-1.07063
ILVBL	-1.12258	1.18317
SRCAP	-1.0353	-1.09103
LEFTY2	1.10244	-1.16611
SHOX	1.12646	-1.18587
NT5M	-1.15682	1.21646
OR52B6	-1.37374	-1.13402
NEFH	-1.43191	1.29372
TIMM50	-1.22016	1.11546
POFUT1	-1.47131	1.25275
AKR1E2	-1.19215	1.2851
TOR1AIP2	-1.14966	1.15281
PRKX	-1.15509	1.08747
TMEM185A	-1.51088	1.67266

SLC52A2	-1.34327	-1.1658
SNORD26	1.87475	1.21237
CST6	1.2842	-1.29235
LRRC25	1.15555	-1.12413
H6PD	1.32607	-1.2362
SYNPR-AS1	1.09846	-1.11393
CDC25C	-1.13046	1.16973
DEGS1	-1.1544	1.10171
METTL22	-1.20282	1.35427
USP33	1.05299	-1.07997
LSM2	-1.20621	1.25728
NAGPA-AS1	1.36308	-1.30974
SPATA16	-1.10578	1.17315
SIK2	-1.11015	1.09226
TESK1	1.14216	-1.11076
GDF7	1.2847	-1.24163
PDGFA	-1.1632	1.22555
APOL6	-1.17229	1.24684
CLPSL1	-1.52283	1.59385
CA5A	1.19717	-1.22226
SRP72	-1.14804	1.12069
PDZK1P1	1.53006	-1.31707
ING4	1.17924	1.07232
LOC151475	1.11323	-1.14249
ATL3	1.10334	-1.1102
INSL5	-1.11944	1.11316
SCARNA18	-1.25352	1.28597
SYT3	-1.29511	1.40158
SPRYD4	1.20739	-1.1953
C1orf131	-1.21725	1.23301
TTC25	1.17828	-1.15539
ALKBH4	-1.07622	1.10393
ATRN	-1.30582	1.27042
RPS6KA6	-1.05998	1.07829
BID	-1.19751	1.20292
DSN1	-1.28303	1.35944
ZNF784	1.22333	-1.22918
SNORD68	-1.27358	1.25698
HS2ST1	1.13012	-1.16941
OR4K2	1.30299	1.75232
CHCHD7	-1.14312	1.16837
CLIP1-AS1	-1.32616	1.41305
MCM8-AS1	-1.16863	1.18131
KLHL24	1.11751	-1.10213
PLAC4	-1.13376	1.14628
LRP3	1.32716	-1.32789

C2orf91	-1.07535	1.06961
SIX1	1.44105	1.14412
DPH7	1.11451	1.24272
DDX11L2	-1.11509	-1.34592
MMAA	1.46051	1.15721
GALNT2	1.12559	1.31587
OTUD5	-1.09547	-1.06426
FBXO36	1.32015	1.65663
LURAP1L	-1.13323	-1.29686
C5orf66-AS2	-1.28941	-1.11341
BCL2	-1.08503	-1.0531
ARHGAP5-AS1	1.31924	1.13897
C19orf18	-1.20012	-1.11286
ADGRA1	-1.15439	-1.07138
RNF148	-1.08177	-1.1859
TMEM210	-1.10993	-1.21879
RBCK1	-1.20302	-1.09486
ARHGEF1	1.18057	1.08836
SHCBP1L	1.24008	1.11491
IGLV1-36	-1.4841	-1.29077
USP32P2	-1.29373	-1.47477
HSPB8	-1.99048	-1.49988
HAND1	-1.12342	-1.18305
PCNT	1.14886	1.09722
ZCRB1	-1.07858	-1.12106
IVL	-1.26819	-1.14587
COPS8	1.10942	1.19805
MGC27345	1.15671	1.08599
LOC101929535	-1.5817	-1.34716
LOC102724601	1.46406	1.29181
GAP43	1.17197	1.10154
LOC105379199	1.24456	1.40182
WDR53	1.2846	1.20216
LCMT1	1.28844	1.19265
ZDBF2	1.24196	1.14491
PTGES	-1.25126	-1.15699
RAPGEFL1	-1.38324	-1.24881
CST9	-1.1839	-1.12207
SHISA8	1.13489	1.21189
ATP7A	1.10166	1.15869
CPNE3	1.1477	1.09696
IFT172	1.16901	1.23831
BLM	1.18573	1.28079
C11orf73	-1.2721	-1.17797
UBE2V1	-1.14878	-1.21568
KRTAP4-9	1.19343	1.13179

OR5D14	1.12948	1.18809
KIAA1841	1.4017	1.29562
WDR73	1.16109	1.22799
IRX2	1.19533	1.26302
HMCES	1.12237	1.1604
ELMO1-AS1	1.16908	1.22775
FBXW5	1.19286	1.23759
SLC30A3	-1.19013	-1.14602
OR6C1	-1.29203	-1.3965
CCT6P1	-1.12871	-1.17264
TPH1	1.2292	1.31369
CORO6	1.06195	1.07515
OR1E2	1.56246	1.77816
PIPOX	-1.34905	-1.2921
OR52B2	1.37861	1.45931
PCGF2	-1.22419	-1.19613
FRMD4B	-1.16392	-1.14172
ARL6IP5	-1.10182	-1.12815
KIAA0556	-1.15403	-1.12386
ADRB1	1.21126	1.22485
HEATR5B	1.08451	1.069
ARRDC3-AS1	1.23716	1.20817
XPR1	1.18221	1.20406
KRT15	-1.1246	-1.11097
TNFRSF25	1.10365	1.11299
OR7E91P	1.33727	1.30031
FAM110B	1.42099	1.47063
TINCR	1.26521	1.28952
FOXJ1	-1.16162	-1.15162
DCTN3	1.15639	1.16989
CYP27B1	-1.31417	-1.29011
ZDHHC12	-1.16082	-1.17618
DND1	1.2409	1.22655
MCM2	-1.15025	-1.16232
TRIM38	1.24168	1.22226
NDUFS6	1.11494	1.12303
PRPF18	1.05949	1.05506
CCDC34	1.23192	1.22054
KNDC1	-1.20552	-1.2185
PLEKHG5	-1.22472	-1.21315
MCOLN3	1.1003	1.09479
RNF175	1.70441	1.73551

ADAM5	1.10845	1.10604
GAS2L3	1.39535	1.40747
TSPAN6	-1.13706	-1.13916
SNORD114-28	1.07227	1.07043
CRYM-AS1	-1.15133	-1.15436
RNF113B	-1.17185	-1.16885
AXIN1	1.15534	1.1523
DEFB124	1.21256	1.21163
RGAG1	-1.25306	-1.25427

Supporting Table 2. Calculated binding energies of CID heptapeptides to PLCγ1-SH3 domain.

Relative fold change in the quantity of transcripts significantly ($p \leq 0.05$) and differentially expressed in Th17 and Treg cells stimulated vs unstimulated with cl-CD95L (100 ng/mL). Data for each experimental group (n = 2 per condition) are shown.

Table 3

	interaction energy (kcal/mol)	van der Waals energy (kcal/mol)	Ligand Contact Surface Area (Å)	Receptor Contact Surface Area (Å)	RMSD vs 1YWO all heavy atoms (Å)	RMSD vs 1YWO backbone atoms (Å)
Predicted SH3-PLCγ1 / CID-CD95 complex (TCRKHRK peptide)						
protein protein docking	-122	-26.5	203	200	na	na
homology modelling	-143	-24.4	225	222	na	na
SH3-PLCγ1 / SLP-76 complex (PPVPPQR peptide)						
PDB : 1YWO	-118	-35	238	229	0	0
redocking (pose 6)	-90	-40	238	232	6.6	5.1
redocking (pose 29)	-118	-37	243	233	2.2	2.2
protein protein docking (pose 10)	-98	-36	220	218	5.5	3.6
protein protein docking (pose 20)	-138	-30	236	213	3.9	2.5

Supporting Table 3. Calculated binding energies of CID heptapeptides to PLCγ1-SH3 domain.

The binding energy computed for the best complex obtained by the two molecular modelling approaches is compared to calculated binding energy of the PLCγ1 SH3 - SLP-76 complex. This control is either the co-crystallized molecules (PDB:1YWO), redocking of SLP-76 (protein-protein docking, using co-crystallized conformations), or protein-protein docking

using the same protocol as for CID docking (short molecular dynamics simulation of the free peptide, then protein-protein docking).

Supporting table 1

Click here to access/download

Supplemental Movies & Spreadsheets

Table1.xlsx